







### TECHNICAL UNIVERSITY OF CIVIL ENGINEERING BUCHAREST

Faculty of Building Services Engineering
Thermo-Hydraulic Systems and Atmosphere Protection Department

## RESEARCH REPORT

NUMERICAL STUDY REGARDING THE IMPLEMENTATION OF PHASE CHANGING MATERIALS WITHIN AIR SOLAR COLLECTORS

PhD. Student

Eng. Andrei - Stelian BEJAN

**Scientific Coordinator** 

Assoc. Prof. Tiberiu CATALINA

BUCHAREST 2018

## **TABLE OF CONTENTS**

	TA	BLE C	OF CONTENTS	2
	FIG	SURE	S LIST	3
	TA	BLES	LIST	6
	AB	STRA	CT 7	
	1.		Introduction. Bibliographic study	9
		1.1.	Bibliographic study - general approach	9
		1.2.	Numerical modelling of solar collectors and phase changing materials	15
		1.3.	Conclusions and perspectives	18
	2.		The real collector geometry and results of experimental studies - synthesis	19
		2.1.	Geometry and materials	19
		2.2.	Results in permanent regime	21
	3.		The objectives of the numerical study and the infrastructure used	24
	4.		Numerical modelling of the airflow through the lobed orifices (absorbent metal plate)	25
		4.1	Creating the geometrical model	25
		4.2	Creating the mesh (mesh independency study)	27
plan		4.3	Experimental validation of the numerical model – comparison of velocity profiles in longitudinal 37	
		4.4	Experimental validation of the numerical model – comparison of outlet temperature	43
		4.5	Final parameters of the numerical model and results	45
PCMs	5.		Creating a numerical model for the transpired solar collector with lobed orifices and integra 49	ated
		5.1.	Creating the simplified model	49
		5.2.	Creating the optimum mesh (mesh independency study)	51
		5.3.	Experimental validation of the numerical model-comparison of the temperature variation	59
		5.4.	Final parameters of the numerical model and results	69
	6.		Conclusions and perspectives	73
	7.		Conferences and publications	76
	RE	FERE	NCES	78

## **FIGURES LIST**

	Figure 1	Example of opaque solar collector (TSC) [4]
	Figure 2	Types of geometries used for the absorbent plate orifices [20]11
[20]	Figure 3	Rise in temperature obtained for the 5 types of geometries at 110 ${\rm m}^3/{\rm h/m}^2$ and 190 ${\rm m}^3/{\rm h/m}^2$ 11
	Figure 4	Thermal efficiency of the solar collector depending on the airflow [20]11
	Figure 5	The geometry of the solar collector: a – front view b – section19
	Figure 6	Geometry of solar collector: a – sensors positioning, b – PCM layer position20
collecto	Figure 7 r cavity, c –	Solar collector geometry: a – absorbent metal plate, b – suction grille for the air inside the mixing box, d – collector backwall, e – medal framework for the PCM layer20
	Figure 8	Experimental setup21
	Figure 9	Temperature variation in the case of TSC without PCM21
	Figure 10	Temperature variation in the case of TSC with PCM22
	Figure 11	Thermal stratification in the solar collector 2 <sup>nd</sup> cavity without PCM22
	Figure 12	Thermal stratification in the solar collector 2 <sup>nd</sup> cavity with PCM22
tempera	Figure 13 ature) with a	Rise in temperature (difference between air temperature on the outlet and ambient air and without PCMs23
	Figure 14	Lobed orifices layout and geometry with equivalent diameter of 5mm (De=5mm)25
	on of a 4x4	Designing the 3D model in AutoCAD: a – absorbent metal plate with lobed orifices, b - lcm part, c – embedment in the computing domain, d –3D computing domain (4x4cm plate rallelepiped)
comput	_	Importing the geometry from AutoCAD to ANSYS DesignModeler: a -4x4cm metal plate, b - and its geometry26
	Figure 17	Importing the geometry from AutoCAD to ANSYS DesignModeler – isometric view26
	Figure 18	Extracting the 4x4cm metal plate from the computing domain (airflow)27
detail fo	_	Different mesh levels for six different cases analysed: overview, orifice detail and boundary 0.62, c) 1.5, d) 3, e) 5.3, f) 7.3 million elements28
	t air), metal	Computing grid for 3 zones: inlet (the computing domain limit corresponding to the inlet of the (the boundary of the metal absorber) and outlet (the computing domain limit corresponding to distance from the metal plate)29
	Figure 21	Importing results in Tecplot 360 in order to be properly processed31
	Figure 22	31
cases a)		Velocity profiles (u [m/s] – velocity magnitude) for longitudinal planes XY and XZ for the six, c) 1.5, d) 3, e) 5.3, f) 7.3 million cells
d) 3, e) !	_	Temperature profiles in the longitudinal planes XY and XZ for the 6 cases a) 0.2, b) 0.62, c) 1.5 illion elements
from the		Velocity profiles (u [m/s] – velocity magnitude) in transverse plane at distance 5De (2.5cm) e in all the six cases analysed: a) 0.2, b) 0.62, c) 1.5, d) 3, e) 5.3, f) 7.3 million elements35
the met	_	Velocity profiles (u [m/s] – velocity magnitude) in transverse plane at distance 10De (5cm) from II the six cases analysed: a) 0.2, b) 0.62, c) 1.5, d) 3, e) 5.3, f) 7.3 million elements
	Figure 27	Velocity profiles in transverse plane37

•	The use of the PIV technique in order to measure air velocity profiles as a results of a metal d orifices – small size collector (according to [85])38
Figure 29	Longitudinal planes used for experimental validation38
	Velocity fields in longitudinal XY plane according to PIV experimental measurements at Re2500 e jet (Z=0mm) (according to [4])39
	Velocity fields in longitudinal XY plane according to PIV experimental measurements at Re2500 from the jet centre (Z=2.5mm) (according to [4])39
Figure 32 the jet (Z=0mm)	Velocity field in longitudinal XY plane according to numerical study at Re2500, in the centre of 41
_	Velocity field in longitudinal XY plane according to numerical study at Re2500, at 2.5mm from et (Z=+2.5mm)41
Figure 34 jet Z=0mm)	Normalized velocity magnitude variation: numerical study vs. experimental study (centre of the 42
_	Normalized velocity magnitude variation: numerical study vs. experimental study (at 2.5mm the jet Z=+2.5mm)42
Figure 36	Temperatures variation in the case of experimental measurements43
Figure 37	Temperature fields obtained for the point 1 – numerical study44
Figure 38	Temperature fields obtained for the point 2 – numerical study45
Figure 39 – until 2000 iteratio	Typical images for the convergence of non-dimensional residues for a stady state simulation: a ons, b – after 10000 iterations46
Figure 40	Velocity fields at different distances from the absorbent plate47
Figure 41	Velocity and temperature fields in longitudinal XY and XZ planes47
Figure 42	Velocity vectors in longitudinal XY plane47
Figure 43	Velocity vectors in different transverse planes48
Figure 44	Velocity and temperature fields in longitudinal XY plane for 7 orifices48
Figure 45 "slice" from the sol	Designing the geometry in AutoCAD: a – absorbent plate with lobed orifices, b – extraction of a lar collector and its components49
Figure 46 view	Importing the geometry from AutoCAD to ANSYS DesignModeler: a – side view; b – isometric 50
Figure 47 PCM body	Defining bodies in ANSYS DesignModeler: a – body corresponding to the collector cavity; b – 50
previous chapter w	Creating specific air intake areas (inlet) where the velocity and temperature profiles from the vill be entered: a – 50 zones on the inlet; b – the outlet of the previous study became the inlet of velocity field which will be integrated on the new inlet51
_	Meshing levels for the analysed cases without PCM: a) 0.2 (0.18), b) 0.66 (0.61), c) 1.3 (0.7), d) 6 (3.5) million elements53
Figure 50	Areas where boundary conditions were imposed54
Figure 51	Velocity fields imported from the previous model and processed in Tecplot54
Figure 52 integrate PCMs	Velocity fields imported from the previous model in the new model of the solar collector with 54
Figure 53 2.8 (1). e) 5 (2.5). f)	Temperature fields in longitudinal plane (symmetry): a) 0.2 (0.18), b) 0.66 (0.61), c) 1.3 (0.7), d) 6 (3.5) million elements (the legend represents temperature in °C)

(1), e) 5		Velocity fields in longitudinal plane (symmetry): a) 0.2 (0.18), b) 0.66 (0.61), c) 1.3 (0.7), d) 2.8 .5) million elements (the legend represents velocity in m/s)58
	Figure 55	Velocity vectors in longitudinal plane - vortices58
	Figure 56	The mesh which will be used – the final case with PCM (5 million elements)59
respecti	-	Time interval extracted from the experimental study for the experimental validation – hours, econds59
the phe	_	Ambient temperature variation and metal plate temperature variation – the three stages of ing 120minutes of experimental campaign60
variation	n equation	Extracting the metal plate temperature variation equation and ambient air temperature in order to obtain variable boundary conditions (UDF): heating (I), stopping solar radiation (II) 61
orifices	Figure 60	Experimental validation of the numerical model – airflow through the metal plate with lobed 63
	Figure 61	a - the geometry of solar collector with PCM and b – mesh with PCM (5 mil. cells)64
	Figure 62	Energy storage capacity variation depending on the temperature [88]65
	Figure 63	Temperature variation in the case of experimental studies – 120 minutes65
(UDF): h		Extraction of temperature variation at 10De in order to obtain the variable boundary conditions copping the solar radiation (II) and cooling (III)66
	Figure 65	Results of the numeric study vs. experimental study at T10068
	Figure 66	Results of the numeric study vs. experimental study: Toutlet and Tinlet69
simulati	_	Typical images for the convergence of non-dimensional residues for the transient regime 1700 iterations (until 550 iterations – steady state regime), b – after 4000 iterations70
the tran	_	The results of the numerical study in steady state regime after 550 iterations (starting point for estudy): a – temperature field, b – velocity field71
velocity	_	The results of the numerical study in transient regime after 600s: a – temperature field, b – 71
velocity	_	The results of the numerical study in transient regime after 1200s: a – temperature field, b – 71
velocity	Figure 71 field	The results of the numerical study in transient regime after 1800s: a – temperature field, b – 72
velocity	_	The results of the numerical study in transient regime after 2400s: a – temperature field, b – 72
velocity	Figure 73 field	The results of the numerical study in transient regime after 3000s: a – temperature field, b – 72
velocity	Figure 74 field	The results of the numerical study in transient regime after 7200s: a – temperature field, b – 73
	Figure 75	Results dissemination – Solar World Congress SWC 2017, Abu Dhabi, EUA77
	Figure 76	Results dissemination – EENVIRO Conference 2017, București, România77
	Figure 77	Results dissemination – I P2M2F Laboratory Cadi Avvad University Marrakech Morocco 77

## **TABLES LIST**

	Table 1.	Software used for numerical modelling of air solar collectors	15
	Table 2.	Software used for numerical modelling of PCMs	16
	Table 3.	Boundary conditions used in the mesh independency study	29
	Table 4.	Boundary conditions used for the experimental validation	40
	Table 5.	Boundary conditions used for point 1	43
	Table 6.	Boundary conditions used for point 2	44
	Table 7.	Boundary conditions used in the mesh independency study	53
n transi	<i>Table 8.</i> ent regime	Boundary conditions for the model used in order to simulate the airflow through lobed orifical	ices
	Table 9.	Characteristics of the PCM use in the experimental and numerical studies [88]	64
PCMs	Table 10.	Boundary conditions use in case of experimental validation of the solar colector with integra 68	ted

### **ABSTRACT**

The current paper represents the third report within doctoral studies and presents the state of preliminary numerical studies conducted so far. The three research reports were structured as follows:

- a) Research Report no. 1, respectively the complex bibliographic study on the implementation of phase changing materials (PCMs) in buildings and solar collectors
- b) Research Report no. 2, respectively the experimental study regarding the implementation of phase changing materials within air solar collectors
- c) Research Report no. 3 (the current one), respectively the experimental study regarding the implementation of phase changing materials within air solar collectors

The paper is composed by multiple chapters which analyse the implementation of phase change materials (PCM) in solar collectors with air, respectively:

- Bibliographic study regarding the implementation of PCMs in air solar collectors (from a numerical view)
- The geometry of the real collector and component materials
- Study of the numerical model which analyses the airflow through the collector lobed orifices
- Study of the numerical model which analyses the implementation of PCMs in the air solar collector proposed
- Conclusions and perspectives

In the current energy context, of continuously increasing energy consumption, continuous global development and very high  $CO_2$  emissions worldwide it is essential to implement advanced materials, systems which are using renewable energy sources and energy-efficient solutions in the buildings sector in order to achieve the proper indoor comfort with minimum energy consumption.

The implementation of PCMs is a strategy with an enormous potential, an increasingly attractive topic for researchers around the world. PCMs have the potential to reduce energy consumptions for cooling by absorbing latent heat from the environment or by improving night-time cooling (additional thermal mass), to reduce energy consumption for heating by increasing heat storage capacity, especially in case of low-inertia buildings, to enhance thermal comfort by improving indoor temperature variations and by taking over the peak loads and finally by contributing to the design of low-capacity HVAC systems. PCMs materials have been integrated over the time into building outdoor walls, indoor walls, HVAC systems, Trombe walls, solar air collectors and in many other systems. They have the potential to increase the overall efficiency of systems

using renewable energy sources by storing the energy during the periods when the source is available. Air solar collectors are systems with low investment cost which have the potential to reduce the energy consumption for heating and ventilation, moreover the transpired solar collectors are, according to the literature, one of the most cost-effective that can be used for this purposes. Transpired solar collectors have been studied for over 30 years, but have not yet reached their full potential.

According to the bibliographic study, the PCMs have not been implemented so far in perforated solar collectors, this system being an absolute novelty in literature. The lobed orifices implemented in air solar collectors have the potential to enhance thermal transfer and to increase the efficiency of the solar collector. Moreover, thermal energy storage (TES) materials contribute to the improvement of temperature variations at the collector outlet and the accumulation of thermal energy stored for later use, when the solar radiation is missing (cloudy periods or during the night). The biggest advantage of PCMs is that they have a high heat storage capacity due to the latent heat stored during phase change and also occupy less space than conventional materials.

Solar collectors with embedded TES materials have the potential to reduce energy consumption for space heating, reduce energy consumption regarding the heating of fresh air which is mandatory for the health of building occupants, dry indoor air, maintaining minimum safety temperature inside buildings and improve indoor thermal comfort. The addition of inertial materials to the solar collectors has a number of benefits, namely the improvement of temperature variations on the collector air outlet and the accumulation of energy for the use during periods when there is not enough solar radiation thus increasing the operating time of the solar collector and its overall efficiency.

The present paper represents the last part of the doctoral studies which has the purpose to analyse the implementation of PCMs in transpired solar collectors (TSCs) in a numerical manner and comes next to the extensive bibliographic study conducted before and the experimental studies carried out so far. The paper presents and complex bibliographic study regarding the numerical modelling of TSCs with PCMs, a synthesis of experimental results obtained until now, the study of the numerical model which analyses the airflow through the collector lobed orifices, the study of the numerical model which analyses the implementation of PCMs in the air solar collector proposed and the experimental validation related.

The last chapter of the paper outlines the research perspectives that will be followed until the end of the PhD. studies and the preliminary conclusions of the studies. The results of this paper will be further developed and expanded.

The software used for numerical modelling and data processing are ANSYS Fluent 15.0, respectively Tecplot 360 and the hardware used is part of the laboratories within Faculty of Building Service Engineering, Technical University of Civil Engineering Bucharest.

The sources used for the bibliographic study were: <a href="www.sciencedirect.com">www.sciencedirect.com</a>, <a href="www.scholar.google.com">www.scholar.google.com</a> and <a href="www.researchgate.net">www.researchgate.net</a>.

### 1. Introduction. Bibliographic study

### 1.1. Bibliographic study - general approach

Solar collectors are a method of using solar energy as a renewable energy source. These solutions have been used and studied since earliest times and can be classified into: water solar collectors water (WSCs) and air solar collectors (ASCs). WSCs are widely used solutions for domestic hot water production and for the preheating of thermal agent (water) in case of space heating. ASCs are used for preheating the fresh air needed by occupants, for heating, drying or in order to maintain a minimum safety indoor temperature during the winter. Unlike water collectors, the air collectors have the advantage that there is no risk of frost and have a lower impact on the environment [1]. According to Goyal et al. [2] ASCs could provide an outlet temperature up to 65°C.

Depending on the geometry and construction characteristics, ASCs can be classified in several ways. According to Lai et al. [3] solar air collectors can be grouped into:

- a) Opaque solar collectors (with or without orifices)
- b) Transparent or glazed solar collectors (GSCs).

Opaque solar collectors may be also classified in several types: solar collectors with plane absorber plate, solar collectors with transpired absorber plate (TSCs) or solar collectors where the absorber plate is protected by a glass layer.

Regardless of their type, the running principle of air solar collectors is the same. Solar radiation is captured by an absorbent element (generally a metal plate) that transfers the heat to the airflow within the collectors' air cavity. In the case of opaque solar collectors, the heat is usually captured by a planar metal panel (absorber) or a black perforated panel (Figure 1), then it is released to the air which is then collected at the top of the solar collector and introduced into the room by a fan (in winter or during transition periods). If there are inertial elements, the energy stored during the daytime can be later released at night. During the daytime, in summer, the solar collector can work as a thermal buffer that reduces the cooling loads determine by the building envelope or as a ventilated facade with the same role.

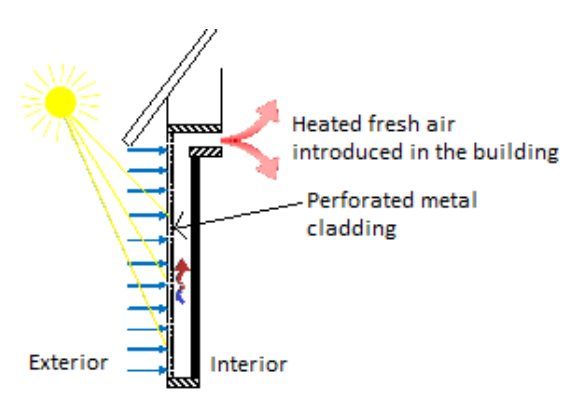


Figure 1 Example of opaque solar collector (TSC) [4]

TSCs typically have a lower investment costs and high efficiency in the case of heating systems, fresh air preheating systems or drying systems [5] and

moreover, they have lower lifetime costs [1]. Opaque solar collectors are typically used for applications where the required temperature is lower [6] and side winds are not very strong [7].

According to the literature studied so far [5, 8-14], ASCs could be used in the following applications, with enormous potential for reducing power consumption and operating costs [10]:

- heating of buildings
- maintaining a minimum safety indoor temperature in industrial applications
- drying solutions for industrial spaces
- drying solutions for food industry
- preheating fresh air needed by occupants
- heating and drying greenhouses
- improving the efficiency of photovoltaic systems
- improving the efficiency of HVAC systems
- reduction of energy consumptions for cooling.

According to Leon and Kumar [10], solar air collectors were often used for drying, by using collectors with surfaces ranging from 90m² to 1300 m² providing an air temperature from 27°C to 70°C. Regarding their implementation in buildings, air solar collectors were mounted [8, 9, 11, 15]: in the exterior walls (as solar façades or ventilated façades), in the roof (as a ventilated roof) or as individual systems mounted on the roof, facade or on the exterior wall of the building. Another interesting solution involves the use of air solar collectors for heating the air or the heating water required for heat pumps [16,17], in this way the coefficient of performance of the air-to-water heat pumps can be improved. According Ciriminna et al. [13] the main obstacle regarding the implementation of air solar collectors is poor market awareness and difficult access to this type of technology.

According to the literature [11, 18] the most important parameters defining the functioning of TSCs are:

- the pitch of orifices (and absorber plate porosity)
- orifice diameter and geometry
- dimensions of mixing box and air cavity
- absorption coefficient of the absorbent plate
- ambient temperature
- air density
- kinematic viscosity
- thermal conductivity of the air
- solar radiation incident on the solar collector

- air flow and suction speed
- wind speed (lateral or front)
- temperature of the absorbent plate
- temperature of the exhaust air.

A numerical study conducted by Van Decker et al. [19] on a TSC shows that about 62% of the thermal energy is transferred to the air in front of the absorbent plate, 28% in the orifices (so the geometry of orifices has an important role) and about 10% behind the plate. The thermal transfer efficiency decreases as the air velocity increases and the orifices pitch increases. Moreover, the thermal transfer efficiency increases as the wind speed increases and if the absorber plate is thicker.

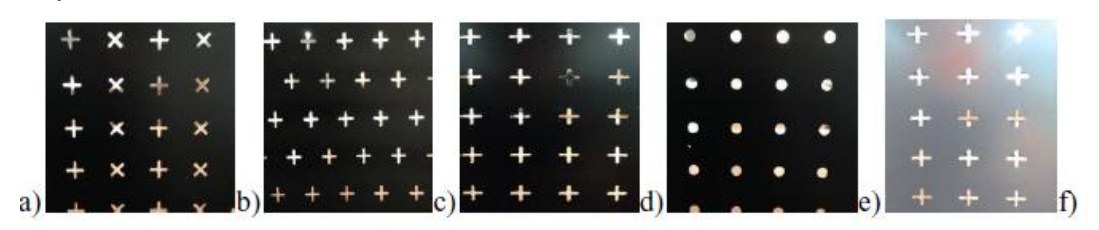


Figure 2 Types of geometries used for the absorbent plate orifices [20]

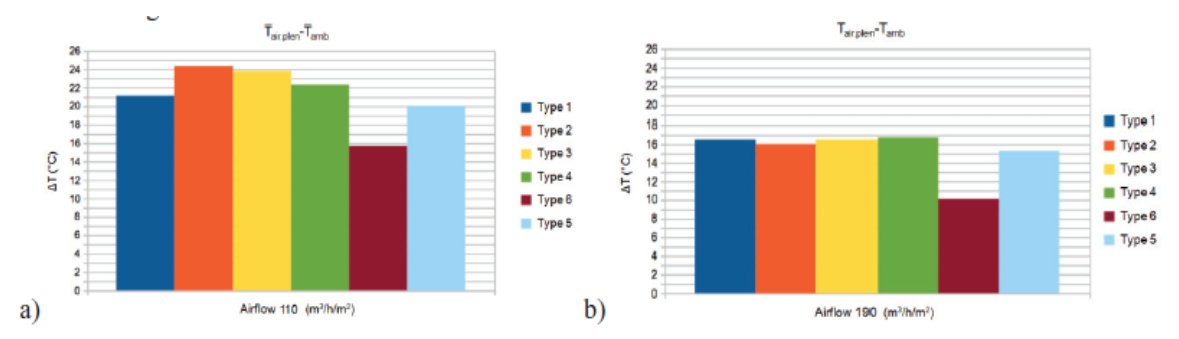


Figure 3 Rise in temperature obtained for the 5 types of geometries at 110  $m^3/h/m^2$  and 190  $m^3/h/m^2$  [20]

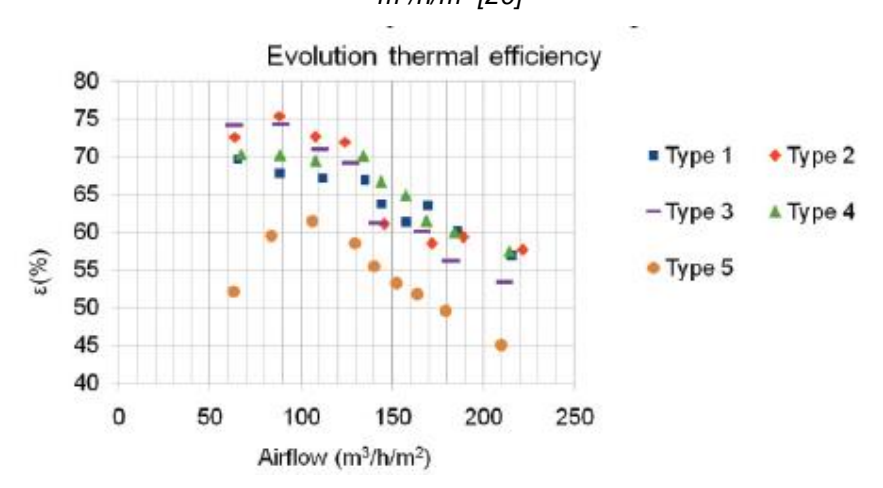


Figure 4 Thermal efficiency of the solar collector depending on the airflow [20]

An opaque solar collector with orifices with high efficiency was propose by Croitoru et al. [4, 20]. The study proposes the use of lobed geometries instead of circular ones used as orifices in classical solar collectors. Figure 2 shows the

types of holes studied and Figures 3 and 4 show the results obtained. The lobed geometries used are 15% more efficient for flows ranging from 80m³/h/m² to 220m³/h/m² and can determine an outlet air temperature higher with up to 2°C. The unconventional shape of the lobed orifices determines a more complex flow that improves heat transfer by approximately 40% [4].

Although for the efficiency of a Trombe wall the thermal mass is essential [21] and the type of thermal energy storage material used is very important, inertial materials are not very often implemented in the case of TSCs. In order to be able to use the solar energy at times when it is necessary, it is very important to store it in inertial systems [22]. According to Navarro et al. [23] systems using solar energy combined with inertial elements are a very good alternative to classical systems and the integration of phase changing materials (PCMs) that store latent heat has a greater impact than the classical materials.

Thermal energy storage materials can be classified depending on the energy storage principle, such as: sensible heat storage, latent heat storage and heat storage from chemical reactions [24]. Among these, latent heat storage methods using Phase Change Materials (PCMs) are among the most promising because they can store 5-14 times more energy than conventional energy storage methods [25, 26]. According to Soares et al. [25], the implementation of PCMs in buildings could bring the following benefits:

- enhance the thermal comfort by: reduce the number of overheating hours, changing the temperature of the surfaces and decreasing the temperature peak values;
- increasing the building envelope performance (increase thermal resistance, thermal capacity increase);
- decreasing the heat and cooling loads by taking over the peak loads (designing HVAC systems with lower capacities)
- reducing energy consumption for cooling and/or heating;;
- reduction of operating costs and CO<sub>2</sub> emissions;
- improving the efficiency of systems using renewable energy sources.

TES materials that can be used to increase the performance of the solar collectors can be classical materials that store sensible heat (stone, brick, concrete, water, granite, sand, earth) or materials that store latent heat [2], like phase changing materials. Conform Goyal et al. [2] by using thermal mass in solar collectors, thermal energy is stored during the day and then discharged during the night, the temperature of the exhaust air reaching up to about 46°C. The same author points out that as the thickness of the thermal mass layer increases, the efficiency of the collector decreases as the material stores and cesses the thermal energy over a longer period of time.

According to Alkilani et al. [8] air solar collectors with embedded inertial materials are one of the most efficient methods of using solar energy and could create a solution that stores energy, integrated into the system (in the absorbent element or a wall) or separate from the system (in storage batteries). When the collector is separated from the system, the heat can be used, for example, directly

for space heating and the surplus can be stored in a "battery" with inertial materials (concrete, PCM, water etc.). If the medium that stores the heat is integrated into the solar collector, the processes of energy absorption, storage and energy release to the air are happening in the same time and when solar radiation is not enough, thermal inertia materials transfer heat to the air, streamlining and prolonging the solar collector number of hours of functioning. When solar energy storage elements are being implemented, the solar energy storage capacity is greatly improved [7].

According to literature studied so far, organic phase change materials (e.g. paraffin) presents a number of advantages and disadvantages that determine their possibility to be implemented in buildings and building integrated systems [24, 25, 27, 28]:

### a) Advantages:

- available in a large range of phase change temperatures (20 –70°C)
- chemically inert
- stable over time (many phase change cycles)
- high latent heat values in case of phase change (120-210 J/g)
- high specific heat values (unlike hydrated sales)
- non-corrosive (only fatty acids are slightly corrosive)
- low cost (especially for commercial paraffin, fatty acids cost about 2-2.5 times higher than paraffin)
- compatible with materials used in construction processes
- small variations of volume during the phase change
- harmless (not toxic or irritating, only certain nonparaffin have a certain degree of toxicity)
- stable below 500 °C
- recyclable

#### b) Disadvantages:

- low thermal conductivity (approximately 0.2 W/mK)
- highly flammable at high temperatures
- not compatible with classic plastic containers.

According to Paloma et al. [29] the most important property of PCMs when implemented in buildings is the thermal energy storage capacity (which must be as high as possible). Also, according to the same author, the phase change temperature, thermal conductivity, density, viscosity, flammability and stability over time are very important. Several researchers have studied and classified the

useful properties of PCM [24, 25, 27, 30-32], the most important criteria governing their selection in order to store thermal energy are:

- a) Thermal and physical properties:
  - phase change temperature according to operating temperatures (e.g. indoor temperatures in a building or working temperature for a solar collector)
  - high thermal conductivity values
  - high specific latent heat storage capacity
  - high density and high specific heat
  - thermal stability over time and stability during phase change
  - small volume variations during phase change
  - low vapour pressure at operating temperature
- b) Kinetic properties:
  - high crystallization rate (full phase change cycle)
  - without overcooling
- c) Chemical properties:
  - complete reversible melting / solidification cycles
  - chemical stability over time and preservation of properties over time after a large number of phase change cycles
  - non-corrosive and compatible with building materials
  - non-toxic, non-flammable, non-explosive
- d) Economical properties:
  - available on the market in large quantities
  - low cost
- e) Environmental impact properties:
  - low value of the embodied energy used in order to produce the material
  - recycling potential (the possibility of being separated from the materials they are embedded in)
  - non-polluting materials.

According to the studied literature, there are several ways in which phase-change materials can be used in buildings [24, 28, 32-35] and the most commonly used methods are micro-encapsulation and macro-encapsulation. According to Iten and Liu [36] in order to choose the proper container for different applications, it is important to know: details about the application and available space, boundary conditions and related materials used. The same authors point out that metal containers are most used in order to increase thermal conductivity (especially

aluminium, copper and steel) and also rectangular containers are most often used due to fast fabrication and high stocking density of the material (up to 90% of total volume). At the same time, they are very easy to install and fit into the available spaces. In addition to geometry and the material used, another important aspect of the metal container with PCMs is its position with respect to the vertical [37] which can have a determining role in the thermal transfer and influences the natural convection inside the cavity created [38]. In the most experimental and numerical studies, the convection phenomenon inside the cavity is neglected.

According to the extensive bibliographic studies analysed [8, 9, 11, 15, 30, 39] the systems with opaque transpired solar collectors and phase changing materials have been studied rarely. Moreover, there have not been identified in the literature any studies regarding the implementation of phase change materials used as an energy storage medium in transpired solar collectors used as an external wall in the building envelope. According to Nkwetta et al. [9] TSCs with integrated PCMs have the potential to reduce energy consumption and store energy in order to use it during the periods when is actually needed. Taking this into account, the present study represents an absolute novelty.

## 1.2. Numerical modelling of solar collectors and phase changing materials

According to the bibliographic study conducted, various types of simulation programs (software) were used for numerical analysis of solar collectors, which are presented in the table below:

Software	Title of study	Reference
TASCflow	A CFD heat transfer analysis of the transpired solar collector under no-wind condition	
	Effect of wind on flow distribution in unglazed transpired plate collectors	
	Flow distribution in unglazed transpired plate solar air heaters of large area	[42]
	Development of a flow distribution and design model for transpired solar collectors	[5]
Retscreen	The performance of first transpired solar collector installation in Turkey	[43]
TRNSYS	Validation of Unglazed Transpired Solar Collector Assisted Air Source Heat Pump Simulation Model	[17]
	Performance analysis of a solar air heating system with latent heat storage in a lightweight building	[44]
Ansys Fluent	PCM thermal storage system for 'free' heating and cooling of buildings	[45]
	Numerical Study of Convective Heat Transfer for Flat Unglazed Transpired Solar Collectors	[46]
	Energy and exergy analyses of Photovoltaic/Thermal flat transpired collectors: Experimental and theoretical study	[47]
	Experimental and two-dimensional numerical simulation of an unglazed transpired solar air collector	[48]

Thermal Performance Analysis of A PCM Combined Solar Chimney [49] System for Natural Ventilation and Heating/Cooling		
	Comparison of modelled heat transfer and fluid dynamics of a flat plate solar air heating collector towards experimental data	[1]
EnergyPlus Glazed building wall as a solar thermal collector [		[22]
Comsol	A Three-Dimensional Modelling of Photovoltaic Thermal Collector	[50]

u

As it can be observed from the table above, in order to study in a numerical manner the transpired solar collectors, many researches used ANSYS Fluent, a CFD software (Computational Fluid Dynamics).

Many researchers have turned their attention to experimental studies on the implementation of phase-change materials in buildings [23, 51-58]. However, in order to choose the proper PCM and a proper geometry for a specific application in a building the numerical approach is mandatory [59] due to the complexity of the phenomena occurring in the melting / solidification process. The problem that arises is due to the non-linear character of the phenomena and the fact that the two phases, solid and liquid, have different thermophysical properties [60].

According to the bibliography studied, the software used for the analysis of phase change materials are: TRNSYS, EnergyPlus, ESP-r, Ansys Fluent, DesignBuilder, Codymur, WUFlplus or Comsol. The table below summarizes the studies made with these softwares.

**Table 2.** Software used for numerical modelling of PCMs

Software	oftware Title of study	
	Development and validation of a new TRNSYS type for the simulation of external building walls containing PCM	Reference [61]
	Modelling and simulation of a phase change material system for improving summer comfort in domestic residence	[62]
TRNSYS	Reducing energy consumption in buildings using phase change material (PCM)	[63]
	Phase Change Material (PCM) composite insulating panel with high thermal efficiency	[64]
	Thermal energy storage in Swedish single family house – a case study	[65]
	Evaluation of Phase Change Materials for Cooling in a Super-Insulated Passive House	[66]
	Cooling load reduction in office buildings of hot-arid climate, combining phase change materials and night purge ventilation	[67]
EnergyPlus	Economic impact of integrating PCM as passive system in buildings using Fanger comfort model	[68]
EllergyFlus	Verification and validation of EnergyPlus phase change material model for opaque wall assemblies	[69]
	PCM thermal energy storage in buildings: experimental study and applications	[70]
	The energy saving and indoor comfort improvements with latent thermal energy storage in building retrofits in Canada	[71]
ESP-r	Computational Optimization of Passive use of Phase	[72]

Change Materials in Lightweight Low-Energy Houses			
Ansys Fluent	PCM thermal storage system for 'free' heating and cooling of buildings	[45]	
Alisys Fluelit	Performance analysis of a solar air heating system with latent heat storage in a lightweight building	[44]	
	Simulation of Melting Process of a Phase Change Material (PCM) using ANSYS (Fluent)	[73]	
DesignBuilder	The Implementation of Phase Changing Materials in Energy-efficient Buildings. Case Study: EFdeN Project	[74]	
Designbunder	Comparison of different PCMs impact on indoor comfort in an energy positive house	[75]	
Codymur	Optimization of a phase change material wallboard for building use	[76]	
WHEIphia	PCM Application-Effect on Energy Use and IA Temperature	[77]	
WUFIplus	Analysis of simulation models of PCM in buildings under latvia's climate conditions	[78]	
Comsol	Application of Phase Change Materials in Gypsum Boards to Meet Building Energy Conservation Goals	[79]	

As can be seen in the table above, software such as Energyplus, ESP-r, TRNSYS or DesignBuilder were used in order to analyse the effect of PCMs implementation in buildings (generally in passive systems). However, in order to analyse the small-scale effect, in a wall, construction element or an active system, software such as Comsol, Ansys Fluent, TRNSYS, Codymur were used.

Therefore, according to the above mentioned arguments, I have decided to use the ANSYS Fluent CFD Numerical Simulation Software in order to study solar air collectors with integrated phase change materials. CFDs are based on the fundamental equations governing fluid dynamics: the continuity equation, the energy conservation equation and the impulse conservation equation. Because the results of Navier-Stokes equations cannot be solved analytically, the CFD software tries to find an approximate solution by spatial meshing methods that convert partial-derivative equations into algebraic equations (calculations are iterative).

The steps of a CFD numerical simulation that were followed in the present paper are:

- a) Creating the geometry of the model
- b) Creating the calculation grid mesh independency study
- c) Imposing boundary conditions and configuring the numerical case
- d) Validating the numerical model by comparing the numerical results with the experimental ones
- e) Calculation of the solution and post processing

All these stages will be detailed and presented extensively in the following chapters.

### 1.3. Conclusions and perspectives

In recent years, there has been an upward trend in the implementation of PCMs in buildings and more and more researchers are interested on their impact on energy efficiency and thermal comfort in buildings.

According to Arkar et al. [44] PCMs have the advantage of storing a great amount of energy with a very low temperature variation, at temperatures close to those that define indoor thermal comfort. According to the literature studied [15, 25, 30, 60, 80-82] it can be noticed that PCMs can be part of passive or active strategies to reduce energy consumption and improve thermal comfort in buildings, with remarkable results.

According to the literature, there are few experimental and numerical studies on the implementation of inertial materials in opaque solar collectors and no studies regarding the use of PCMs in transpired solar collectors have been identified so far.

As discussed in the previous chapter, PCMs can be implemented in solar collectors thus increasing their efficiency and contributing to space heating or preheating of fresh air introduced into the rooms. Moreover, the implementation of inertial materials in solar collectors has the potential to increase their overall efficiency by discharging the accumulated energy and by storing thermal energy during periods when solar radiation is available and use it when the radiation is not available (cloudy or night periods). In addition, because of the energy storage, the collectors' outlet air temperature during the day is lower, thus improving the thermal comfort inside. According to the studied literature, the PCMs were integrated into glazed solar collectors and especially in Trombe walls, but also in opaque collectors. However, it can be observed that the use of PCM in perforated solar collectors is analysed by very few studies.

Regarding the numerical studies, according to the studied literature it can be noticed that many researchers have opted for the ANSYS Fluent numerical simulation software, both for studying the airflow inside the air solar collector and for studying the implementation of phase change materials in different applications. That's why we decided to use this software in the present doctoral studies. The approach of numerical simulations is extensively addressed in the following chapters.

# 2. The real collector geometry and results of experimental studies - synthesis

### 2.1. Geometry and materials

In the previous two research reports from the doctoral studies we have extensively presented the bibliographic study justifying the hypotheses made, as well as the preliminary experimental study which was further continued and developed. In order to understand the geometrical modelling and the results of the numerical study, it is necessary to present the construction of the real solar collector studied synthetically.

Figure 5 shows the geometry of the transpired solar collector. Its dimensions are 2140x1140mm and the metal absorbent plate with lobed orifices is 2000x1020mm.

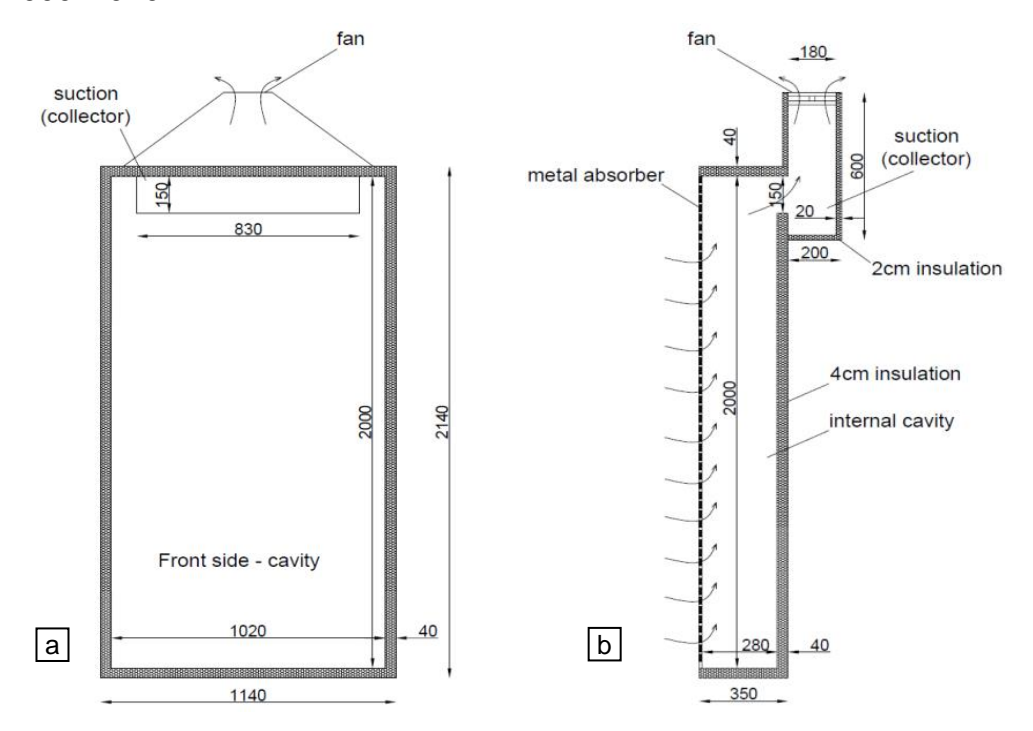


Figure 5 The geometry of the solar collector: a – front view b – section

After the air is sucked through the lobed orifices and the heat is transferred from the absorbent plate to it, the air enters the cavity and follows a downward trajectory due to the phase change materials obstacle (Fig. 6). The obstacle is made of rectangular aluminium containers glued together, with macroencapsulated phase change materials inside. Aluminium has been used in order to increase thermal conductivity and the rectangular shape respects the requirements of the experimental setup. The PCM used is RT35 with a phase change temperature of 35 °C and was chosen to meet the average working temperature in the collector cavity. The total amount of PCMs integrated in the rectangular aluminium containers located in the TSC is up to 28kg. In addition to the eight K-type sensors (precision  $\pm$  0.2 °C) shown in Figure 6, three other sensors were used: one measuring the ambient air temperature, one measuring the temperature on the surface of the PCM bars (reflecting the temperature of

PCMs) and one positioned at 5 cm of the absorbent metal plate (10 equivalent diameters of an orifice).

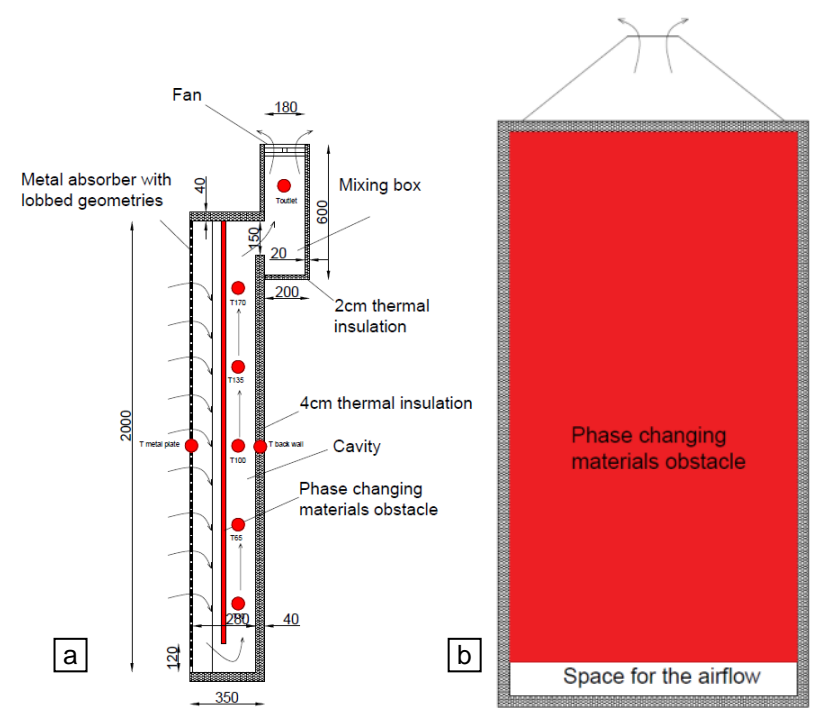


Figure 6 Geometry of solar collector: a – sensors positioning, b – PCM layer position



Figure 7 Solar collector geometry: a – absorbent metal plate, b – suction grille for the air inside the collector cavity, c – mixing box, d – collector backwall, e – medal framework for the PCM layer

Figure 7 shows the components of the solar collector and Figure 8 shows the air solar collector with its real geometry. The solar collector walls are made of OSB and 4cm of thermal insulation. The air is circulated via an axial fan resulting an airflow rate of 400m³/h. The solar radiation was simulated by means of 8 halogen lamps of 500W each. Experimental studies were performed under laboratory conditions, on a permanent regime and the results are presented below.

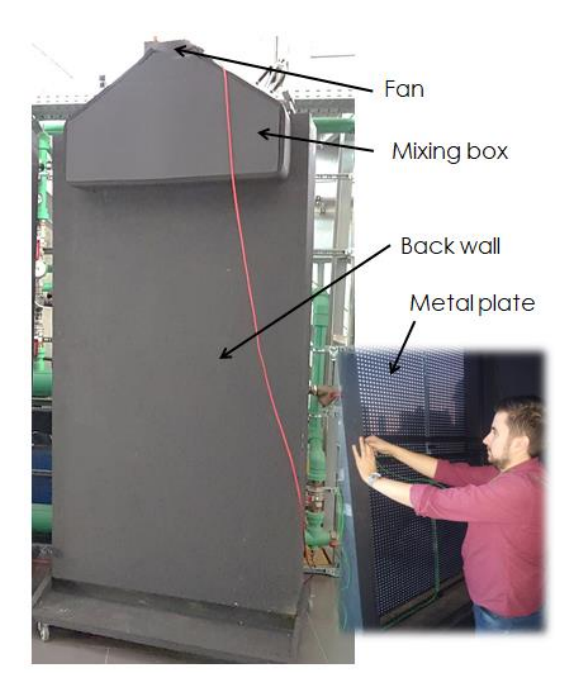


Figure 8 Experimental setup

### 2.2. Results in permanent regime

In the present chapter the experimental results obtained in a permanent regime that will be used for validation of the numerical model are briefly presented. More experimental results useful in order to validate the numerical model are presented in the following chapters.

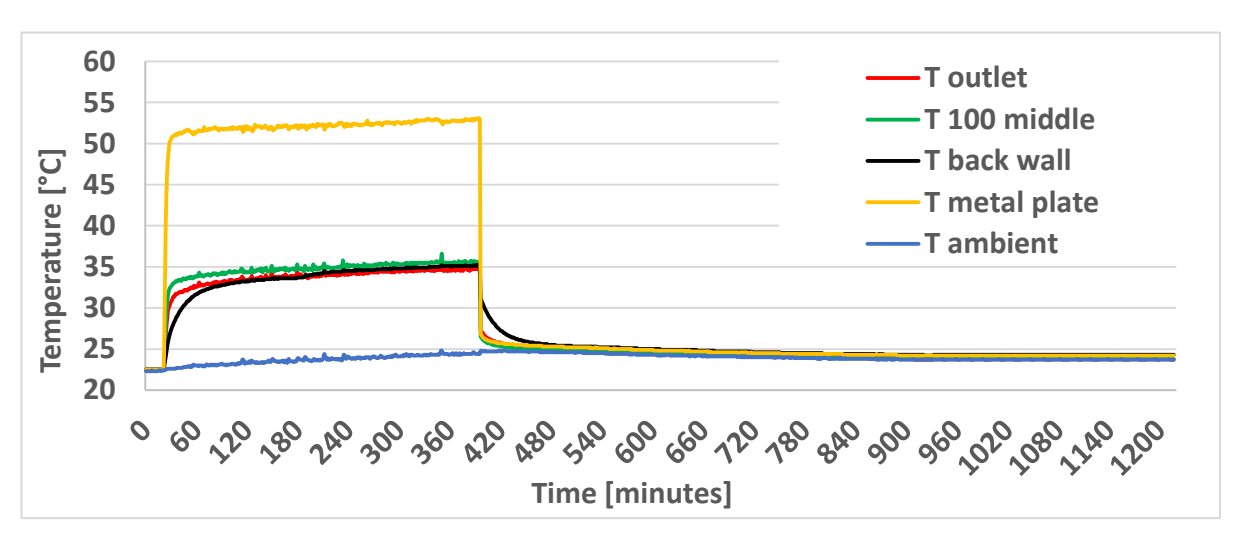


Figure 9 Temperature variation in the case of TSC without PCM

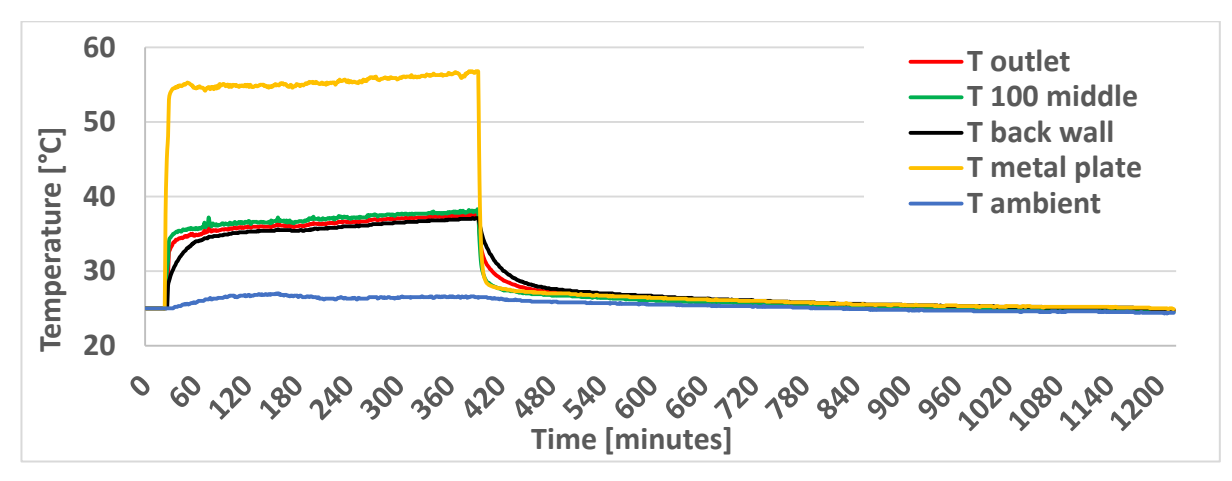


Figure 10 Temperature variation in the case of TSC with PCM

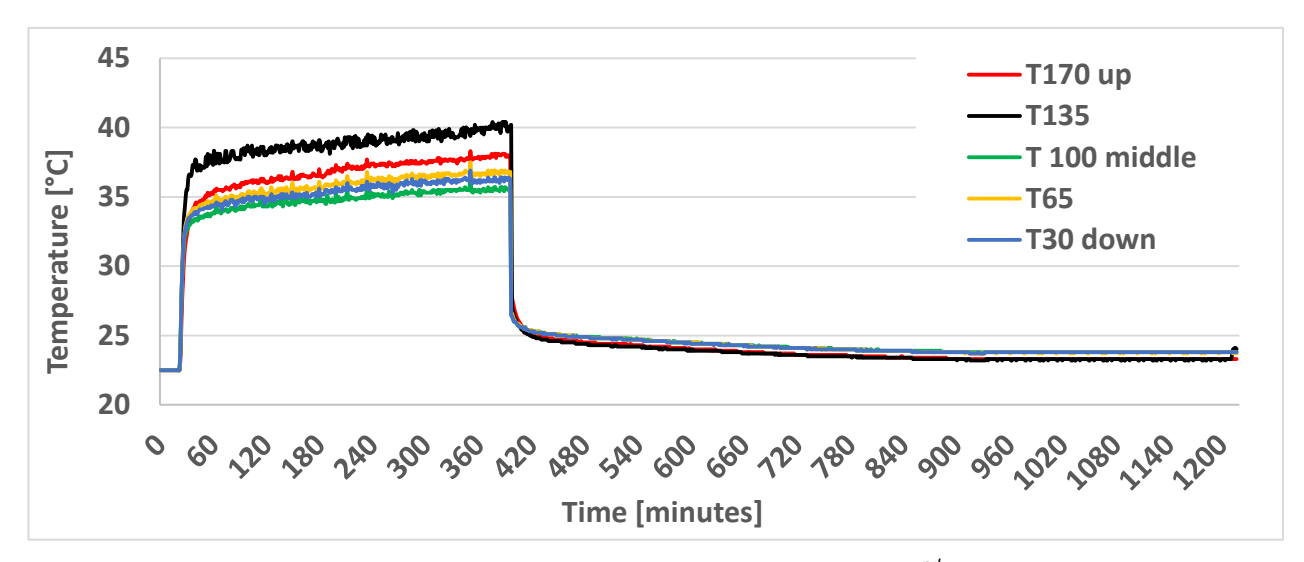


Figure 11 Thermal stratification in the solar collector 2<sup>nd</sup> cavity without PCM

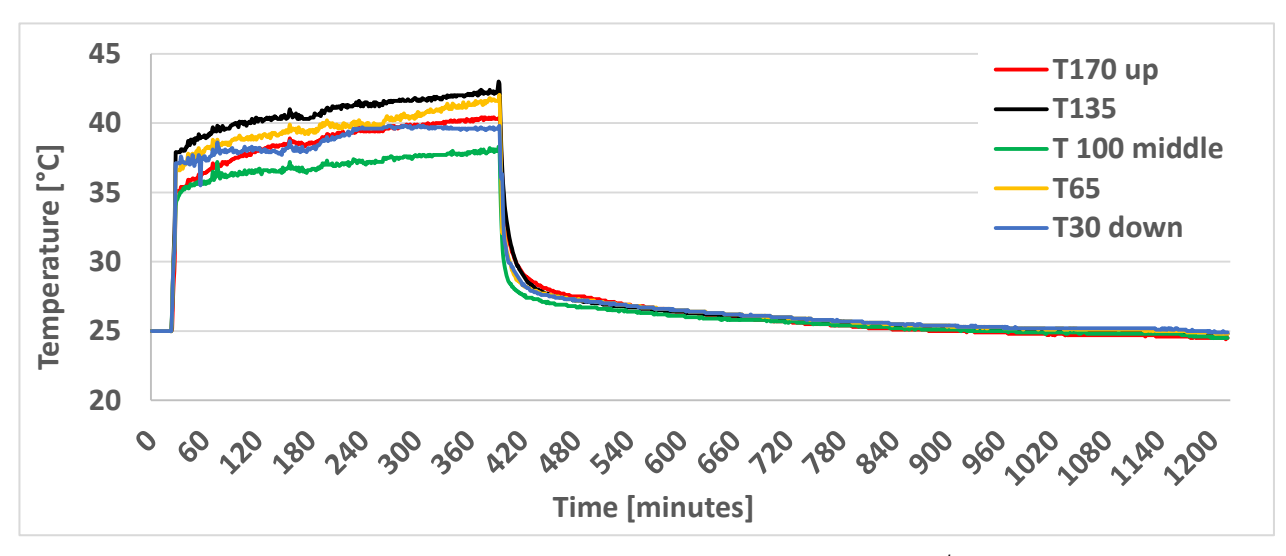


Figure 12 Thermal stratification in the solar collector 2<sup>nd</sup> cavity with PCM

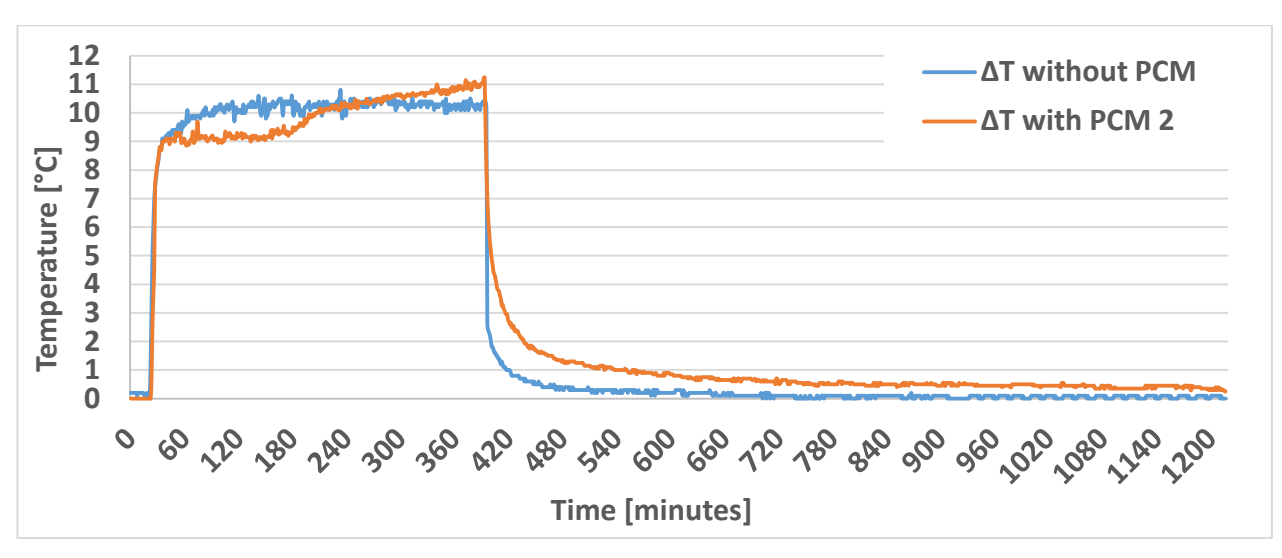


Figure 13 Rise in temperature (difference between air temperature on the outlet and ambient air temperature) with and without PCMs

Figure 9 shows the temperature variation in the case of the solar collector without PCMs and Figure 10 shows the temperature variation in the case of the collector with PCMs. It can be noticed that during the period when solar radiation is available, PCM stores the energy and when the radiation is no longer available, they begin to transfer the heat to the airflow conveyed into the solar collector cavity, having the potential to increase its overall efficiency and increase the number of hours of operation. Figurer 11 and figure 12 show the thermal stratifications inside the solar collector in the second cavity (after the air passes bellow the PCM obstacle).

The most important conclusions of the experimental studies conducts so far are the following:

- In the case of air solar collector without PCM the maximum rise in temperature is  $\Delta T = 10.2^{\circ}C$
- In the case of air solar collector with PCM the maximum rise in temperature is  $\Delta T = 11.2^{\circ}C$ , with 8.8% more
- After the solar radiation is no longer available the rise in temperature is higher up to 800 minutes in case of using PCMs
- The melting process is obvious during 180 minutes
- The maximum heating capacity reached is 0.75 kW/m<sup>2</sup>
- The maximum thermal transfer efficiency achieved is up to 38%.

### 3. The objectives of the numerical study and the infrastructure used

According to the bibliographic study conducted, the implementation of phase change materials in transpired air solar collectors has not been studied so far. The goal of the following numerical studies presented is to create a numerical model that can accurately simulate the airflow through the solar collector with PCMs and the transfer phenomena that take place inside it. With respect to these objectives, the numerical model designing involves two important stages:

- a) Numerical modelling of the airflow through the lobed orifices (absorbent metal plate)
- b) Designing the numerical model of the TSC with integrated PCMs

Chapters 4 and 5 deal with the two steps outlined above. Numerical modelling of the airflow through the lobed holes aims to accurately capture the phenomena that occur in the orifice and after it, and to analyse the impact of the geometry of the orifices on the solar collector. Simulating the solar collector to its real size would require a very long calculation time due to a very large number of mesh cells, a period of time that would be virtually impossible to complete the studies (and it would also require a high performance computing). The temperature and speed profiles obtained from the first study will be integrated into the numerical model of the solar collector with PCMs.

Numerical simulation software CFD ANSYS Fluent 15.0 and all its components: ANSYS DesignModeler, ANSYS Workbench and ANSYS Mesher were used to carry out the numerical study. Tecplot 360, Notepad and Microsoft Excel were used for data processing and the C ++ programming language was used to perform the transient variation functions for some input parameters (UDF = User Defined Functions). Moreover, two computing stations which are in the endowment of Faculty of Building Service Engineering laboratories were used:

- 1) Laptop used in the 1<sup>st</sup> part of the studies (with limited performances)
  - Processor: Intel Core i7 6500 2.5Ghz, 4 processors
  - 12 GB RAM
- 2) Computing station used in complex numerical simulation which require a higher computing power
  - Processor: Intel Xeon 3.4Ghz, 16 processors
  - **128 GB RAM**

# 4. Numerical modelling of the airflow through the lobed orifices (absorbent metal plate)

### 4.1 Creating the geometrical model

In order to be able to perform the numerical modelling of the solar collector with lobed perforations with integrated PCMs in a feasible period of time, we have simplified as much as possible the geometry of the absorber plate that is part of the solar collector, starting from the premise of the thermal transfer phenomena symmetry and velocity fields symmetry. As it could be observed from the literature, the shape of the orifices considerably influences the efficiency of the solar collector [4, 20], it can improve thermal transfer and can cause a higher air temperature in the collector cavity. The unconventional lobed geometry of the absorbent plate orifices determines complex airflows thus improving the heat transfer and according to the literature is the geometry that helps to obtain the greatest rise in temperature between the ambient air (inlet) and the exhaust air (outlet). The orifices layout in the case shown in Figure 14 is also the most efficient solution for large values of the airflow. Taking into account all these arguments, I decided to consider the effect of orifices on the solar collector flow and efficiency. Moreover, this approach will create future premise of studies regarding the orifices influence on the PCMs integration.

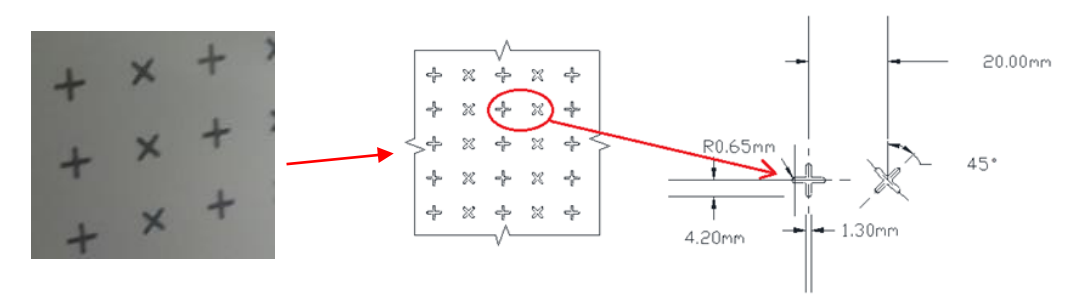


Figure 14 Lobed orifices layout and geometry with equivalent diameter of 5mm (De=5mm)

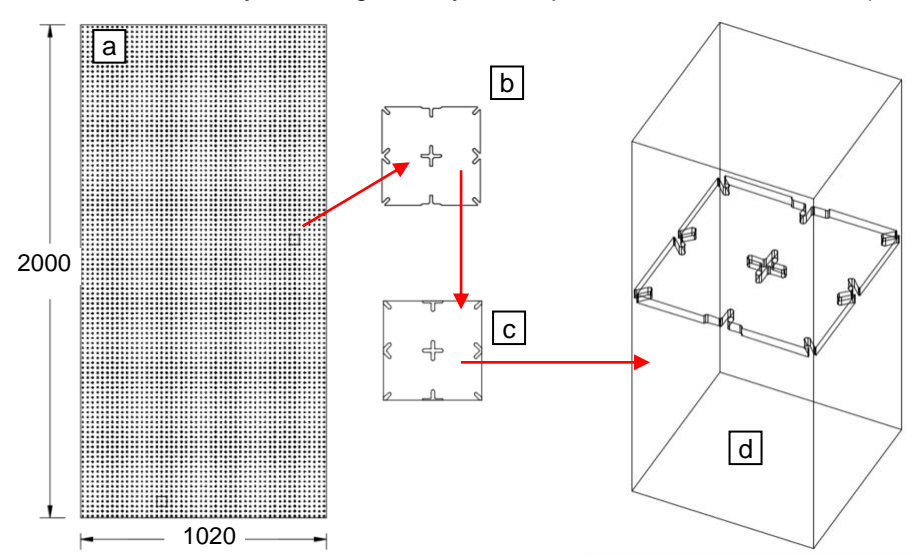


Figure 15 Designing the 3D model in AutoCAD: a – absorbent metal plate with lobed orifices, b – extraction of a 4x4cm part, c – embedment in the computing domain, d –3D computing domain (4x4cm plate surrounded by a parallelepiped)

Figure 14 shows the layout and geometry of the lobed holes. The orifices are alternately positioned horizontally (+, x, +, x, +... etc.) at a pitch of 20 mm and with an equivalent diameter of 5mm.

As can be observed in Figure 15a, the absorbent plate with a surface area of approximately 2m<sup>2</sup> and a thickness of 2mm has a large number of lobed orifices on its entire area (5000 holes). Modelling the entire absorbent plate with lobed holes would require a complex mesh and a large number of mesh cells in the computing domain in order to accurately capture the phenomena that occur near the orifices. This would lead to a very long time necessary in order to carry out the numerical studies. Taking into account airflow symmetry and transfer phenomena symmetry we selected a 4x4cm metal plate containing 4 equivalent orifices for the present study (Figure 15b).

The 4x4cm extracted metal plate was then enclosed in a 9.2x4x4cm parallelepiped that will represent the airflow in the computing domain, with respect to the flow direction (Figure 15c and 15d). The plate is positioned at 4cm distance from the computing domain limit (inlet - upstream) and at 5cm distance from the outlet (downstream) which represents ten equivalent equivalents (10De=5cm). From the experimental studies carried out at the Faculty of Building Services Engineering we noticed that after 10De, in the case of lobed orifices the airflow and velocity profiles are stabilizing. The velocity fields thus obtained at a distance of 5cm from the metal plate will then be used (introduced as boundary limits on the inlet) into the simplified numerical model of the solar collector.

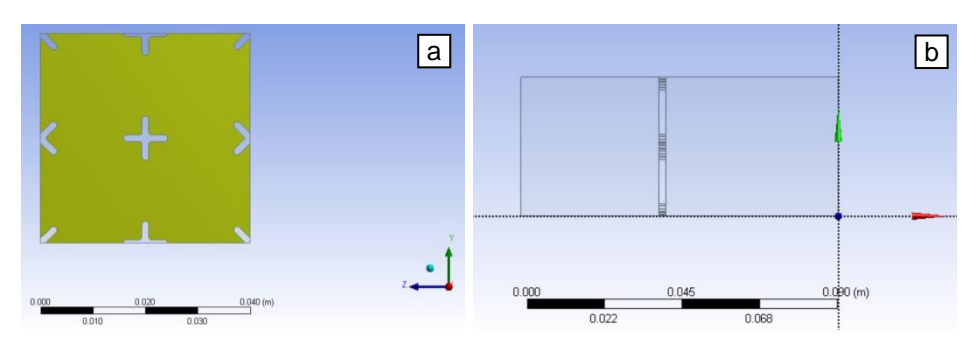


Figure 16 Importing the geometry from AutoCAD to ANSYS DesignModeler: a –4x4cm metal plate, b – computing domain and its geometry

The 3D geometry was designed in AutoCAD and converted in .igs format that can be imported in ANSYS DesignModeler (Figure 16 and Figure 17).

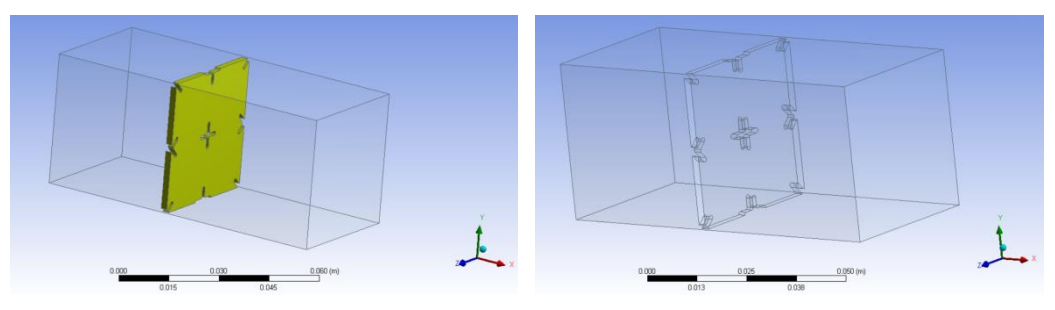


Figure 17 Importing the geometry from AutoCAD to ANSYS DesignModeler – isometric view

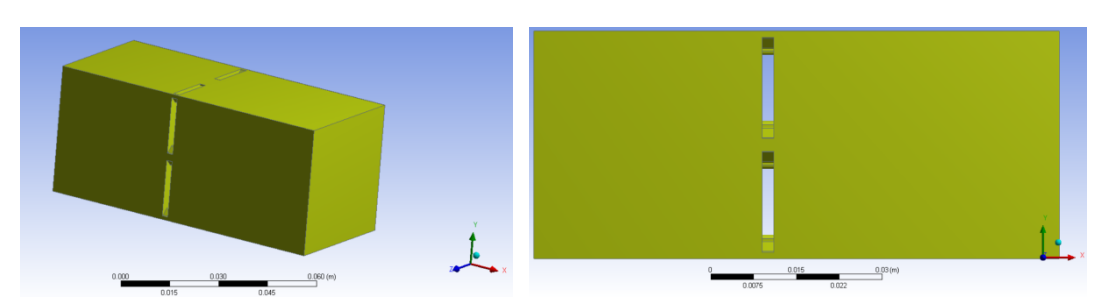


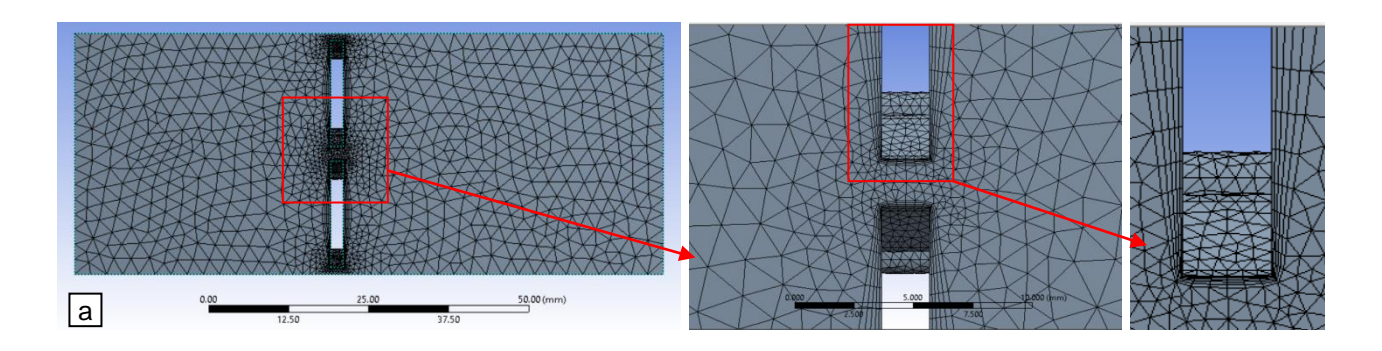
Figure 18 Extracting the 4x4cm metal plate from the computing domain (airflow)

Taking into account that the 2 mm thick metal plate is made of aluminium which has high thermal conductivity, the heat transfer is very fast thus resulting a relatively uniform temperature across the surface. The internal transfer phenomena are not very complex and do not influence the result of the simulation. Therefore, the 4x4cm metal plate was extracted from the computing domain, leaving only the air circulated (Figure 18).

After the geometry of the model was created and proper surfaces were named, it was imported into ANSYS Meshing in order to achieve spatial meshing.

### 4.2 Creating the mesh (mesh independency study)

After building the geometry, the next step in creating the numerical model is the choice of the optimum mesh. In order to determine the number of computing elements (cells) useful to solve the problem, it is necessary to make a solution independency study based on the quality of the mesh or mesh independency study. The study aims to achieve a correct numerical result, but the accuracy of the results is directly related to the number of cells (more cells = more accurate result). Furthermore, if the number of cells is higher, the calculation time becomes higher and the necessary computing resources will also increase. The mesh independency study begins by choosing multiple levels of meshing with more and more cells. From a certain number of cells up, the results obtained vary insignificantly, this computational grid representing the optimal solution regarding the result-computing ratio.



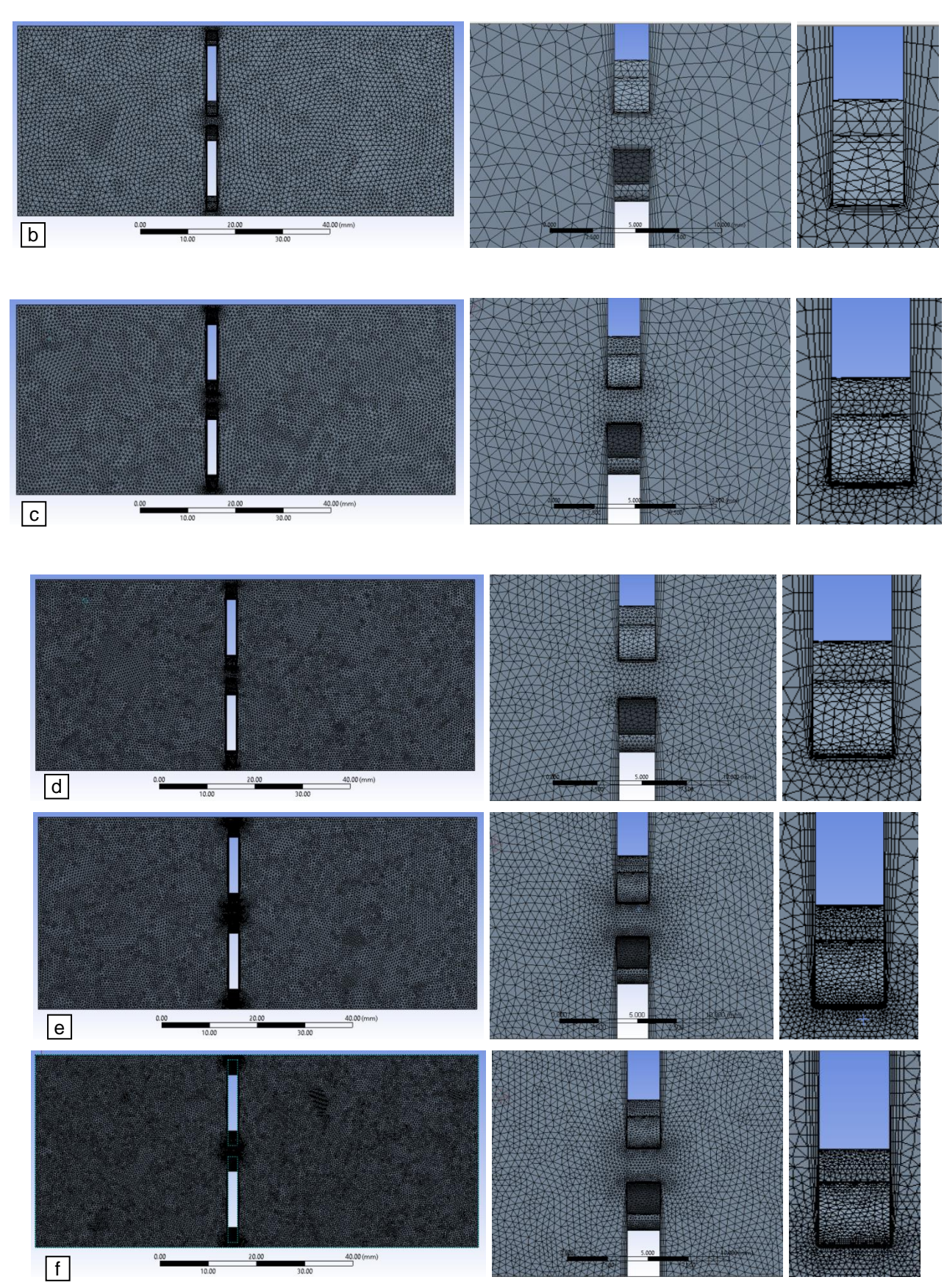


Figure 19 Different mesh levels for six different cases analysed: overview, orifice detail and boundary detail for a) 0.2, b) 0.62, c) 1.5, d) 3, e) 5.3, f) 7.3 million elements

In order to conduct the mesh independency study I have chosen 6 levels of meshing (Figure 19), respectively: 0.2, 0.62, 1.5, 3, 5.3 and 7.3 million tetrahedral computing elements. The optimum meshing level will be chosen by conducting individual numerical simulations, using similar boundary conditions and cases.

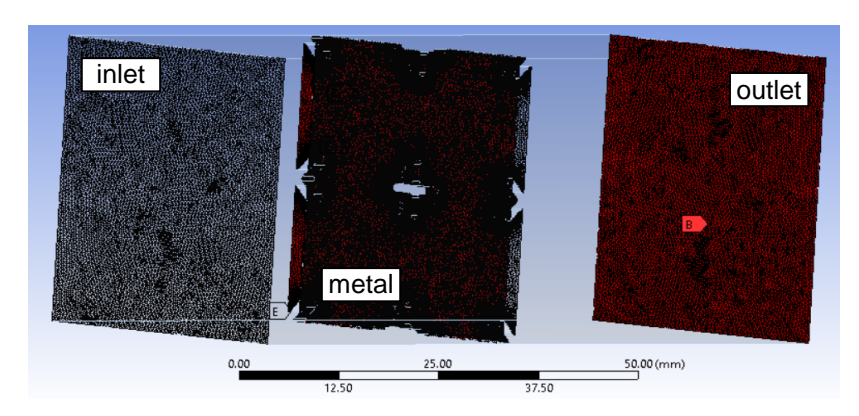


Figure 20 Computing grid for 3 zones: inlet (the computing domain limit corresponding to the inlet of the ambient air), metal (the boundary of the metal absorber) and outlet (the computing domain limit corresponding to the outlet at 10De distance from the metal plate)

**Table 3.** Boundary conditions used in the mesh independency study

Boundary limit	Value	Unit
Average velocity at the computing domain limit (velocity inlet)	0.05555	m/s
Inlet temperature (inlet)	25	°C
Metal plate temperature (metal)	50	°C

The six meshing levels were sequentially imported into ANSYS Fluent and for each I imposed the same boundary conditions as presented in Table 3. The air velocity (in the inlet area) is 0.05555 m/s corresponding to the nominal airflow rate of 400m<sup>3</sup>/h for the entire collector (according to the equations below), the inlet air temperature is 25°C and the metal plate temperature is 5 °C (corresponding to a solar radiation value of approximately 530 W/m<sup>2</sup>).

$$Q = 400 \frac{m^3}{h} = 0.1111 \frac{m^3}{s}$$

$$N_o = 5000$$

$$Q_o = \frac{Q}{N_o} = \frac{0.1111}{5000} = 0.00002222 \frac{m^3}{s}$$

$$S_o = \frac{\pi \cdot D_e^2}{4} = \frac{\pi \cdot 0.005^2}{4} = 0.000019635 m^2$$

$$v_o = \frac{Q_o}{S_o} = \frac{0.00002222 \frac{m^3}{s}}{0.000019635 m^2} = 1.312 \frac{m}{s}$$

$$Q_{4x4} = (0.00002222) \cdot 4 = 0.00008888 \frac{m^3}{s}$$

$$S_{4x4} = 0.04 \cdot 0.04 = 0.0016m^2$$

$$v_{4x4} = 0.00008888 \div 0.0016 = 0.05555 \frac{m}{s}$$

, where:

Q = airflow value for the entire collector

Q<sub>o</sub> = airflow value for in the orifice

 $N_o$  = number of orifices

 $Q_{4x4}$  = airflow value for the metal plate (4x4cm);

 $S_0$  = orifice surface

 $S_{4x4}$  = metal plate surface, with its 4 equivalent orifices (4x4cm);

Vo = velocity in the orifice

 $v_{4x4}$  = inlet air velocity.

Regarding the turbulence model I chose the k-ε RNG model (with Enhanced Wall Function - EWF) which is suitable, according to the literature studied [83], in the cases with swirling flows and in the case of flows with small Reynolds numbers (Re≈422 in the present study according to the equations below - laminar flow). Although experienced CFD researchers recommend the analysis of multiple combinations of meshing levels and turbulence models [84], the reduced time available for the present study didn't allowed us to compare several models of turbulence in this case. With respect to the above presented arguments, I performed several numerical simulations for the 6 computational grids chosen, the results being imported into Tecplot software and analysed further.

$$Re = \frac{\rho_{aer} \cdot v_o \cdot De}{\mu_{aer}}$$
 
$$Re = \frac{1.185 \cdot 1.312 \cdot 0.005}{0.0000184} = 422$$

, where;

 $\rho_{aer}$  = air density at 25 °C = 1.185 kg/m<sup>3</sup>;

D<sub>e</sub> = lobed orifice equivalent diameter

 $\mu_{aer}$  = dynamic viscosity = 0.0000184 kg/m·s.

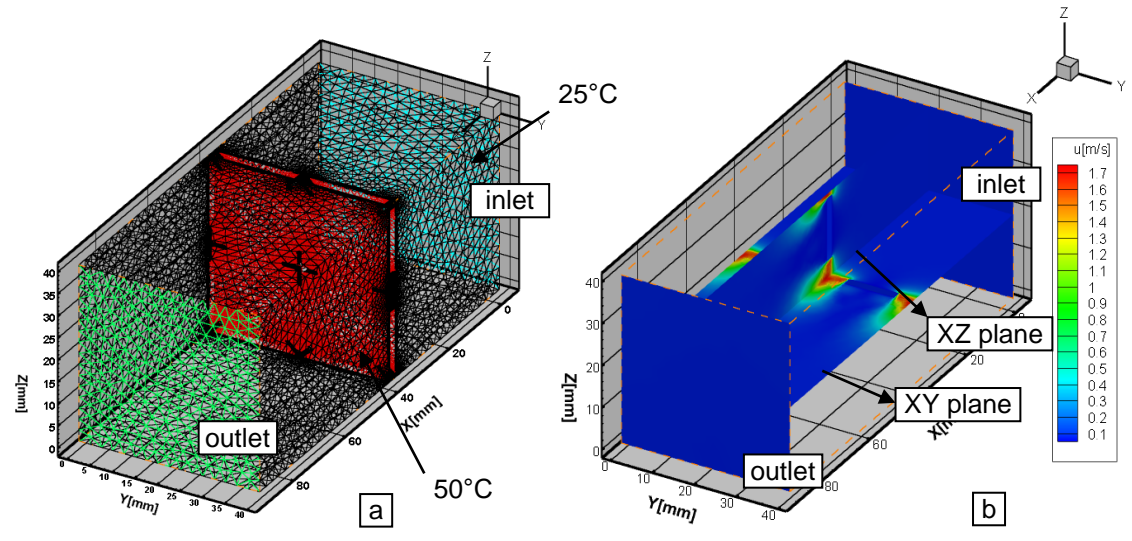
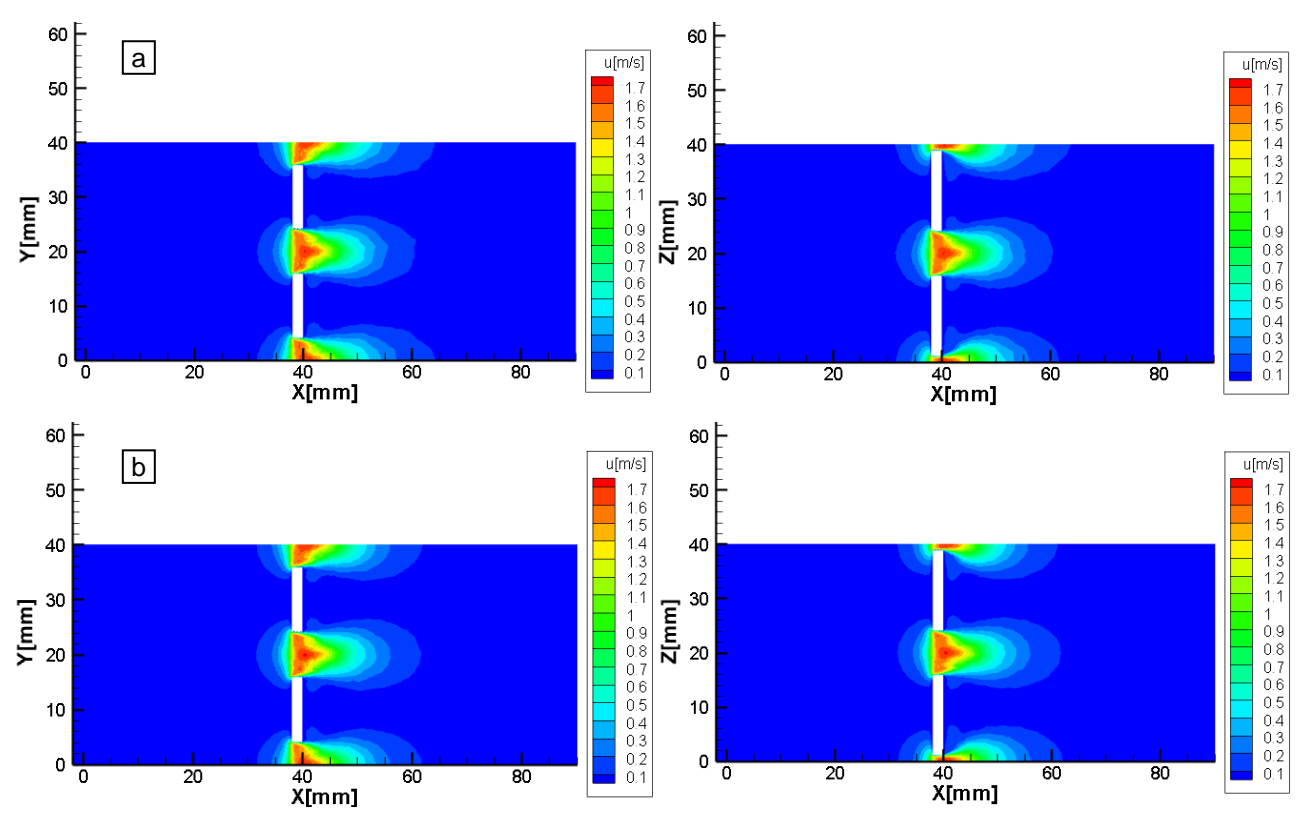
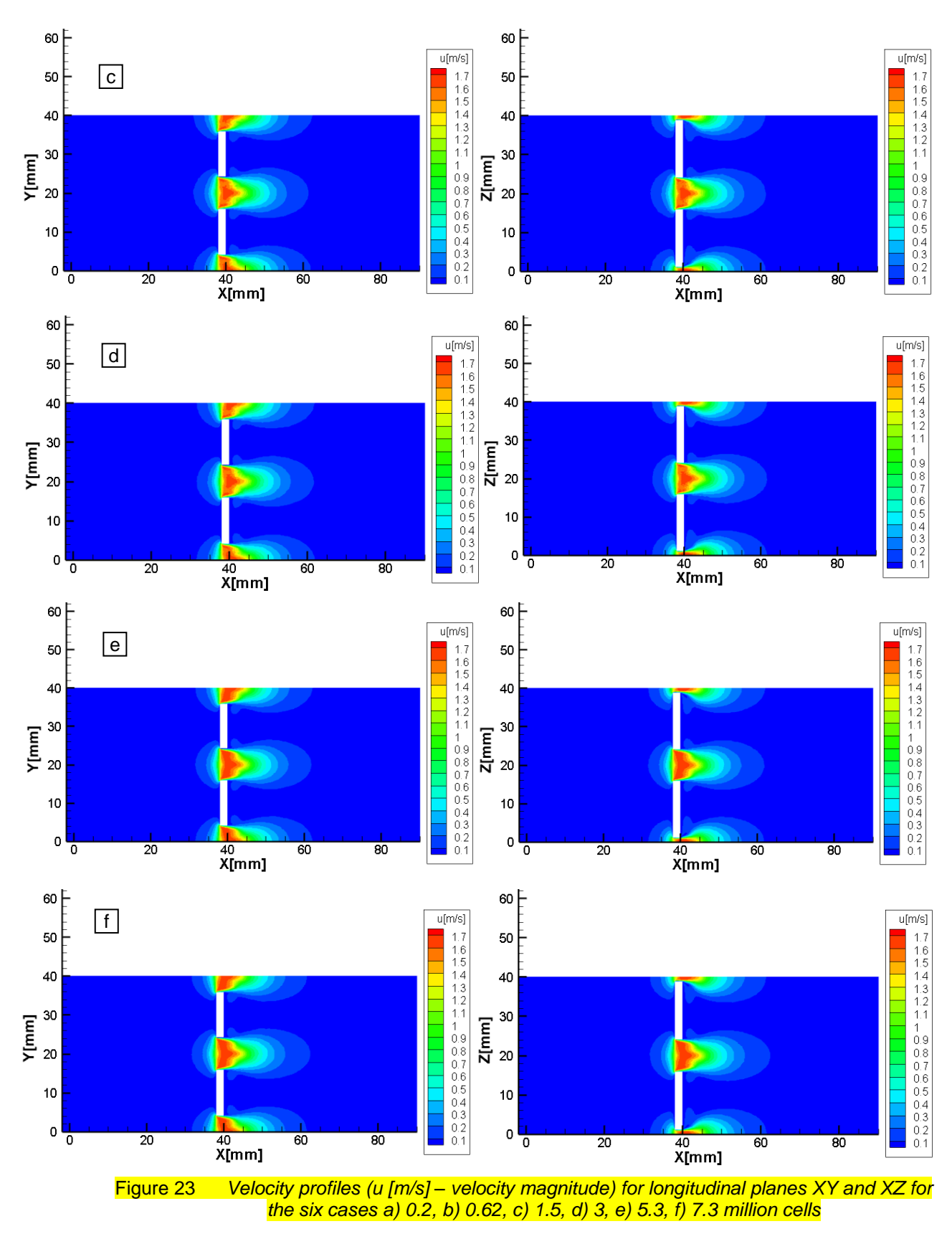


Figure 21 Importing results in Tecplot 360 in order to be properly processed

Figure 22

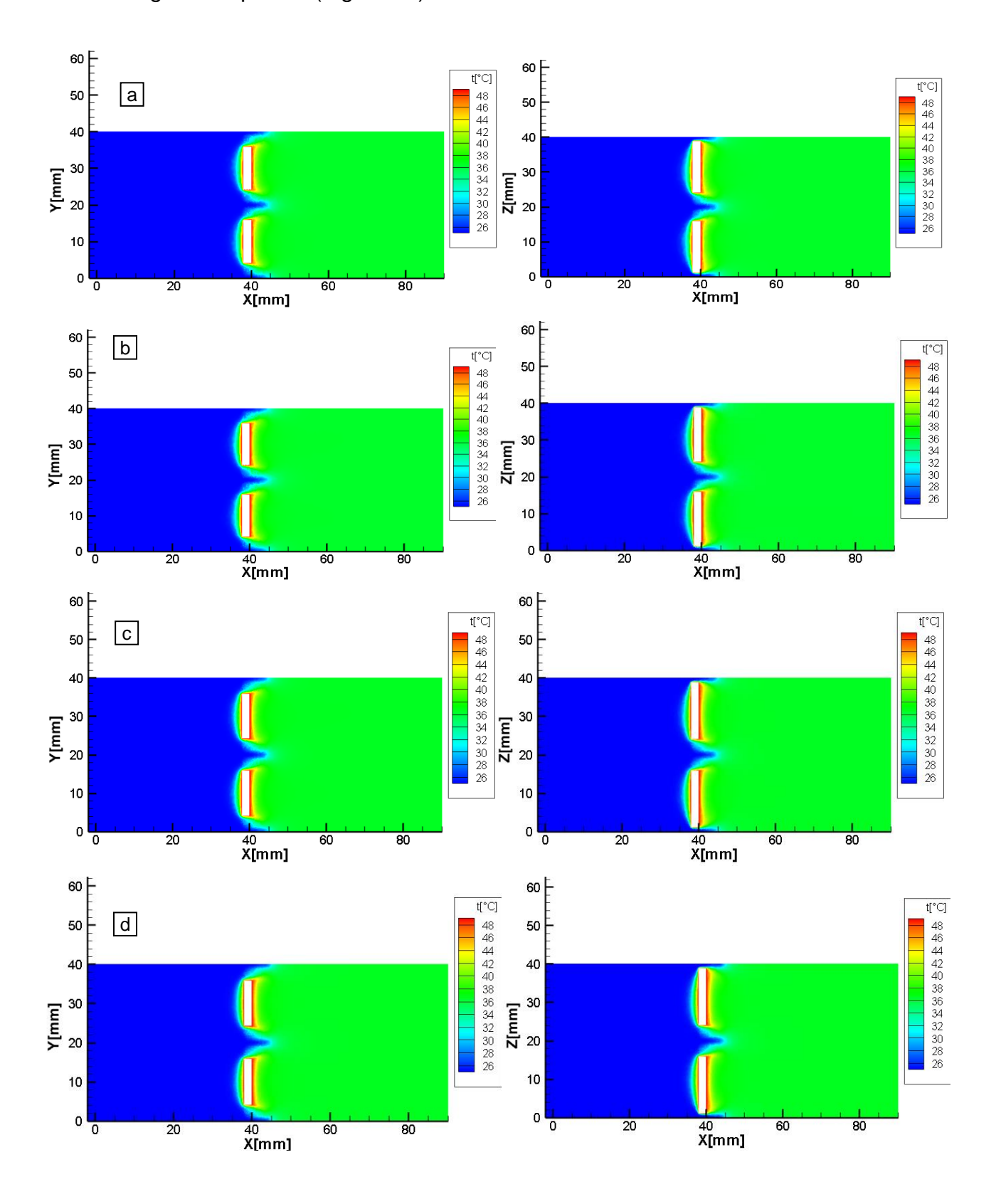
Figure 21 presents the results imported into the Tecplot data processing software. Figure 21a shows the cell distribution for one of the six cases and Figure 21b shows the velocity magnitude distribution in two longitudinal planes: XY and XZ. Further, the velocity profiles for the two planes will be analysed for each of the 6 cases mentioned above.





As it can be observed in Figure 23, the velocity profiles on XY and XZ planes are relatively similar for all 6 cases without important differences. Taking

into account these results we will analyse the temperature distribution in the same longitudinal planes (Figure 54).



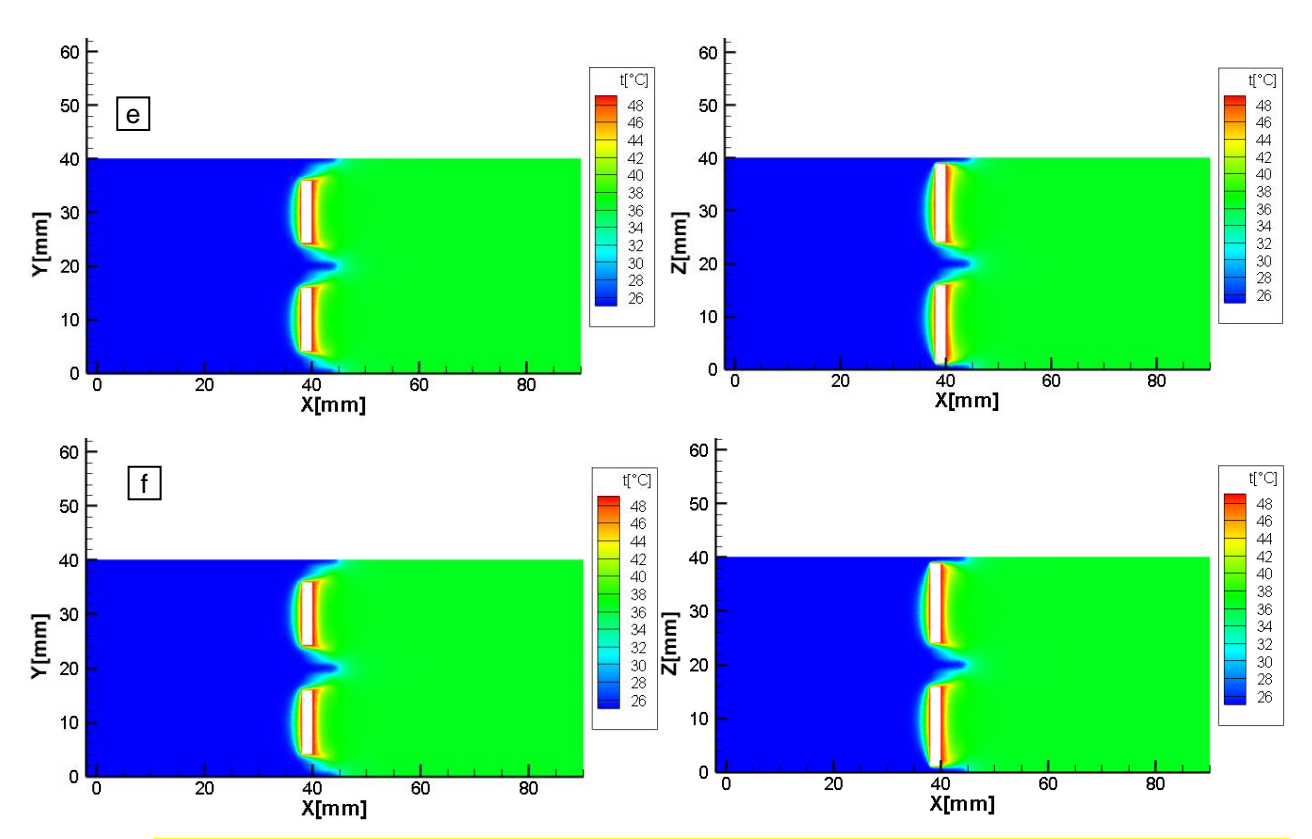


Figure 24 Temperature profiles in the longitudinal planes XY and XZ for the 6 cases a) 0.2, b) 0.62, c) 1.5, d) 3, e) 5.3, f) 7.3 million elements

As it can be noticed from Figure 24, the temperature profiles in the XY and XZ longitudinal planes are similar in all the 6 cases and we cannot precisely determine the optimal solution for the spatial meshing. Taking into account these results, we will further analyse the velocity profiles at 5De distance from the metal plate and 10De distance from the metal plate in transverse planes. In the present study, the 10De velocity profiles are the most relevant to the numerical model.

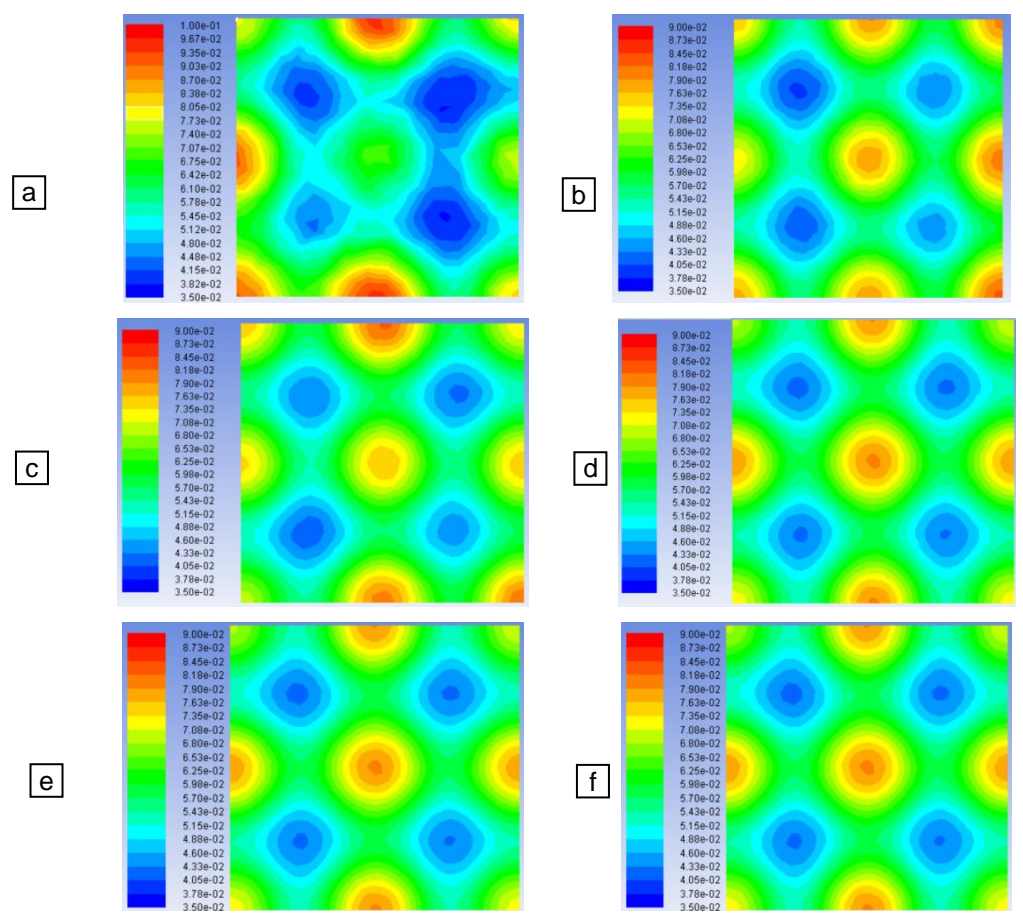


Figure 25 Velocity profiles (u [m/s] – velocity magnitude) in transverse plane at distance 5De (2.5cm) from the metal plate in all the six cases analysed: a) 0.2, b) 0.62, c) 1.5, d) 3, e) 5.3, f) 7.3 million elements

Figure 25 shows the velocity fields at 5De distance from the metal plate for all six cases analysed. It can be noticed that starting with 3 million elements, there are no significant variations regarding the velocity fields. Moreover, Figure 26 shows the velocity profiles at 10De distance from the metal plate for all six cases. It can be observed that at 0.2, 0.62 and 1.5 million elements the profiles resulted are uneven. Beginning with 3 million and even 5.3 million elements no visible variation of the velocity profiles is observed and these are becoming more and more stable.

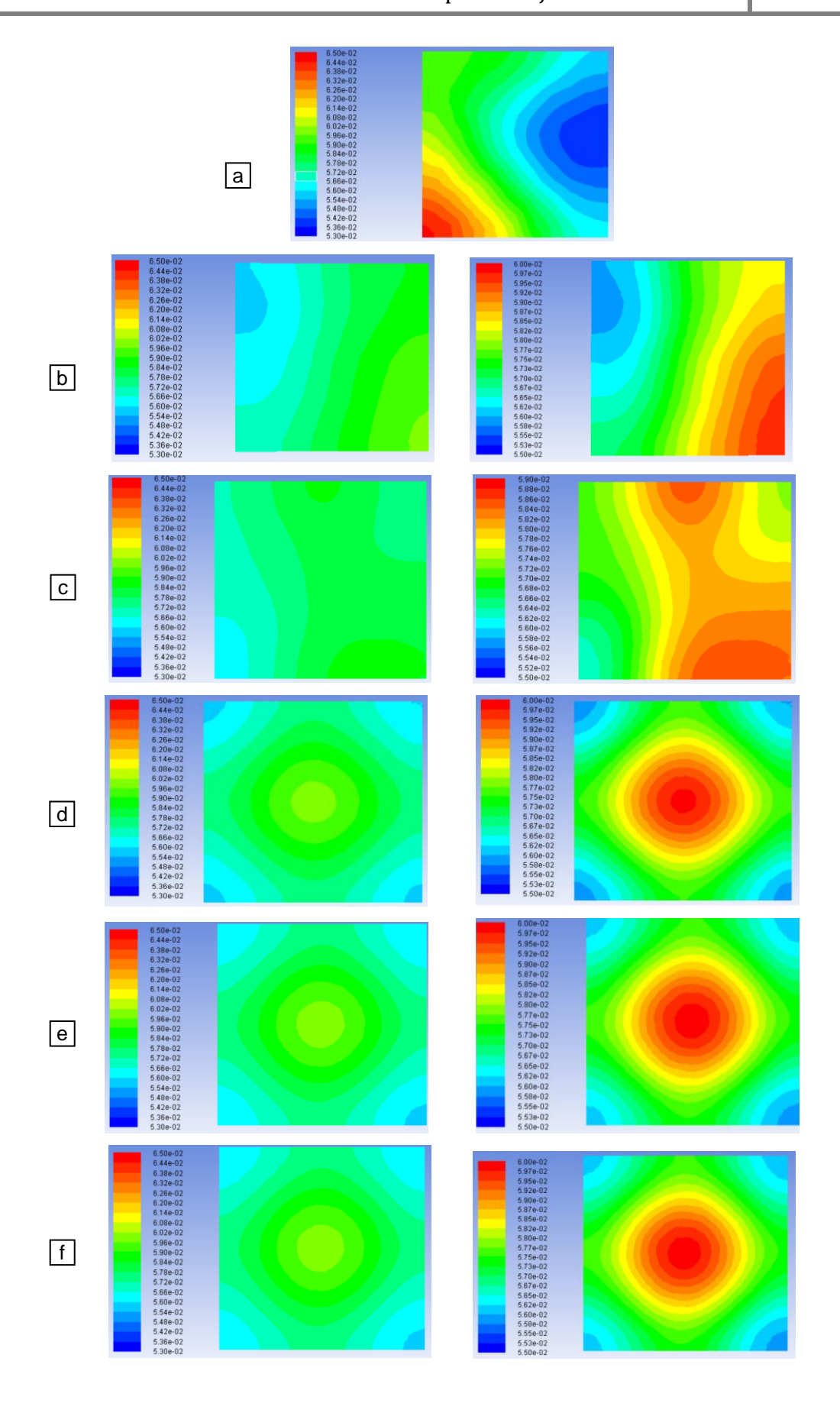


Figure 26 Velocity profiles (u [m/s] – velocity magnitude) in transverse plane at distance 10De (5cm) from the metal plate in all the six cases analysed: a) 0.2, b) 0.62, c) 1.5, d) 3, e) 5.3, f) 7.3 million elements

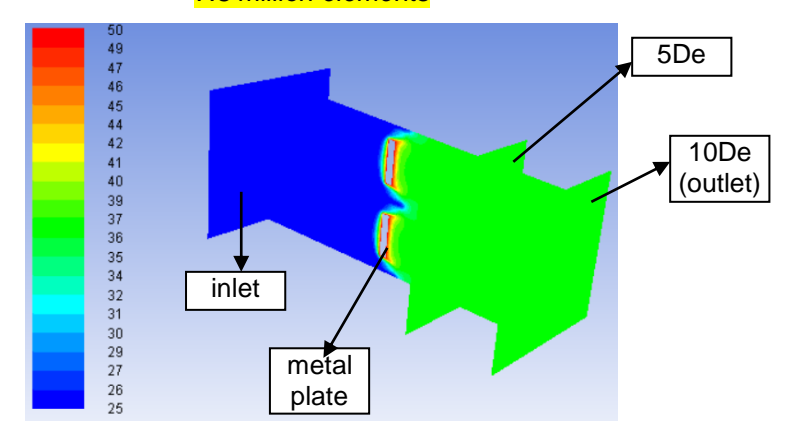


Figure 27 Velocity profiles in transverse plane

In order to perform the mesh independency study, we analysed for all the 6 cases the velocity and temperature profiles in XY and XZ longitudinal planes, respectively at 5De and 10D distance from the metal plate in transverse planes. If there were no significant differences in the first two situations, we can conclude that from the 5.3 million elements mesh there are no visible variations between the velocity profiles. Regarding the 10De transverse plane, although small differences appear in the figure, the velocity distribution is relatively uniform with very small variations between 0.055 and 0.06 m/s. Also, we observed that in the transverse plane there are no visible differences in the temperature fields in all the 6 cases (Figure 27). Considering the imposed boundary conditions for this case, the air temperature at 5De, respectively at 10De is the same around 37 °C.

To conclude, following the mesh independency study conducted, we chose the geometry of 5.3 million cells because it is an independent solution to the computing grid and this will be used in the numerical model analysed.

The mesh independency study must be followed by the experimental validation of the numerical model in order to achieve the final numerical model. This will be achieved through two different approaches:

- a) By comparing the air velocity profiles in longitudinal planes (numerical vs. experimental)
- b) By comparing the temperatures on the outlet (numerical vs. experimental).

# 4.3 Experimental validation of the numerical model - comparison of velocity profiles in longitudinal plane

In order to validate the velocity profiles in longitudinal planes, measurements made using PIV (Particle Image Velocimetry or Particle Image

Speed Measurement) were compared with the results of numerical simulations obtained under similar conditions.

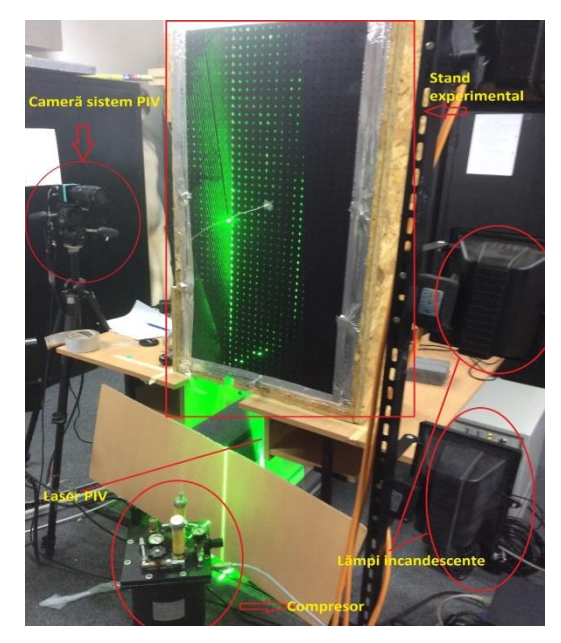


Figure 28 The use of the PIV technique in order to measure air velocity profiles as a results of a metal absorber with lobed orifices – small size collector (according to [85])

The PIV technique is a method of studying the flows generated by various grilles/air diffusion units that allows the measurement of instantaneous velocity fields (Figure 28). The experimental results used to validate the numerical model were taken from previous studies conducted within the Faculty of Building Services Engineering (Technical University of Civil Engineering, Bucharest) [4], studies that pursued the analysis of the velocity profiles for a water flow which passes through similar lobed orifices in case of a certain Reynolds number: Re = 2500.

For the experimental validation of the numerical model, we analysed the XY longitudinal planes, in the plane that traverses the centre of the lobed orifice (the centre of the jet - Z=0mm) and at 2.5mm distance (Z=2.5mm), as can be seen in Figure 29.

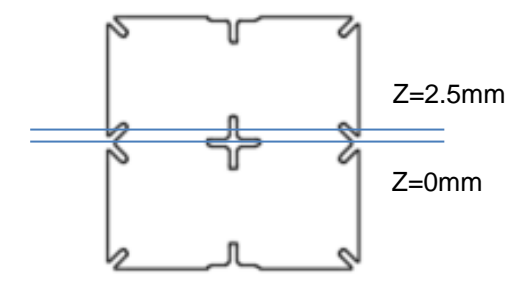


Figure 29 Longitudinal planes used for experimental validation

Figure 30 shows the velocity fields in longitudinal XY plane according to experimental measurements at Re2500 for three different jets (Y00, Y20 and Y40) in their centre (Z = 0mm). Experimental data was imported and processed in Tecplot for the Y40 jet and the data displayed represents the velocity magnitude.

Due to the lack of data in the immediate vicinity of the jet, we decided to process the data starting with x = 10mm and extracted the speed values in 50 points. In the case of the experimental study, the normalized velocity values at the 50 points are shown in Figure 34.

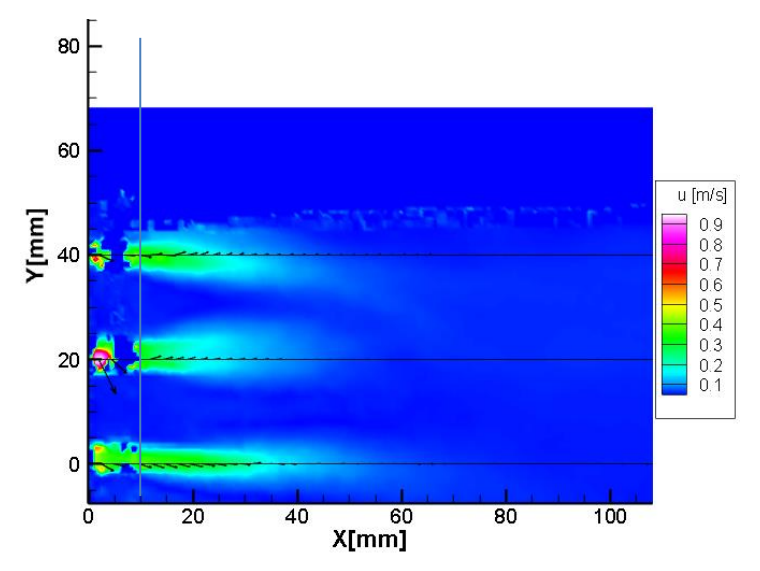


Figure 30 Velocity fields in longitudinal XY plane according to PIV experimental measurements at Re2500 in the centre of the jet (Z=0mm) (according to [4])

Figure 31 shows the velocity fields in longitudinal XY plane according to experimental measurements at Re2500 for three different jets (Y00, Y20 and Y40) at 2.5mm distance from the jet centre (Z=2.5mm). Experimental data was imported and processed in Tecplot for the same Y40 jet and the data displayed represents the velocity magnitude. The normalized velocity values at the 50 points are shown in Figure 35.

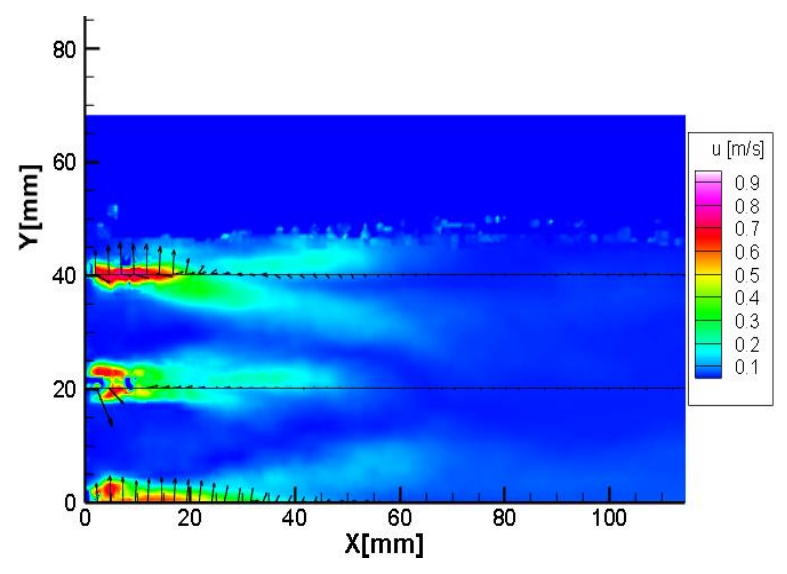


Figure 31 Velocity fields in longitudinal XY plane according to PIV experimental measurements at Re2500 at 2.5mm distance from the jet centre (Z=2.5mm) (according to [4])

In the actual case of the solar collector with lobed holes, the air flow rate is 200 m<sup>3</sup>/h•m<sup>2</sup> (400 m<sup>3</sup>/h), which determines an air velocity in the lobed orifice of

1,312 m/s, the airflow being characterized by a small Reynolds number (Re = 422). In order to be able to compare the results of the numerical model with the experimental results, the air velocity in the inlet must have a value corresponding to a Reynolds number of Re=2500 in the lobed orifice. To do this, we need to calculate the new velocity in the lobed orifice ( $v_o$ ') and then the resulting velocity at the inlet ( $v_{4x4}$ '), as follows:

$$Re' = \frac{\rho_{aer} \cdot v_o' \cdot De}{\mu_{aer}}$$

$$v_o' = \frac{Re' \cdot \mu_{aer}}{\rho_{aer} \cdot De} = \frac{2500 \cdot 0.0000184}{1.185 \cdot 0.005} = 7.764 \frac{m}{s}$$

$$D_o' = 7.764 \cdot 0.000019635 = 0.000152 \frac{m^3}{s}$$

$$D_{4x4}' = 000152 \cdot 4 = 0.0006 \frac{m^3}{s}$$

$$v_{4x4}' = \frac{0.0006}{0.0016} = 0.375 \frac{m}{s}$$

The next step regarding the experimental validation of the numerical model by comparing the velocity profiles in longitudinal planes was the creation of the numerical case. As a result, I imported the 5.3 million cells mesh into ANSYS Fluent and kept the case settings by using the energy conservation equation and k- $\epsilon$  RNG turbulence model (with EWF) according to the previous chapter. The boundary conditions used are presented in Table 4, the new air velocity value at the inlet being essential within the validation.

**Table 4.** Boundary conditions used for the experimental validation

Boundary conditions	Value	Unit
Velocity magnitude (inlet)	0.375	m/s
Ambient temperature (inlet)	25	°C
Metal plate temperature (metal)	50	°C

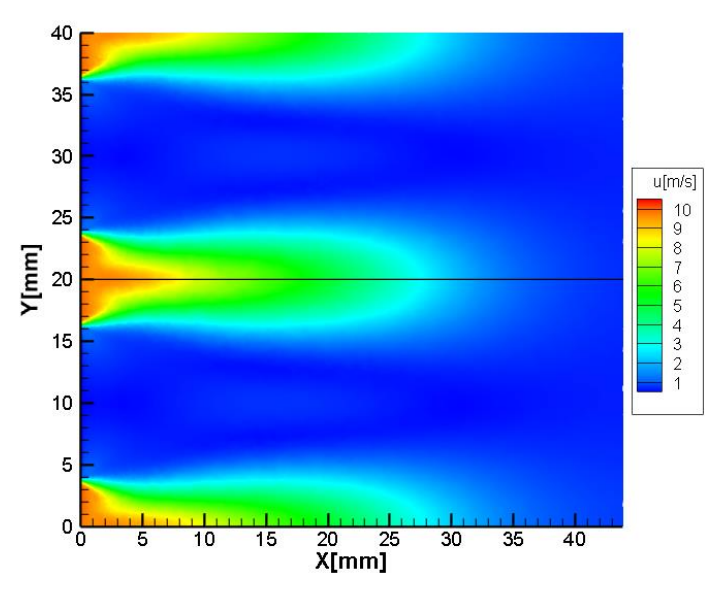


Figure 32 Velocity field in longitudinal XY plane according to numerical study at Re2500, in the centre of the jet (Z=0mm)

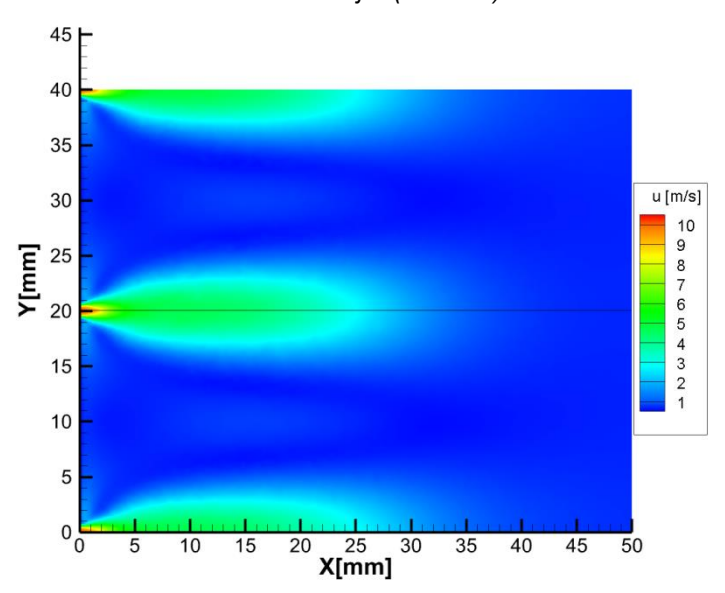


Figure 33 Velocity field in longitudinal XY plane according to numerical study at Re2500, at 2.5mm from the centre of the jet (Z=+2.5mm)

After running the numerical simulation, I obtained the velocity profiles at Re2500 for the airflow through the lobed orifice. The data obtained was imported into the Tecplot data processing software. The XY longitudinal velocity profiles in the centre of the jet and at 2.5 mm from the centre of the jet are shown in Figure 32 and Figure 33. For the Z=0mm case, I extracted velocity values in 50 points, similar to the previous situations to be able to compare velocity profiles. In the case of the numerical study, normalized values of the velocity magnitude in the 50 points are also presented in Figure 34 and Figure 35.

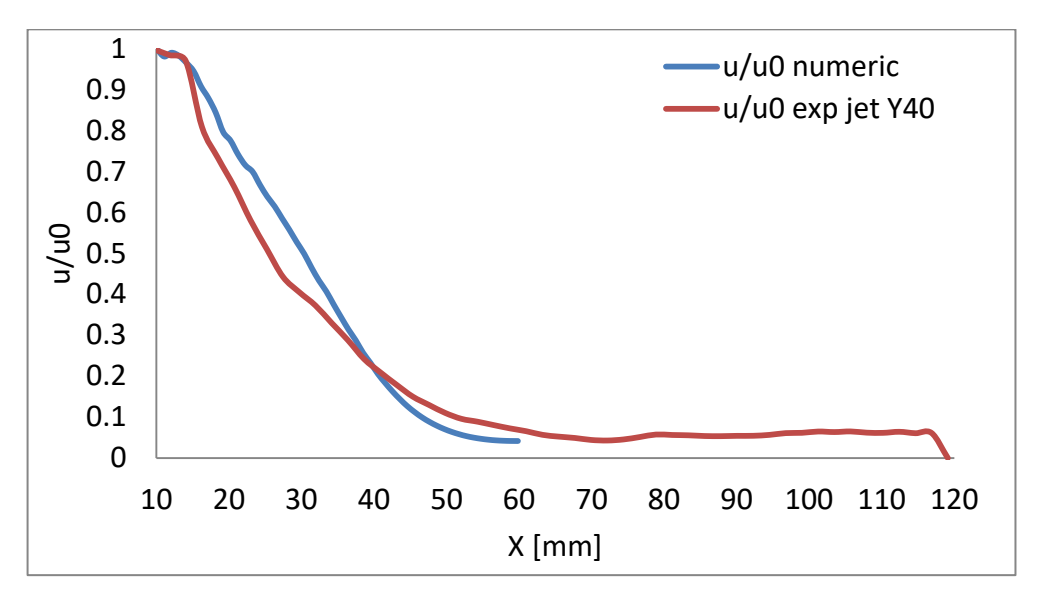


Figure 34 Normalized velocity magnitude variation: numerical study vs. experimental study (centre of the jet Z=0mm)

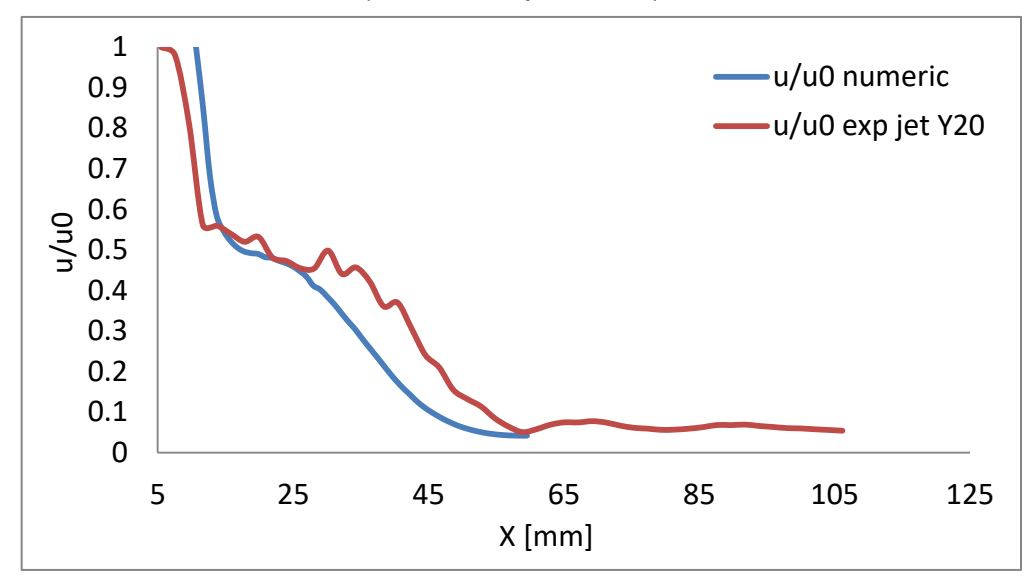


Figure 35 Normalized velocity magnitude variation: numerical study vs. experimental study (at 2.5mm from the centre of the jet Z=+2.5mm)

In order to properly compare the velocity profiles in both cases, both numerical and experimental results need to be normalized. Figure 34 shows the variation of normalized velocities in 50 points in the longitudinal plane XY for the plane passing the centre of the jet (Z = 0mm), both in the case of numerical and experimental study (Y40 jet). It can be observed that the velocity profiles are basically the same and after 10De variation is similar. Figure 35 shows the variation of normalized velocities in 50 points in the longitudinal plane XY for the plane passing at 2.5mm from centre of the jet (Z = +2.5mm), both in the case of numerical and experimental study (Y20 jet). It can be observed that the velocity profiles are basically the same and after 10De variation is similar. The difference between the curves allures is given by the Y20 jet deviation in that zone of the experimental studies.

Therefore, by comparing experimental values with numerical results at Re2500, we can conclude that the numerical model reproduces real flow phenomena within acceptable limits. Moreover, starting with 10De velocity profiles are similar, which confirms the premises assumed in the construction of geometry.

### 4.4 Experimental validation of the numerical model – comparison of outlet temperature

Although the experimental validation of the numerical model by comparing velocity profiles in longitudinal plane is the most relevant in the case of the airflow through the absorbent metal plate with lobed holes, we decided to check the temperature value which results on the outlet of the computing domain. In the case of the study of the implementation of phase change materials in solar collectors, the focus is mainly on temperature variations and less on velocities variations, although they can considerably influence the results.

For this validation, we will compare the results in two points of the experimental study (minute 110 and minute 255) with the results obtained by running the numerical model in steady state regime. The experimental study was conducted in similar conditions with the studies presented in Chapter 2, moreover a new sensor was installed in the first cavity at 5cm distance from the metal plate (10De).

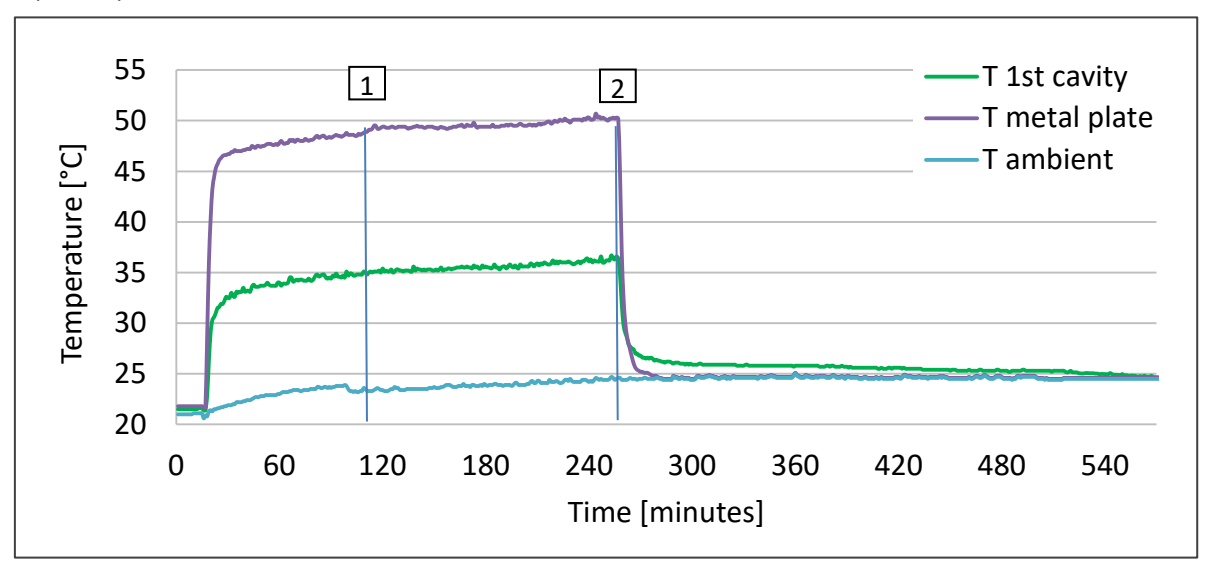


Figure 36 Temperatures variation in the case of experimental measurements

As it can be observed in the experimental results presented in the above figure, regarding point 1 (minute 110) at an ambient temperature of 24 °C and a temperature on the absorbent plate of 49 °C, the air temperature in the cavity at 5cm distance from the absorbent plate is about 35 °C. Also, regarding point 2 (minute 255) at an ambient temperature of 25 °C and a temperature on the absorbent plate of 52 °C, the air temperature in the cavity at 5 cm of the absorbent plate is about 36.5 °C. These were also the boundary conditions used for the numerical study (Table 5 and Table 6).

Table 5. Boundary conditions used for point 1

Boundary condition	Value	Unit
Velocity magnitude (inlet)	0.055	m/s
Temperature on the inlet (inlet)	24	°C
Metal plate temperature (metal)	49	°C

As it can be noticed in Figure 37, the temperature field at the outlet, for the 1<sup>st</sup> studied, has a value similar to that obtained in the case of experimental measurements. Moreover, the temperatures became uniform quickly after the airflow crosses the absorbent metal plate.

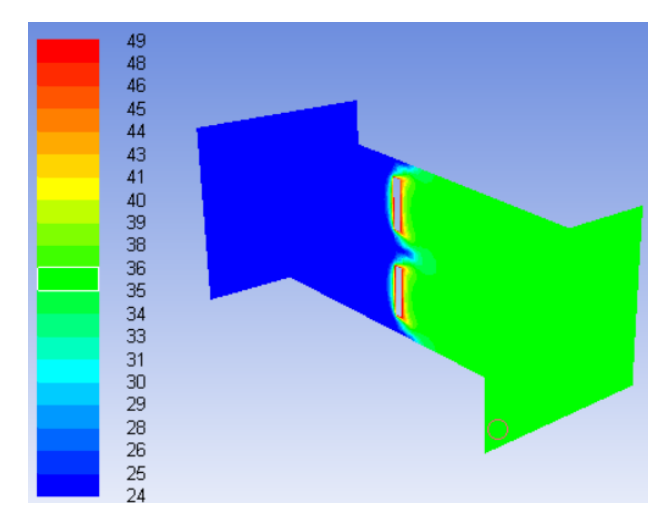


Figure 37 Temperature fields obtained for the point 1 – numerical study

As it can be noticed in Figure 38, the temperature field at the outlet, for the  $2^{nd}$  studied, has a value similar to that obtained in the case of experimental measurements (36.5 ° C).

**Table 6.** Boundary conditions used for point 2

Boundary condition	Value	Unit
Velocity magnitude (inlet)	0.055	m/s
Inlet temperature (inlet)	25	°C
Metal plate temperature (metal)	50	°C

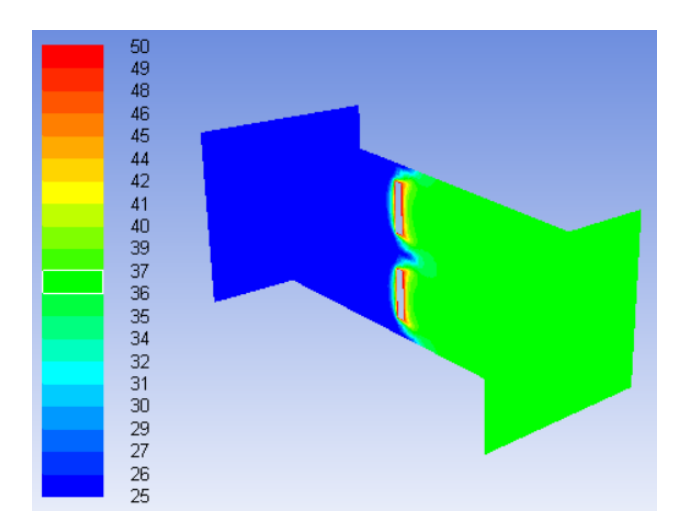


Figure 38 Temperature fields obtained for the point 2 – numerical study

In order to conclude, taking into account all the aspects presented in the last two chapters, we can assert that the numerical model reproduces the real phenomena of the flow and heat transfer that were noticed in the experimental studies and can be further used in the numerical analyses.

### 4.5 Final parameters of the numerical model and results

By considering the analyses elaborated in this chapter, we can conclude the final parameters of the numerical model that studies the airflow through the absorbent metal plate with lobed orifices.

According to the mesh independency study we chose the 5.3 million cells geometry which will not influence the numerical results, being a stable solution.

We also chose the energy transfer model taking into account the energy conservation equation and the k-ɛ RNG turbulence model (with EWF) which according to the literature is suitable for the type of airflow studied. Having the temperature values at different points from the experimental study, we did not use the heat transfer model for radiation in order to obtain a simplified model and to facilitate as much as possible the calculations. This model will be developed in the further studies and will underpin the continuation of post-doctoral studies.

For the air circulated in the computing domain we have selected from the ANSYS Fluent software database the appropriate properties, also for the metal absorber plate we have chosen aluminium as the material. The boundary conditions imposed are those shown in Table 3, but they can be modified to obtain various results and to perform parametric studies (post-processing of the model).

The interpolation scheme used is "second order upwind" for the analysis of convective terms and the pressure-speed coupling scheme is determined by the "SIMPLE" algorithm. According to the studied literature, the convergence of the solution is achieved when the non-dimensional residuals of the flow equations are less than 10<sup>-3</sup>; as a result, in order to obtain the relevant results we have imposed a value less than 10<sup>-5</sup>. Typical images for the convergence of non-dimensional residues are shown in the figure below.

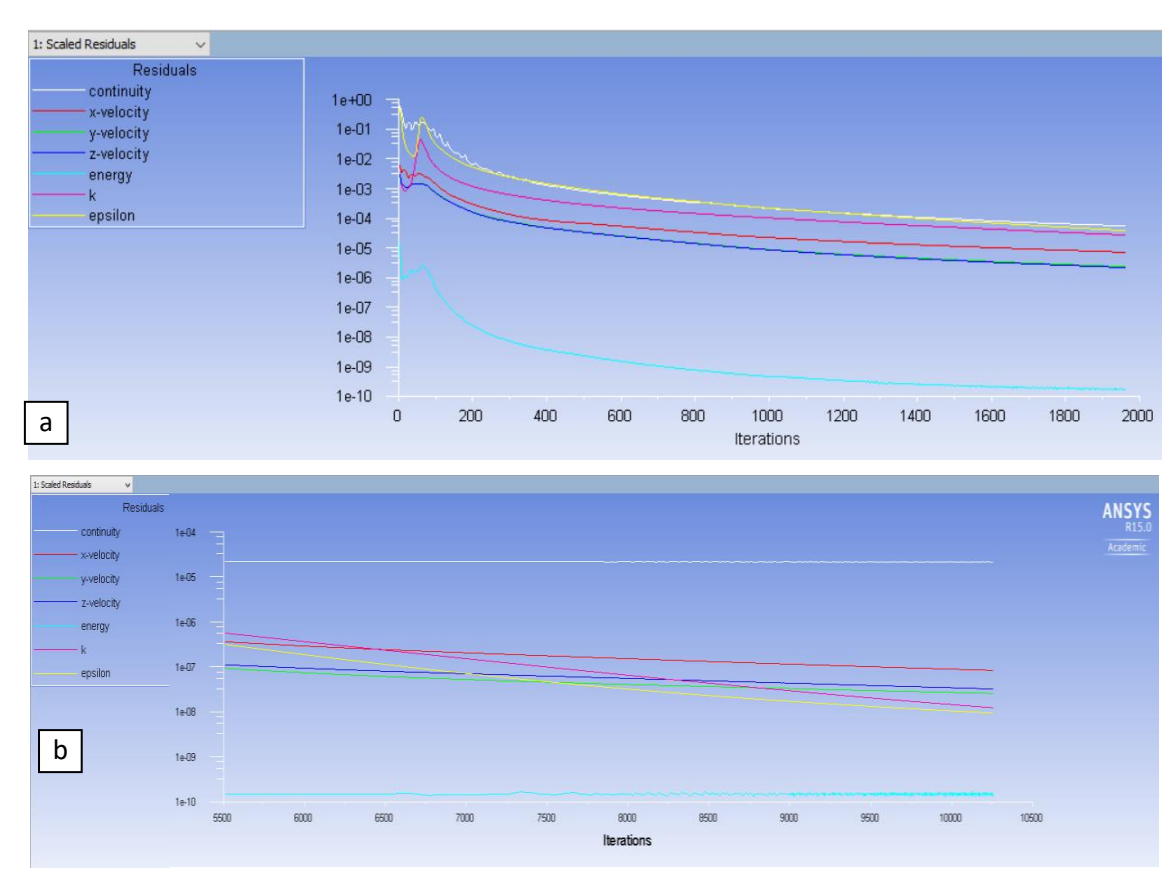


Figure 39 Typical images for the convergence of non-dimensional residues for a stady state simulation: a – until 2000 iterations, b – after 10000 iterations

Obtaining velocity and temperature fields as a result of orifices geometry at 10De will create further opportunity to continue doctoral studying. With these results, we can translate into the numerical model of the solar collector the real impact of the lobed geometry. Also, in the future, we will be able to analyse the impact of the orifices on phase change materials implemented in solar collectors. In the next chapter it will be presented the numerical model of the solar collector with lobed orifices and integrated PCMs. The results obtained in this chapter by using the studied numerical model will be integrated into the real-size model and will constitute input data in the computing domain (inlet of the new model).

Below are some of the results of the numerical model built and analysed in this chapter, taking into account the boundary conditions shown in Table 3 which capture the "heating" stage of the study.

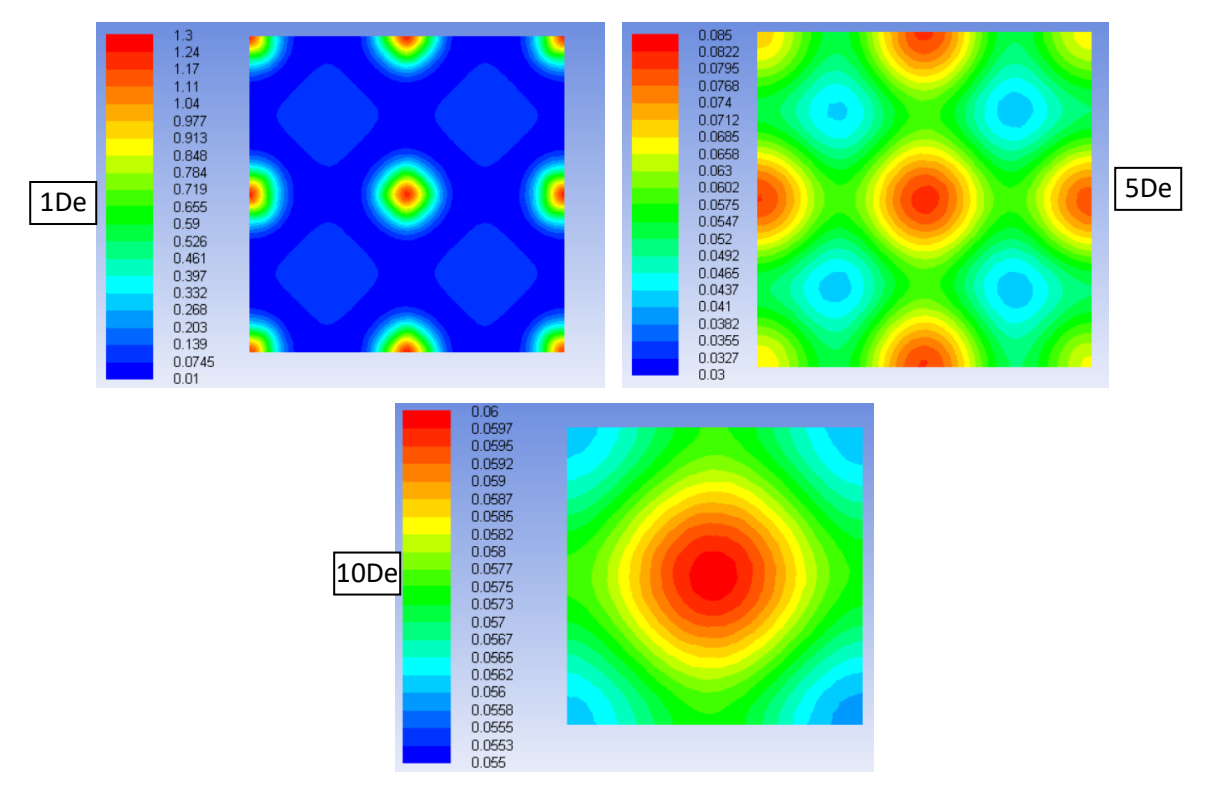


Figure 40 Velocity fields at different distances from the absorbent plate

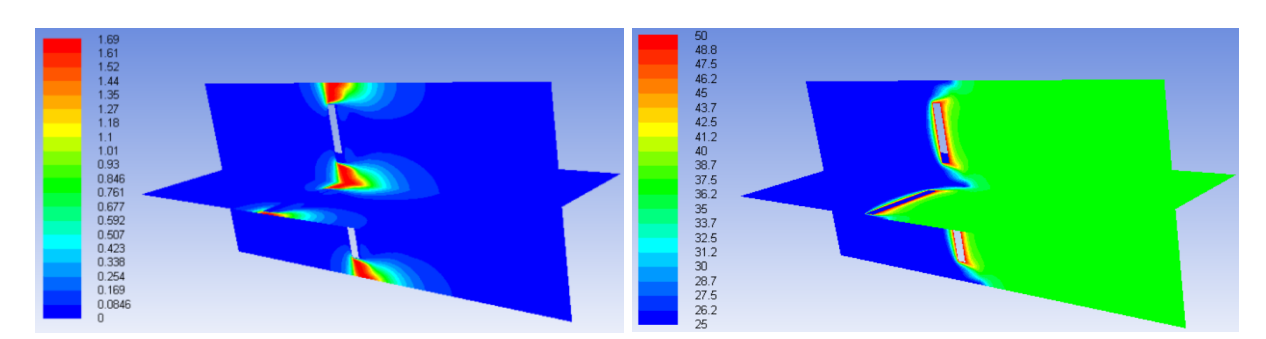


Figure 41 Velocity and temperature fields in longitudinal XY and XZ planes

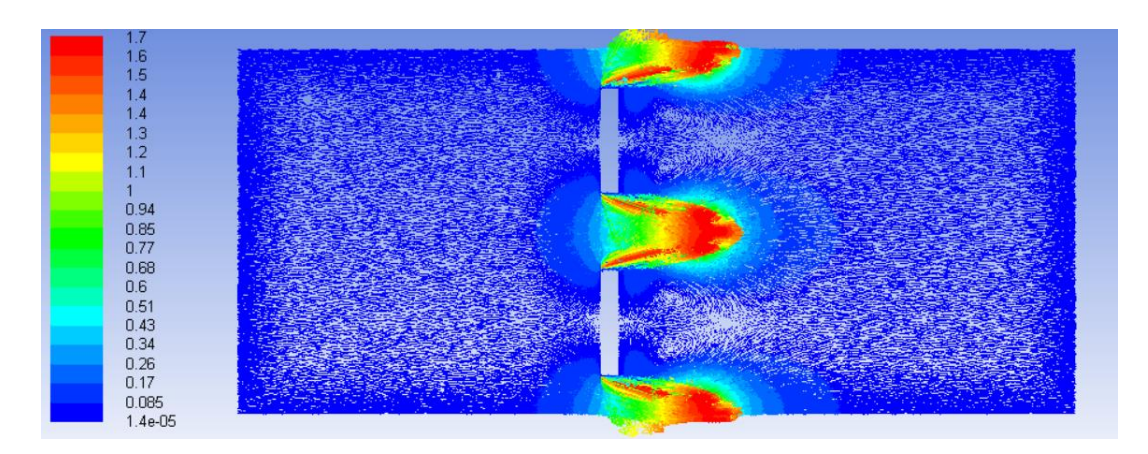


Figure 42 Velocity vectors in longitudinal XY plane

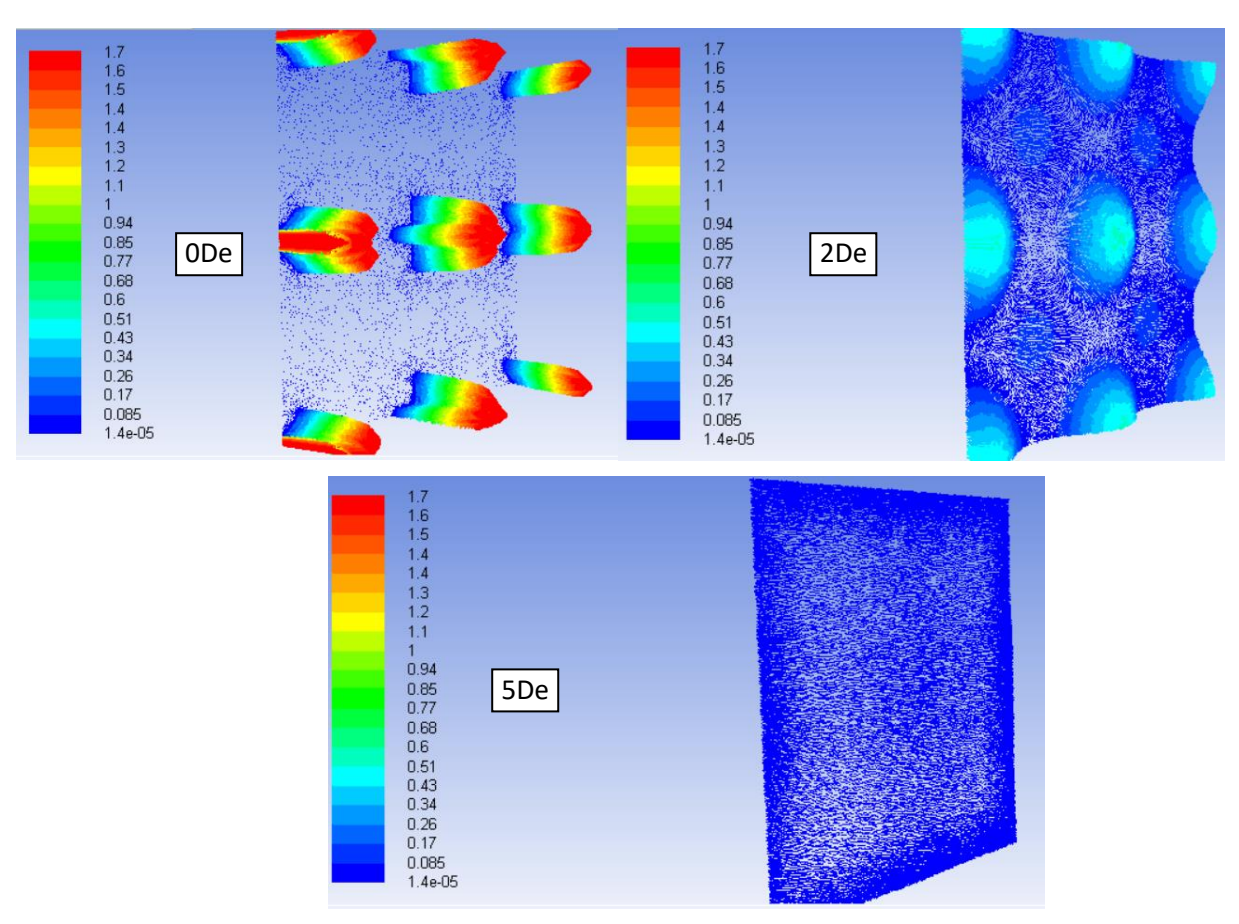


Figure 43 Velocity vectors in different transverse planes

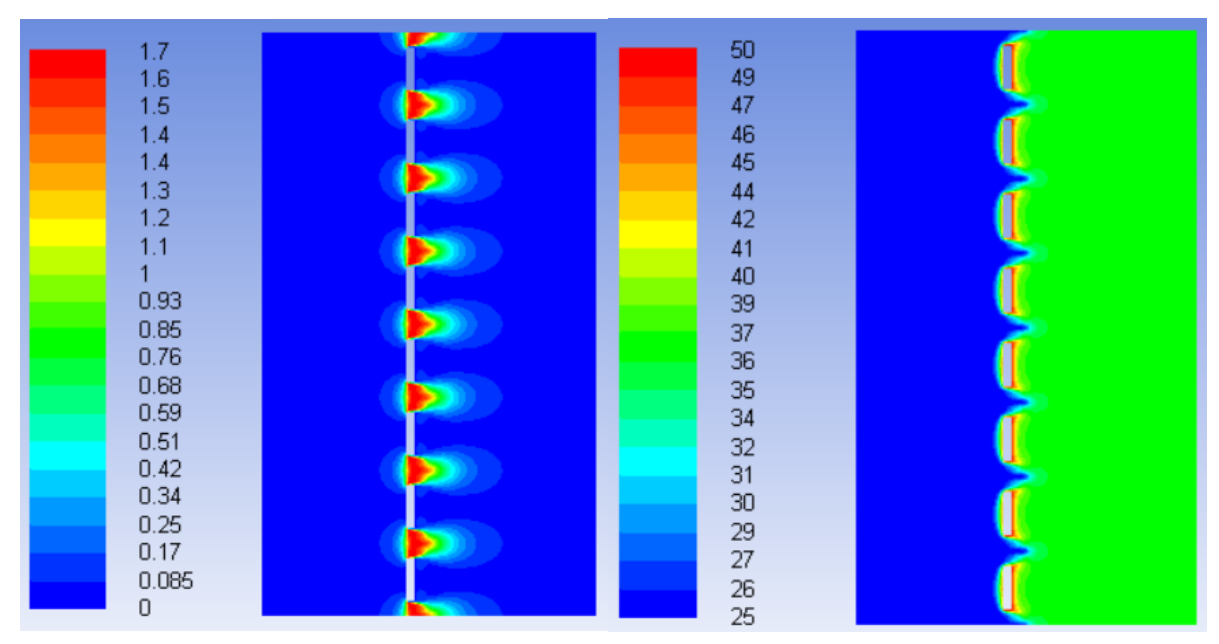


Figure 44 Velocity and temperature fields in longitudinal XY plane for 7 orifices

## 5. Creating a numerical model for the transpired solar collector with lobed orifices and integrated PCMs

### 5.1. Creating the simplified model

After realizing the numerical model analysing the airflow through the lobed orifices (absorbent plate) I continued with the actual modelling of the solar collector with integrated phase change materials. The velocity and temperature fields resulting from the model studied in the previous chapter (outlet at 10De) will constitute input data for the new numerical model (inlet), as shown below.

In order to achieve the numerical simulations within a feasible time period, we decided to simplify the real geometry, starting from the premise of the symmetry of the phenomena which are composing the entire collector. Figure 45 shows the absorbent plate through which ambient air is aspired into the solar collector cavity. From this we extracted a row of orifices (Figure 45a), resulting in a "transversal slice" through the solar collector (Figure 45b). Aspiration (collectors' inlet) is composed of 50 plates with 4x4cm lobes studied in the previous chapter and has the dimensions of 4x200cm. The air circulated through the collector with the properties set at 10De is aspired into the new model, enters the cavity between the metal plate and the phase change materials obstacle, continues the downstream trajectory due to the PCM chicane and after reaching the bottom of the collector will follow an ascending trajectory that ends with the outlet of the air from the solar collector. The dimensions of the "slice" respect the real geometry of the solar collector with integrated PCMs.

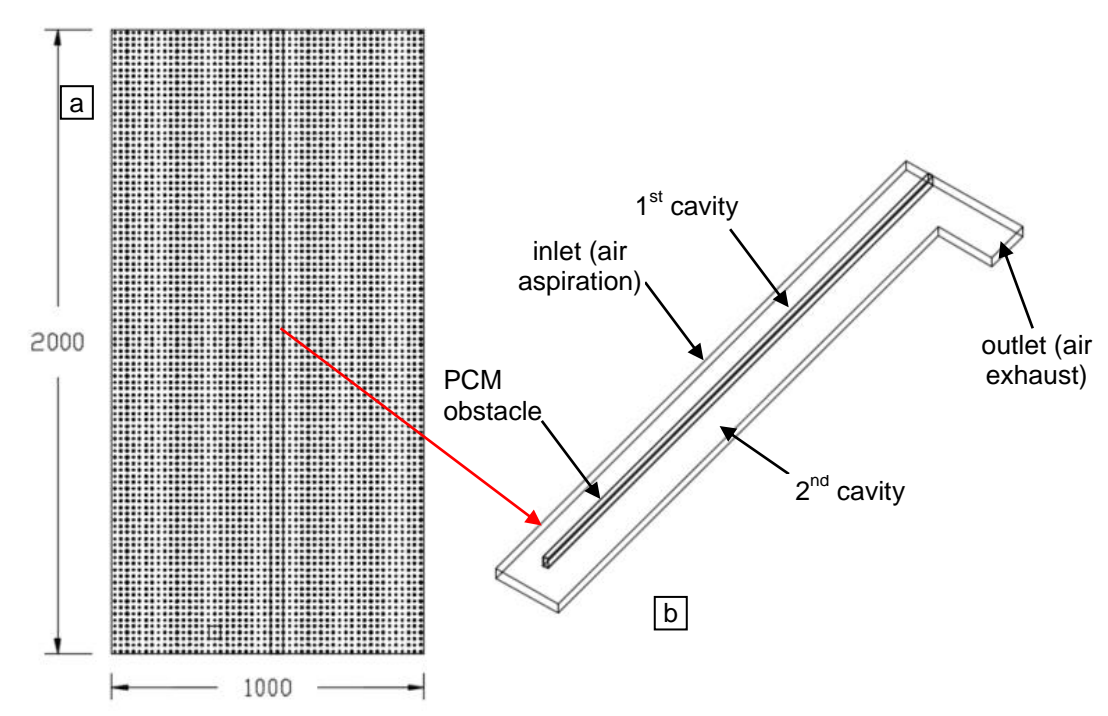


Figure 45 Designing the geometry in AutoCAD: a – absorbent plate with lobed orifices, b – extraction of a "slice" from the solar collector and its components

Modelling of the entire solar collector would involve a complex spatial meshing or a very large number of cells in the computational grid in order to accurately capture the phenomena that take place. After realizing the solar

collector geometry in the AutoCAD design software, the 3D model was saved in .igs and imported into ANSYS DesignModeler (Figure 46).

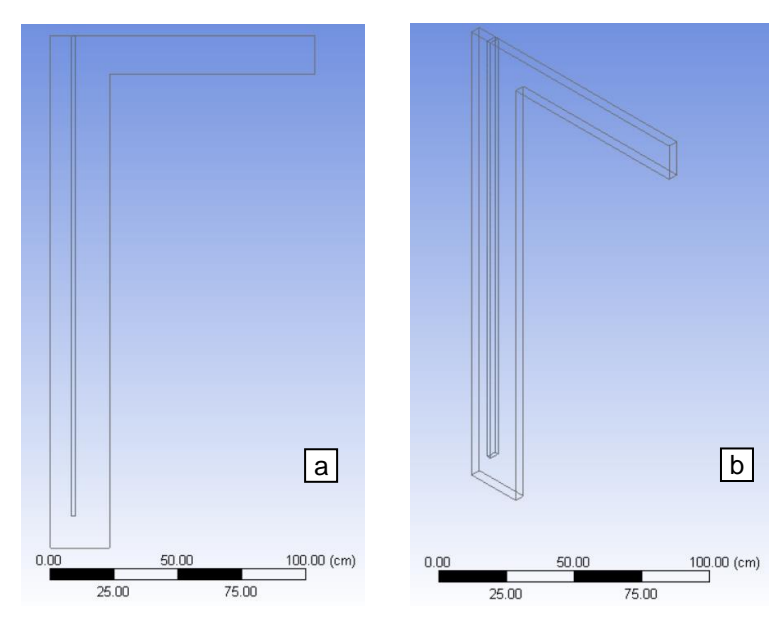


Figure 46 Importing the geometry from AutoCAD to ANSYS DesignModeler: a – side view; b – isometric view

Figure 47 shows the way of defining the bodies in the case of geometry imported ANSYS DesignModeler. In order to obtain a more stable flow to the outlet of the solar collector, the area adjacent to the outlet was extended compared to the real case.

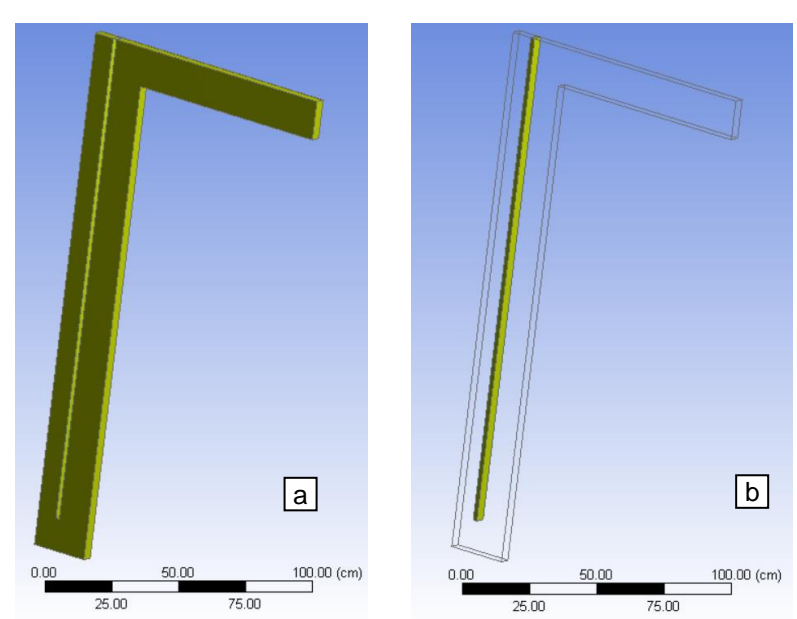


Figure 47 Defining bodies in ANSYS DesignModeler: a – body corresponding to the collector cavity; b – PCM body

The inlet of the solar collector was divided into  $50 \times 4 \times 4$  cm faces in order to integrate the velocity fields obtained at 10De from the lobed orifice plate studied in the previous chapter (Figure 48).

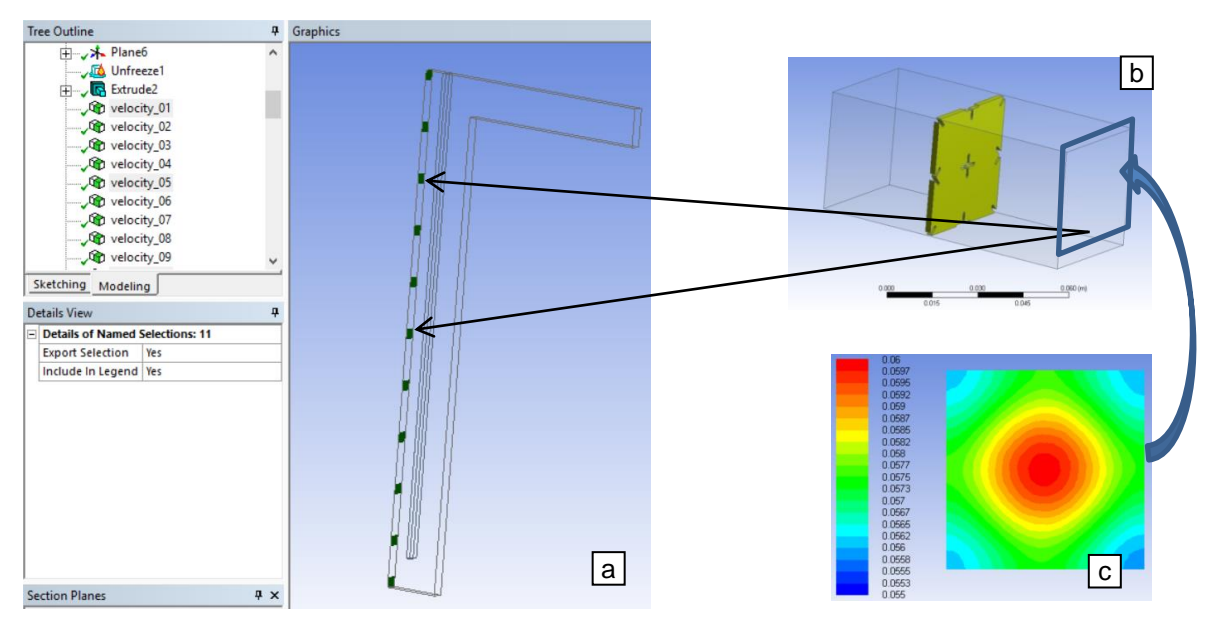


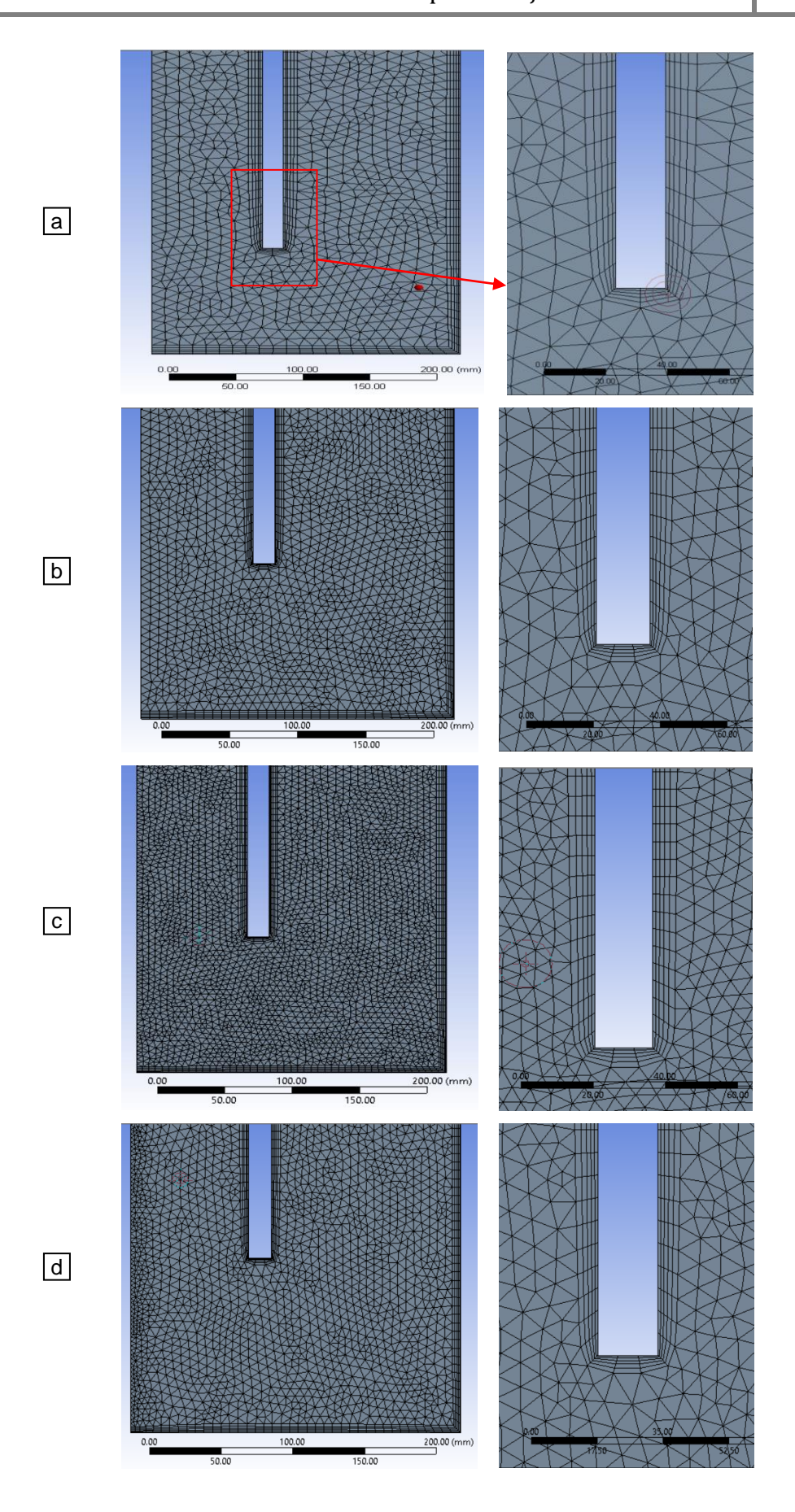
Figure 48 Creating specific air intake areas (inlet) where the velocity and temperature profiles from the previous chapter will be entered: a – 50 zones on the inlet; b – the outlet of the previous study became the inlet of the new study; c – velocity field which will be integrated on the new inlet

### 5.2. Creating the optimum mesh (mesh independency study)

Similar to the steps followed in the previous chapter, after the proper construction of the geometry, the next step of the numerical modelling is choosing the optimum mesh. Moreover, in order to determine the number of computational elements (cells) needed to solve the problem, it is necessary to make a solution independency study with respect to the quality of the meshing.

In order to conduct the mesh independency study I chose also 6 meshing levels, respectively: 0.2, 0.66, 1.3, 2.8, 5 and 6 million cells. In order not to carry out the mesh study in transient regime, which would substantially extend the time needed for the present study, we decided to remove the PCM layer from the model and carry out the study in steady state regime. This will not affect the final result because we aim to study the airflow through the solar collector with PCM and the resulting temperatures (and not the phenomena that occur in the PCM cavity). By extracting the PCM cavity form the entire geometry, results the following meshing levels: 0.18, 0.61, 0.7, 1, 2.5 and 3.5 million.

The meshing levels are shown in Figure 49 and we can observe the gradual increase in the concentration of meshing elements, especially in the boundary layer. The optimal meshing level is determined by individual numerical simulations, using boundary conditions and identical calculation models.



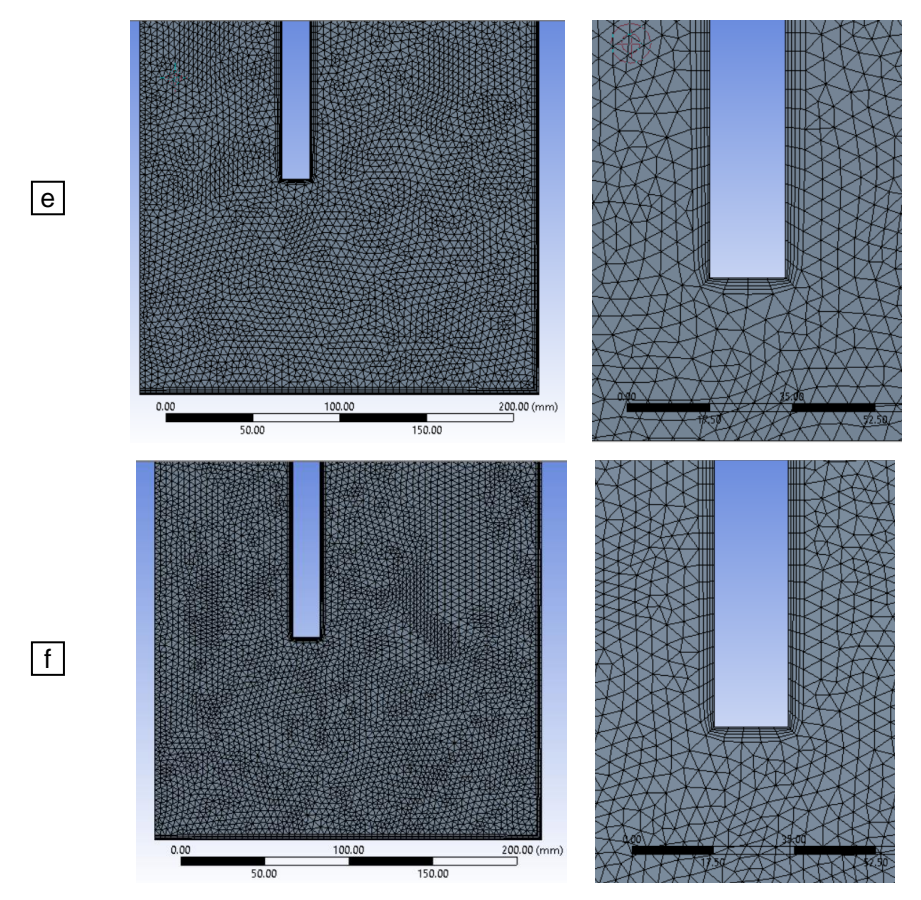


Figure 49 Meshing levels for the analysed cases without PCM: a) 0.2 (0.18), b) 0.66 (0.61), c) 1.3 (0.7), d) 2.8 (1), e) 5 (2.5), f) 6 (3.5) million elements

The six meshing levels were then imported in ANSYS Fluent and for each of them the same boundary conditions were imposed, which are shown in Table 7. The inlet air velocity corresponds to the velocity profiles obtained from the previous study and has values ranging from 0.055 to 0.06 m/s for each of the 50 faces, resulting in a total velocity in the "slice" of about 2.75 m/s. The temperature of the air at the inlet (at 10De) is 26 °C and the temperature of the wall which separates the PCM layer to the cavity is 40 °C. These assumptions represent the cooling stage, respectively the heat transfer from the PCMs to the airflow in periods when the solar radiation isn't available. The areas where the boundary conditions were imposed are presented in figure 50.

**Table 7.** Boundary conditions used in the mesh independency study

Value

Velocity magnitude (inlet)	Velocity field obtained from the previous study with values between 0.055-0.06 m/s for all 50 faces on the inlet		
Inlet temperature (inlet)	26	°C	
PCM temperature (wall between the PCM and the cavity)	40	°C	

**Boundary condition** 

Unit

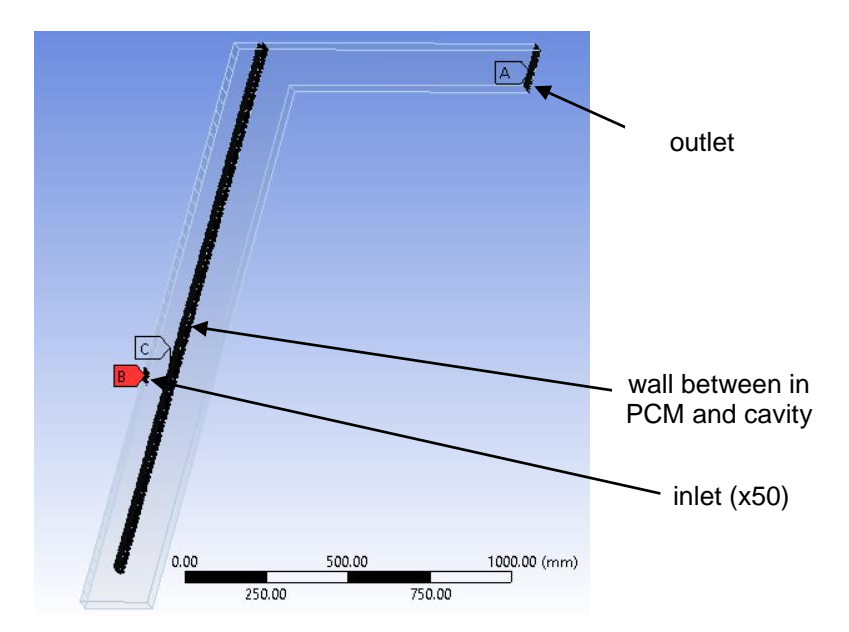


Figure 50 Areas where boundary conditions were imposed

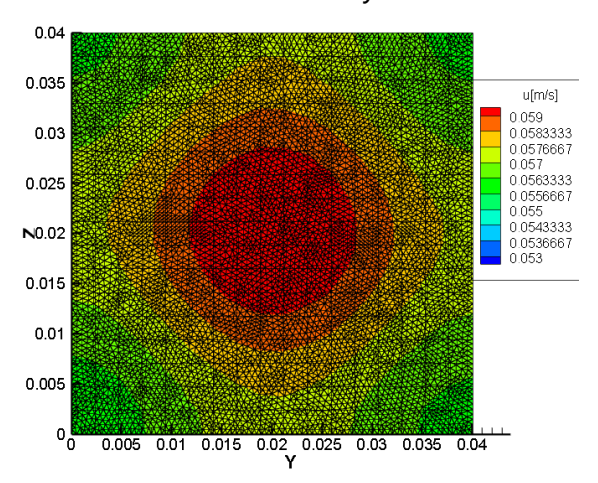


Figure 51 Velocity fields imported from the previous model and processed in Tecplot

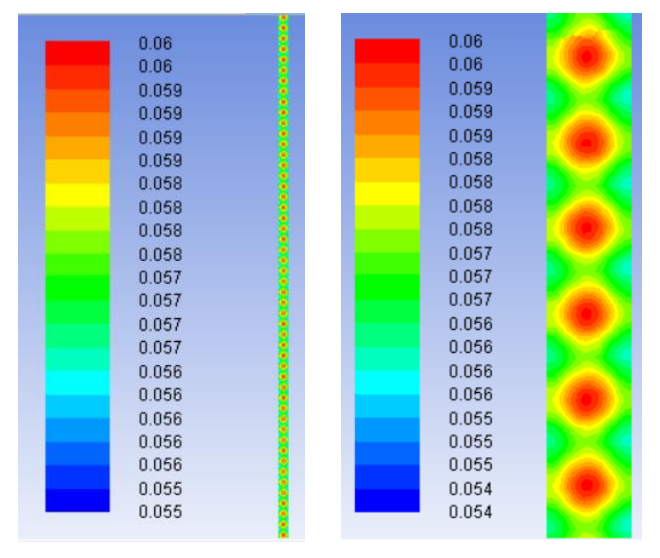
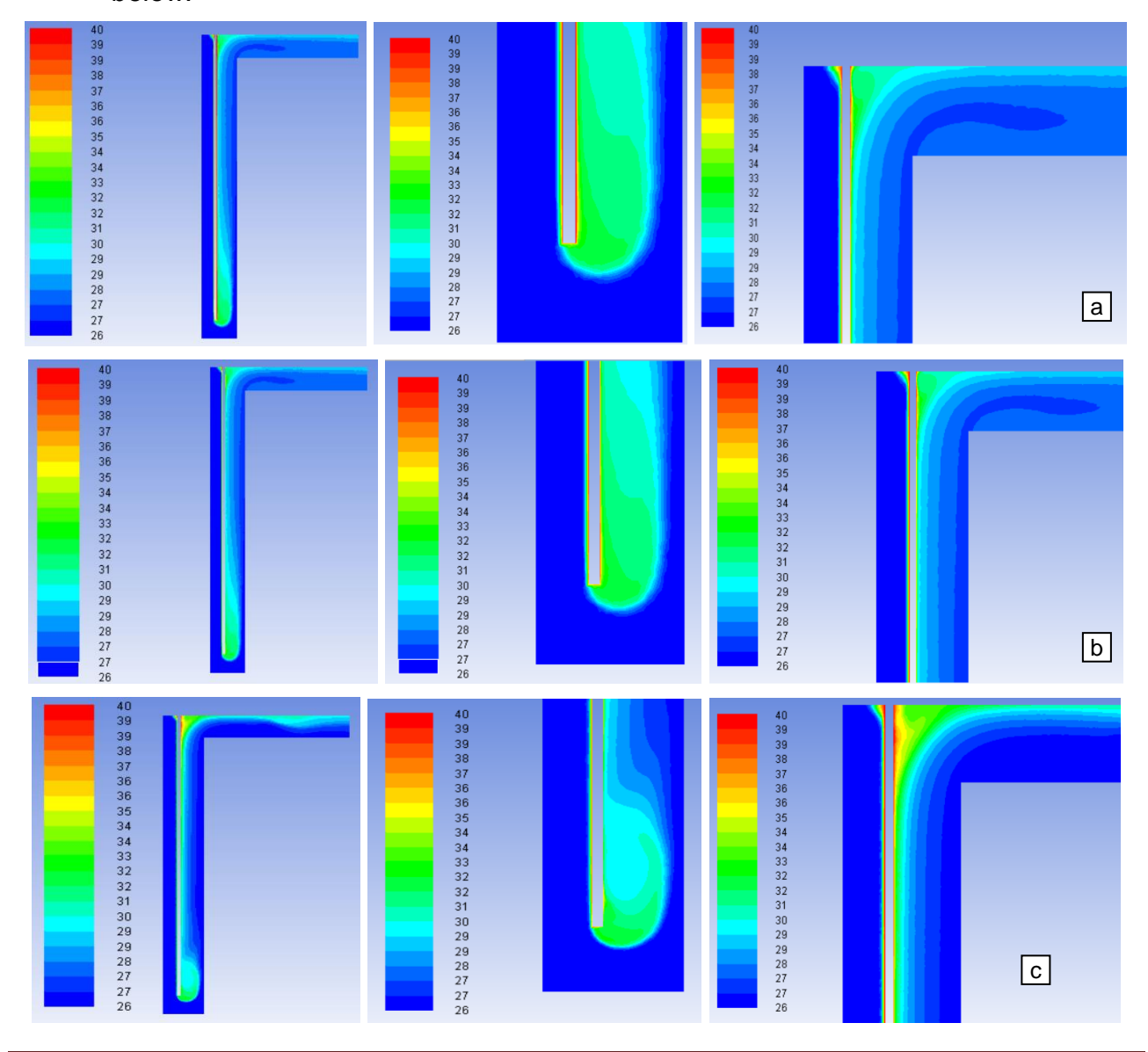


Figure 52 Velocity fields imported from the previous model in the new model of the solar collector with integrate PCMs

The velocity field obtained at 10De in the previous chapter was imported in the Tecplot data processing software (Figure 51). On this I created a matrix of points that were subsequently exported to Notepad and processed in X, Y, and Z coordinates so that they could fit into the new model's coordinates. The newly created profiles were subsequently imported and retrieved under the boundary conditions in the inlet area.

In addition to the energy conservation model, I chose the k- $\Omega$  SST turbulence model (with corrections for a small Reynolds numbers as the case studied and curvature corrections etc.). This is one of the most feasible turbulence models and is suitable, according to the literature, for small Reynolds numbers [86] and for airflows within rectangular air cavities [87]. Although experienced CFD researchers recommend the analysis of multiple combinations of meshing levels and turbulence models, the reduced time available for the present study didn't allowed us to compare several models of turbulence in this case [84]. With respect to the the above mentioned data, we have performed numerical simulations for the 6 computational grids and the results for the steady state study are presented below.



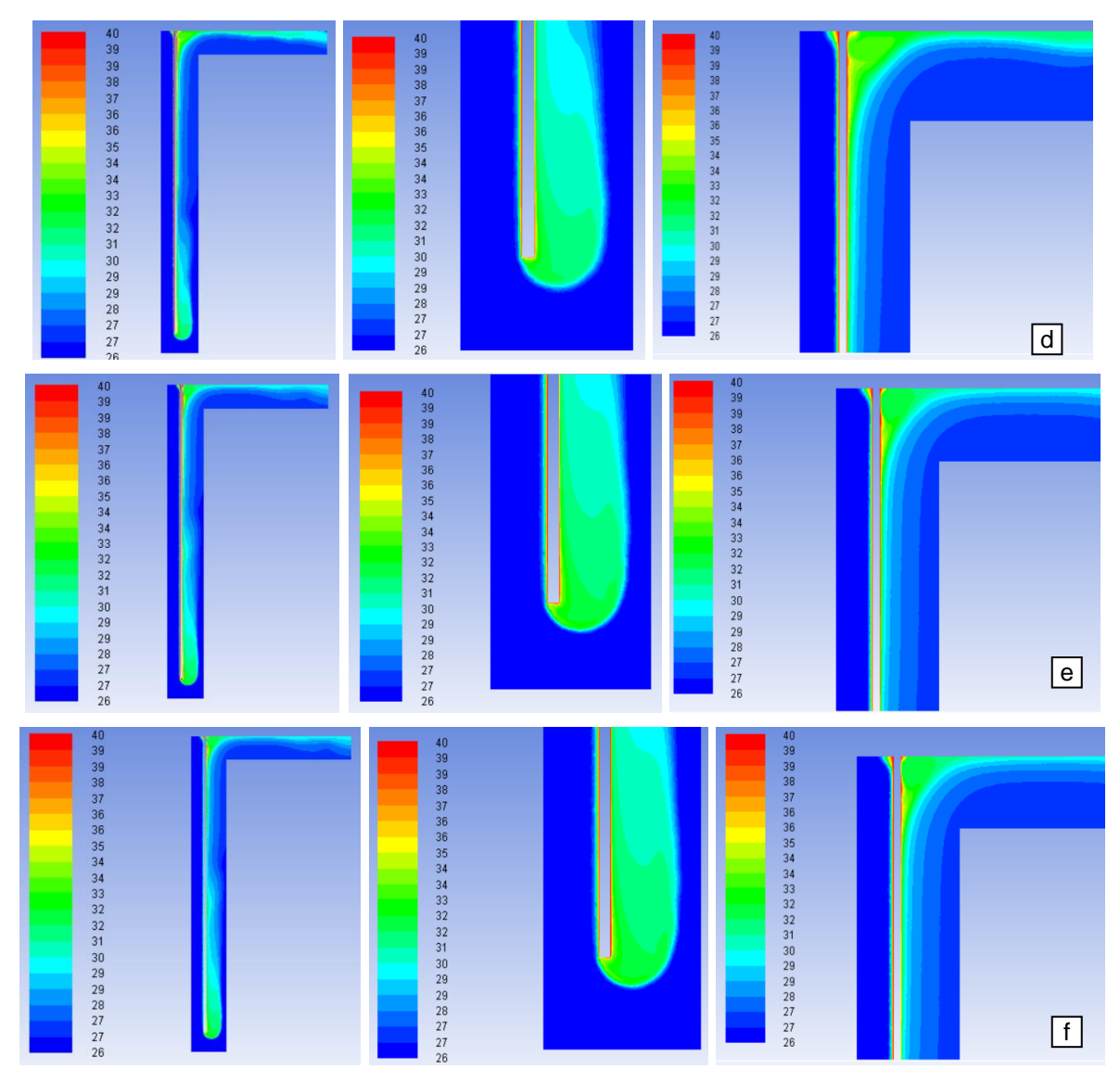
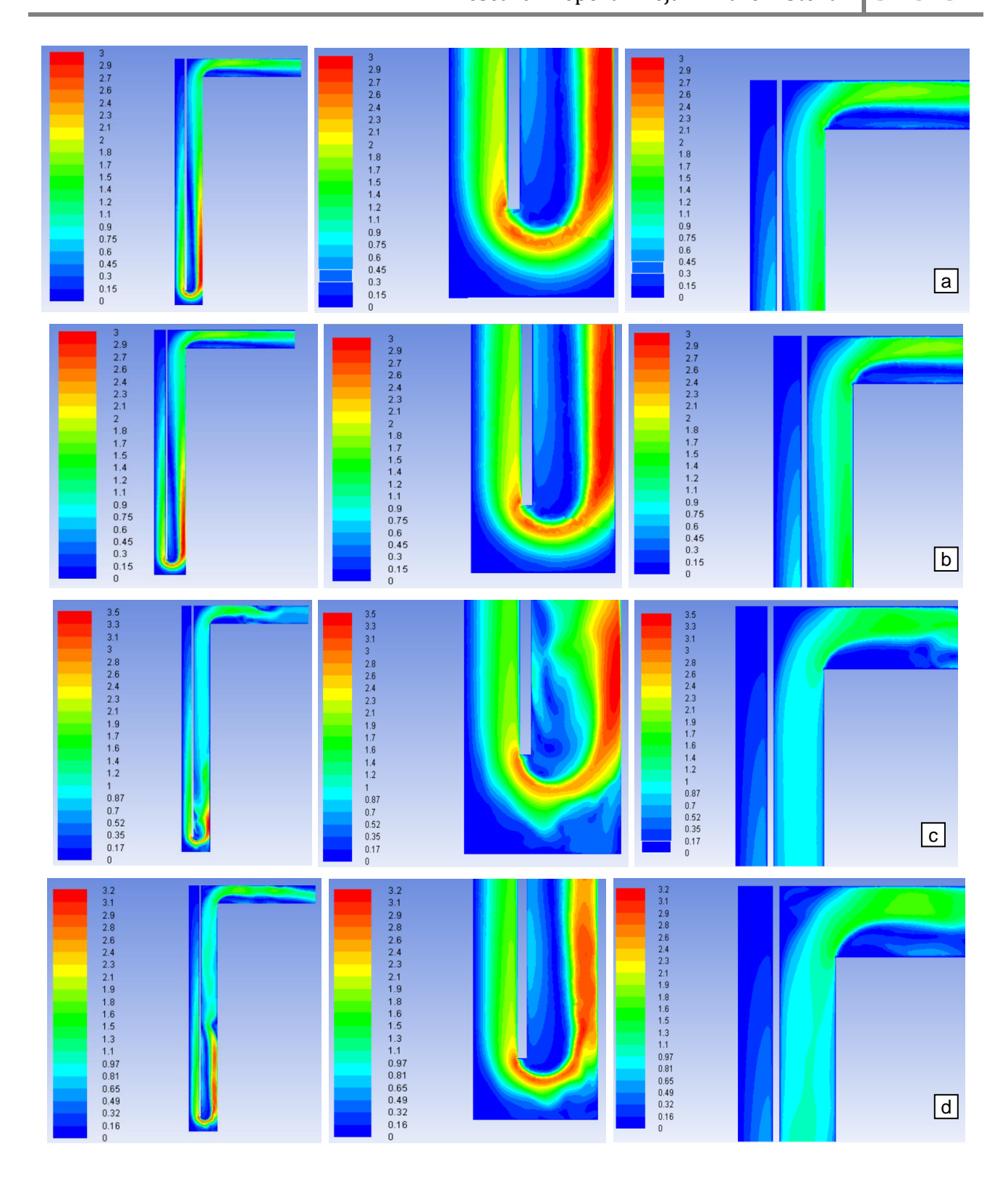


Figure 53 Temperature fields in longitudinal plane (symmetry): a) 0.2 (0.18), b) 0.66 (0.61), c) 1.3 (0.7), d) 2.8 (1), e) 5 (2.5), f) 6 (3.5) million elements (the legend represents temperature in °C)

Figure 53 shows the temperature fields in longitudinal plane (XY) for the 6 meshing levels chosen. It can be observed that for 0.2 and 0.66 million cells the temperature distribution is relatively similar and uniform and starting with 1.3 million cells it begins to change. However, starting with the 2.8 million cells, the temperature distribution begins to normalize again, while at 5 million and 6 million cells the results are virtually similar. It can be seen that at the bottom of the solar collector, the air flow temperature is higher due to the appearance of vortices and air circulation at a relatively low velocity, seen also at the top of the secondary cavity. In the zones where the temperatures are lower we can observe also high values of air velocities (Figure 54).



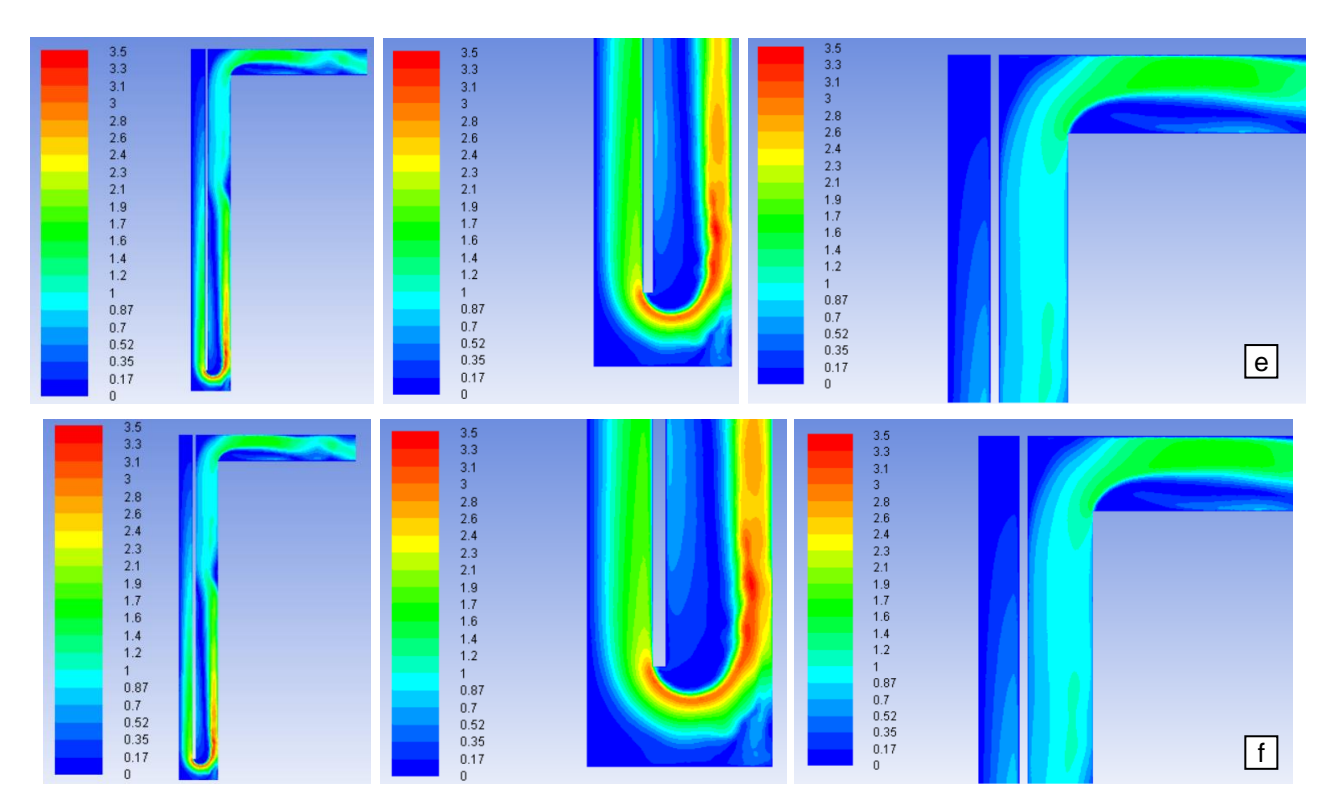


Figure 54 Velocity fields in longitudinal plane (symmetry): a) 0.2 (0.18), b) 0.66 (0.61), c) 1.3 (0.7), d) 2.8 (1), e) 5 (2.5), f) 6 (3.5) million elements (the legend represents velocity in m/s)

Figure 54 shows the velocity fields in the longitudinal planes (XY) for the 6 meshing levels. It can be noticed that for 0.2 and 0.66 million cells the velocity distribution is relatively similar and uniform, while starting with 1.3 million cells it changes similarly to the temperature field. However, starting with the 2.8 million cells, the velocity distribution begins to stabilise, while the results of 5 million and 6 million cells are virtually similar. It can be also observed that at the bottom of the solar collector in the second cavity, the air velocity near the wall increases because of the PCM obstacle presence which causes the apparition of vortices in the vicinity of the chicane and determines the temperature to increase (Figure 55).

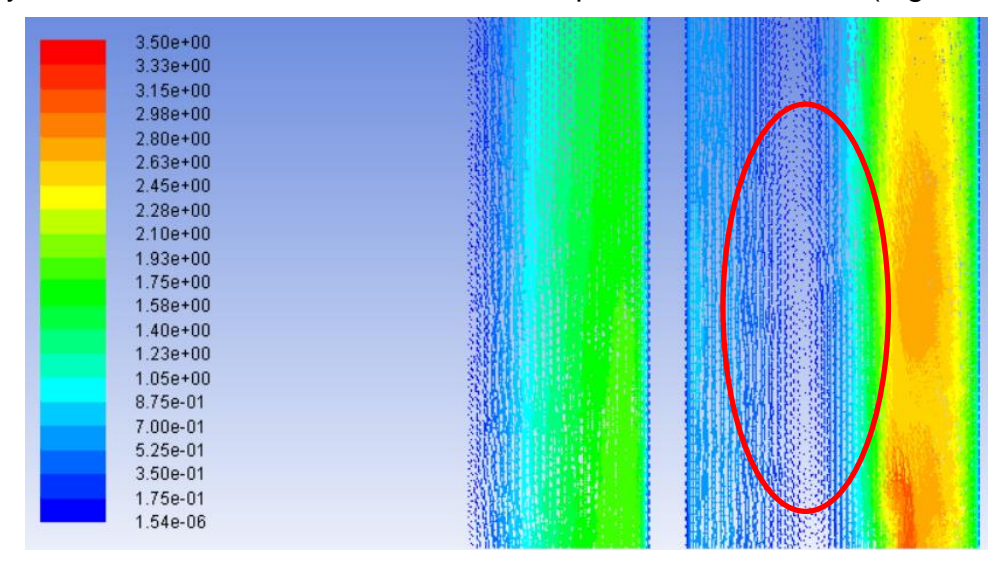


Figure 55 Velocity vectors in longitudinal plane - vortices

In order to conclude, after conducting the mesh independency study, taking into account the above-mentioned aspects, I decided to continue by using the 5 million element mesh because it determines a mesh independent solution (figure 56). This grid is complementary to the mesh presented in Figure 49e and also highlights the mesh obtained for the PCMs cavity.

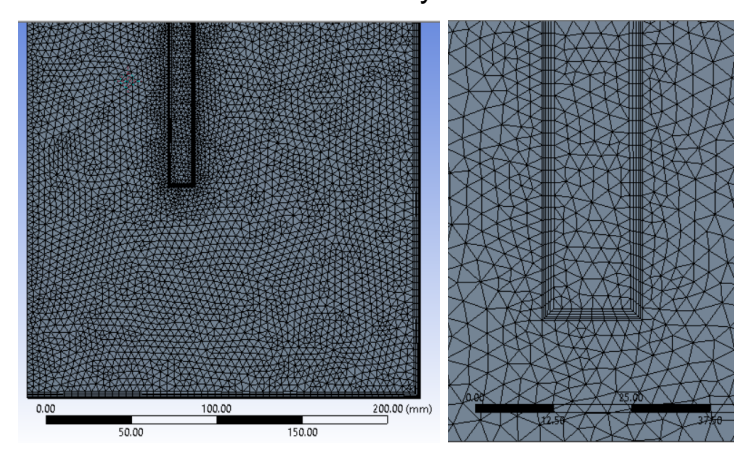


Figure 56 The mesh which will be used – the final case with PCM (5 million elements)

## 5.3. Experimental validation of the numerical model – comparison of the temperature variation

After the mesh independency study presented in the previous chapter, the experimental validation of the numerical model of the solar collector with lobed holes and embedded phase change materials will be conducted. Validation will be realised in two stages. In the first stage we will obtain the temperature variation on 10De in transient regime using the model analysed in Chapter 4 and we will compare it with the measurements made. The temperature variation at 10De will then be imposed on the large scale model (the "slice" through the collector) as boundary conditions.

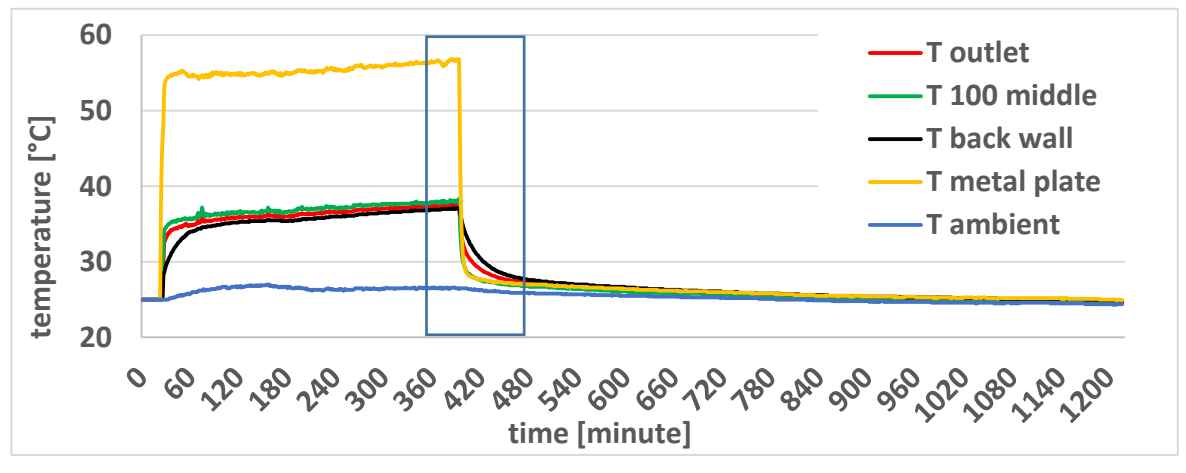


Figure 57 Time interval extracted from the experimental study for the experimental validation – hours, respectively 7200 seconds

In order to validate the model within a feasible time frame, we decided to extract 120 minutes from the experimental results (figure 57) that comprises the main stages (variation levels) of the phenomena studied, namely: heating – absorbing the energy (I), stopping the solar radiation (II) and cooling – slow release of the embodied energy (III). These stages are shown in Figure 58 which emphasises the ambient temperature variation (air aspirated through the lobed orifices) and the metal plate temperature variation during 120 minutes. The variations of the two values are required as input data (boundary conditions) in order to determine the outlet temperature variation, respectively at 10De.

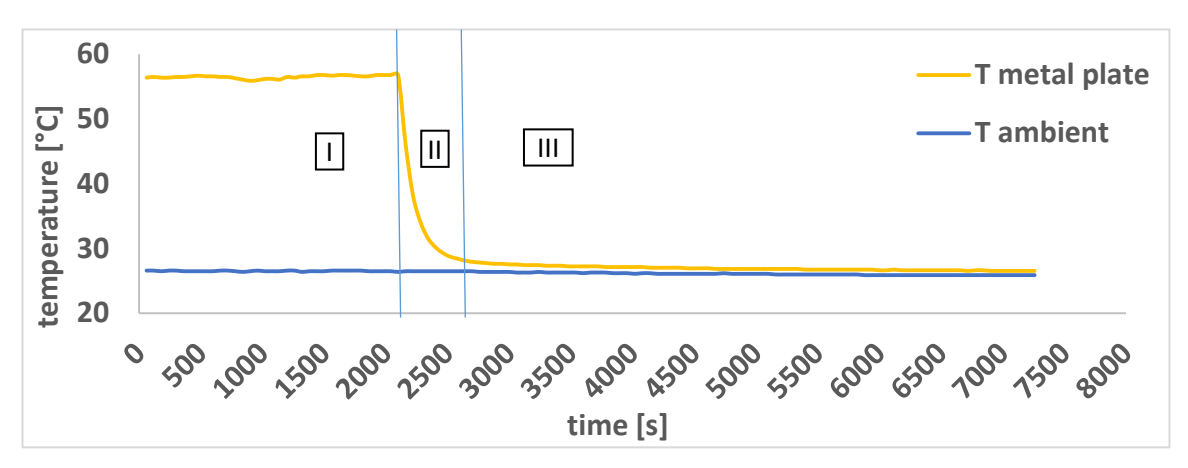


Figure 58 Ambient temperature variation and metal plate temperature variation – the three stages of the phenomena during 120minutes of experimental campaign

In order to in introduce in ANSYS Fluent the variation of a boundary condition in transient regime it is necessary to define a custom function named User Defined Function – UDF. This is a program made in the C ++ programming language that calculates the variation of temperature depending on the time. In order to create this program it is necessary to divide the experimental results into three distinct functions corresponding to the three phenomena stages mentioned above.

The first stage of temperature variation – heating (I) is characterized by a linear variation and it is emphasised in Figure 59-I, where we can find also the equation describing the phenomena. Moreover in the same figure is presented also the linear equation describing the ambient temperature variation. The second stage of the metal plate temperature variation (II) coincides with the sudden stop of the lamps that simulate the solar radiation which determines a rapid temperature drop and it is characterized by a 4<sup>th</sup> degree polynomial equation. Finally, the third stage of temperature variation – cooling (III) is also characterized by a linear equation and describes a slow discharge.

The equations corresponding to the three stages of the metal plate temperature variation and the ambient temperature variation are shown in the figures below.

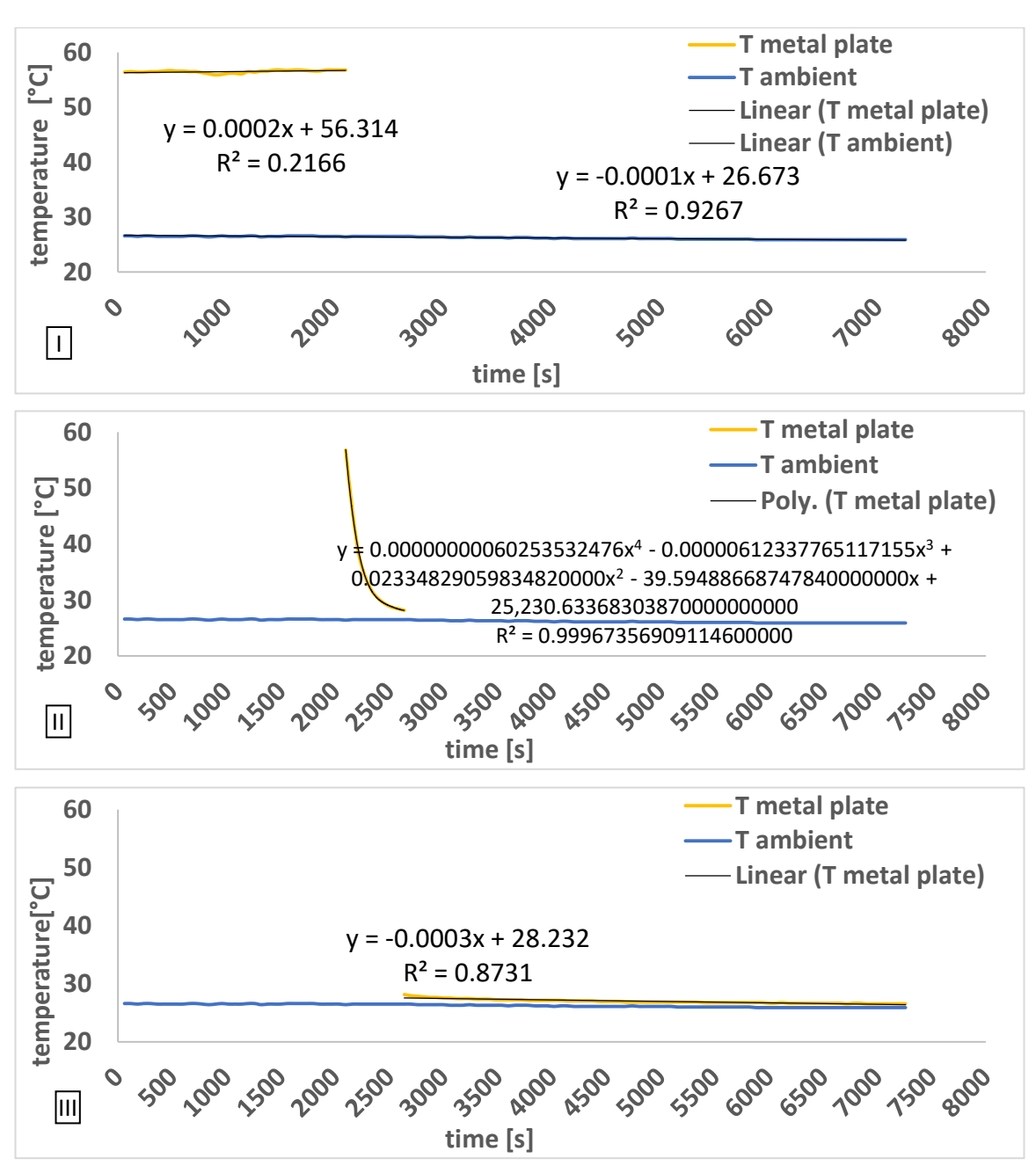


Figure 59 Extracting the metal plate temperature variation equation and ambient air temperature variation equation in order to obtain variable boundary conditions (UDF): heating (I), stopping solar radiation (II) and cooling(III)

After obtaining the four equations needed, we have implemented the C ++ program which will determine the introduction of variable boundary conditions in the numerical model realized in Fluent. The program has gone through several test phases, and its final form is presented below:

```
#include "udf.h"
DEFINE_PROFILE(Tmetal, thread, position)
{
```

```
face_t f;
real t = CURRENT_TIME;
begin_f_loop(f, thread)
              if (t \le 2100)
              F_PROFILE(f, thread, position) = 273.15 + 0.0002*t + 56.314;
              else if (2100 < t && t <= 2640)
              F_PROFILE(f, thread, position) = 273.15 + (6.0253532476*pow(10,-10.00))
                                      (6.12337765117155*pow(10,-6))*pow(t,3)
              10))*pow(t,4)
              0.0233482905983482*pow(t,2)
                                                          39.5948866874784*t
              25230.6336830387;
              else if (t > 2640)
              F_PROFILE(f, thread, position) = 273.15 - 0.0003*t + 28.232;
      }
end_f_loop(f, thread)
}
DEFINE_PROFILE(Tinlet, thread, position)
{
face_t f;
real t = CURRENT_TIME;
begin_f_loop(f, thread)
      {
              F_PROFILE(f, thread, position) = 273.15 - 0.0001*t + 26.673;
      }
end_f_loop(f, thread)
}
```

After creating the UDF required for the transient study I set the case of the numerical model according to chapter 4. We used the k-ε RNG turbulence model and the boundary conditions presented in table 8. We also used the surface temperature monitoring function in order to obtain graphs with respect to time variation. To start from a stable solution we run the calculation on a permanent basis and after stabilizing the solution we set the case for the numerical simulation in the transient regime imposing the following conditions: 20s time step, 360 steps (7200 seconds) and 10 iterations for every time step.

**Table 8.** Boundary conditions for the model used in order to simulate the airflow through lobed orifices in transient regime

Boundary condition	Value	Unit
Velocity magnitude (v ambient)	0.055	m/s
Inlet temperature (T ambient)	Variable according to UDF	
Metal plate temperature (T metal plate)	Variable according to UDF	

In order to compare the results of the numerical study with those of the experimental study we added to the experimental setup a temperature sensor placed at 5 cm distance from the absorbent plate. The overlapped results of the numerical simulation and experimental measurements are shown in Figure 60. As it can be observed, the variation of the ambient temperature and the variation of the metal plate temperature respect the equations imposed as variable boundary conditions. Moreover, the temperature variation at 10De (Toutlet) in the numerical study respects the values from the experimental study, all curves being virtually the same with very small differences.

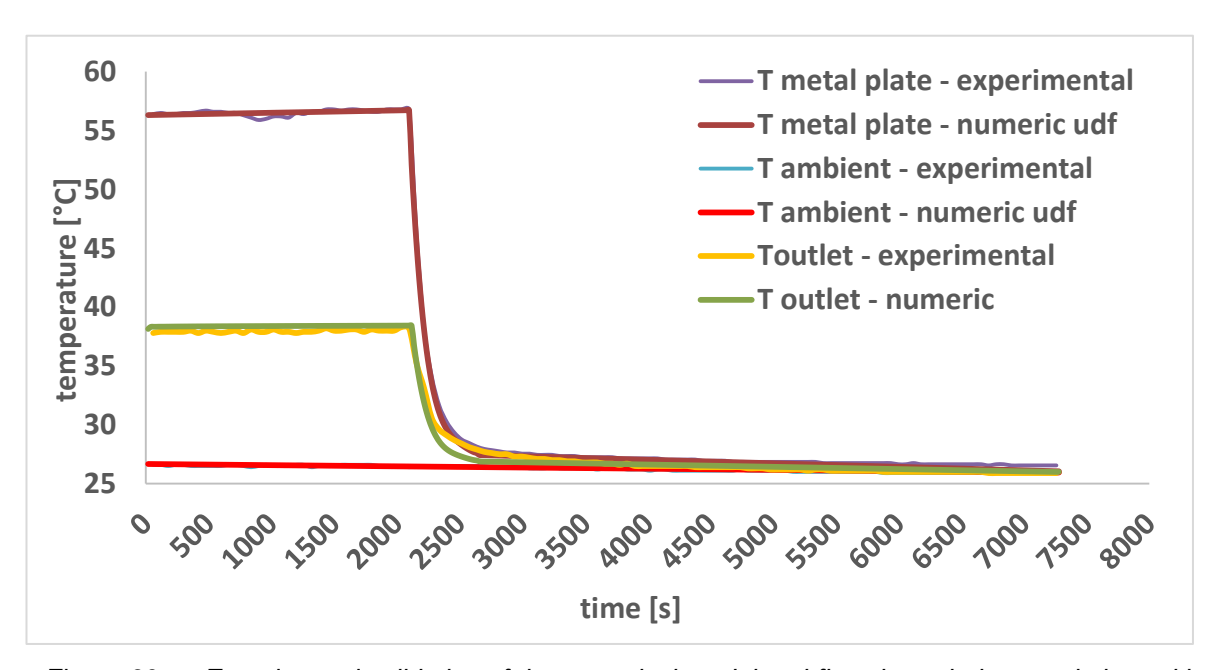


Figure 60 Experimental validation of the numerical model – airflow through the metal plate with lobed orifices

After the validation in transient regime of the numerical model analysing the airflow through the metal plate with lobed orifices, the experimental validation of the solar collector model with integrated phase change materials follows. In this regard, at the geometry and mesh created for the air cavity I added the geometry and mesh related to the phase changing materials (Figure 61). The result is a mesh made of 5 million cells (2.5 million for the air cavity and 2.5 million the PCM).

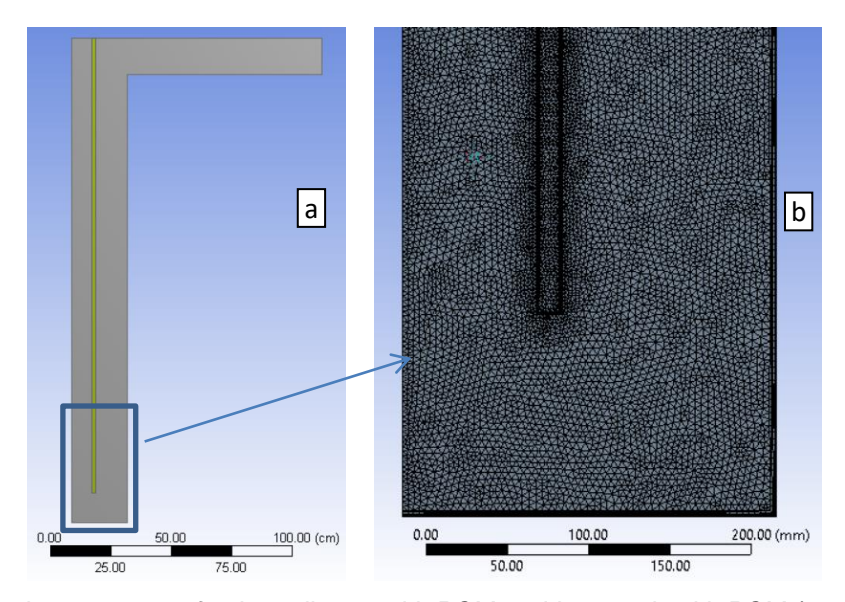


Figure 61 a - the geometry of solar collector with PCM and b – mesh with PCM (5 mil. cells)

After importing the mesh into the Fluent solver I began to set the numerical model case. Therefore, I activated the model using the energy conservation equation and the k- $\Omega$  SST turbulence model according to the previous chapter. The next step was to define the materials used in the numerical study: air and phase change materials. The air properties were taken from the ANSYS Fluent database. For the PCMs we used paraffin RT35 properties presented in Table 9 and used in the experimental study.

**Table 9.** Characteristics of the PCM use in the experimental and numerical studies [88]

Characteristic	Value	Unit
Supplier	Rubitherm	
Model	RT 35 (paraffin)	
Melting temperature	29-36 (main peak: 33)	°C
Solidification temperature	36-31 (main peak: 35)	°C
Heat storage capacity ±7.5% (sensible + latent in the 26-41°C range)	160	kJ/kg
Heat storage capacity ±7.5% (sensible + latent in the 26-41°C range)	45	Wh/kg
Specific heat capacity	2	kJ/kg·K
Density solid (15°C)	0.86	kg/l
Density liquid (45°C)	0.77	kg/l
Heat conductivity (both phases)	0.2	W/m·K
Volume expansion	12.5	%
Max. operating temperature	65	°C

In order to simplify the numerical model, we first considered that the PCMs are solid and have a specific heat capacity variable depending on the temperature. The stored/released energy variation by the PCM at every 1°C variation is

presented in figure 62 and it was introduced in ANSYS Fluent as a material variable property. In this manner, the numerical model takes into account the thermal effect of the PCMs, neglecting the phenomenon which occurs in the rectangular cavity, including the effect of natural convection and solidification/melting processes. The storage capacity is presented as a sum of sensible heat and latent heat.

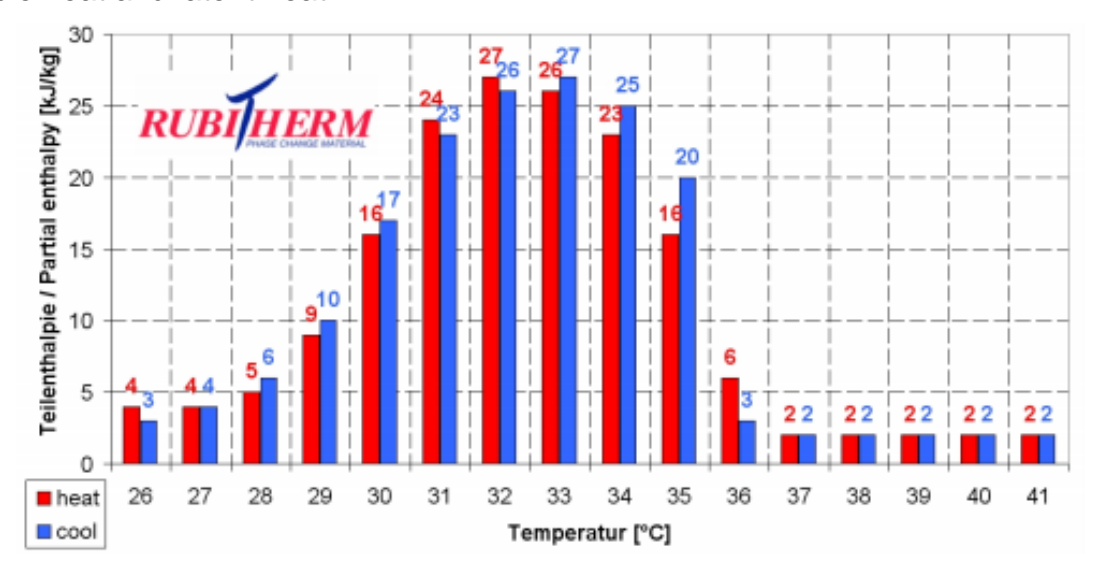


Figure 62 Energy storage capacity variation depending on the temperature [88]

In order to determine the air temperature of the air on the solar collector outlet (T outlet) it is necessary to know the air temperature variation in the 1<sup>st</sup> cavity at 10De and the initial temperature of the phase change materials. To achieve the experimental validation of the numerical model over a feasible time period, we used the same 120-minute study interval and the experimental results being highlighted in Figure 63.

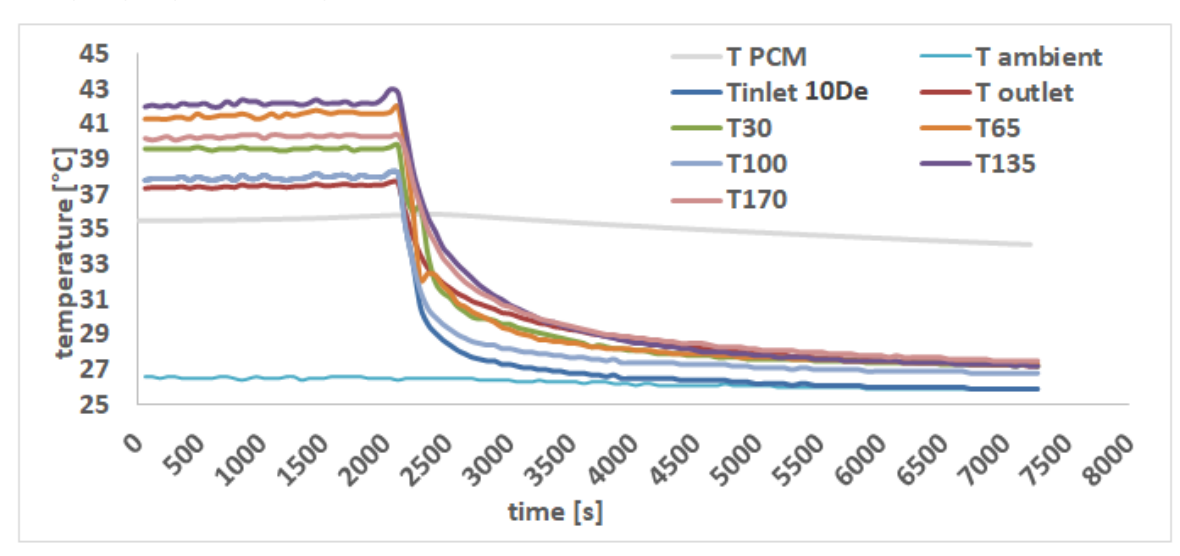


Figure 63 Temperature variation in the case of experimental studies – 120 minutes

In order to impose as boundary condition at the inlet the temperature variation at 10De we used the experimental results instead of the numerical ones presented above, which are practically similar. In order to run the numerical simulation, it is necessary to measure also the temperature of the PCMs, therefore

another temperature sensor was added to the experimental setup in order to measure the temperature on the PCM recipient. To create the program that describes the temperature variation at 10De in the C++ protocol it is necessary to split the results in three stages, similar with the previous case (figure 64).

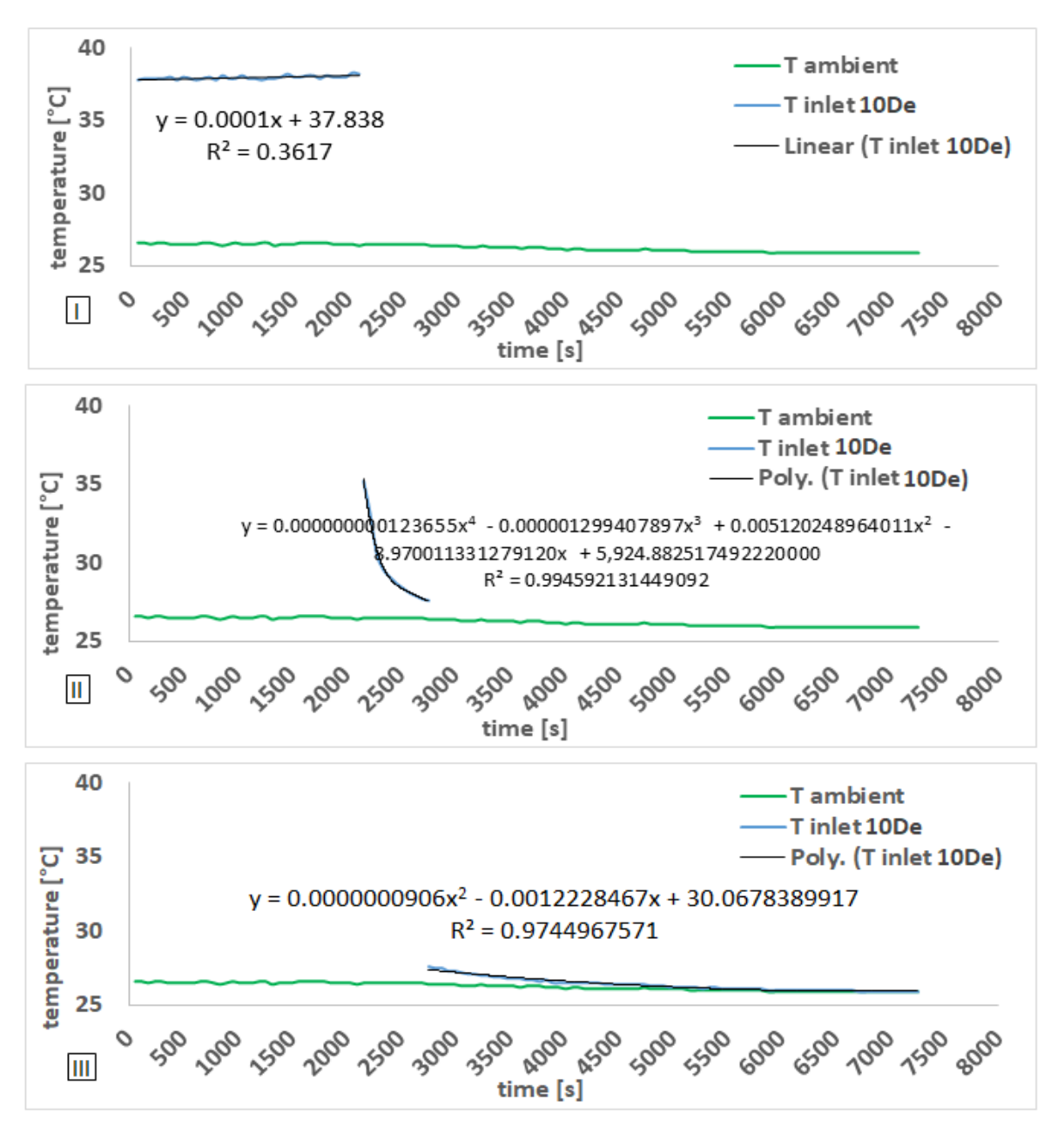


Figure 64 Extraction of temperature variation at 10De in order to obtain the variable boundary conditions (UDF): heating (I), stopping the solar radiation (II) and cooling (III)

The first stage of temperature variation – heating (I) is characterized by a linear variation and it is emphasised in Figure 64-I, where we can find also the equation describing the phenomena. The second stage of the 10De zone temperature variation (II) coincides with the sudden stop of the lamps that simulate the solar radiation which determines a rapid temperature drop and it is

characterized by a 4<sup>th</sup> degree polynomial equation. Finally, the third stage of temperature variation – cooling (III) is also characterized by a 2<sup>nd</sup> degree polynomial equation and describes a slow discharge.

After obtaining the three equations needed, we have implemented the C ++ program which will determine the introduction of variable boundary conditions in the numerical model realized in Fluent. The program has also gone through several test phases, and its final form is presented below:

```
#include "udf.h"
DEFINE_PROFILE(Tinlet, thread, position)
{
face tf;
real t = CURRENT_TIME;
begin_f_loop(f, thread)
             if (t \le 2100)
             F_PROFILE(f, thread, position) = 273.15 + 0.0001*t + 37.838;
             else if (2100 < t \&\& t <= 2760)
             F_PROFILE(f, thread, position) = 273.15 + 0.000000000123655*pow(t,4) -
             0.000001299407897*pow(t,3)
                                                   0.005120248964011*pow(t,2)
             8.97001133127912*t + 5924.88251749222;
             else if (t > 2760)
             F_PROFILE(f, thread, position) = 273.15 + 0.0000000906*pow(t,2) -
             0.0012228467*t + 30.0678389917;
end_f_loop(f, thread)
```

The boundary conditions used within the numerical study conducted are shown in Table 10. Temperature variation at 10De is determined by the UDF presented above and the velocity fields were imported for the 50 faces as a result of the study presented in Chapter 4. Moreover, temperatures were also monitored in different points of the numerical model solar collector as well as the average surface temperatures. The Fluent Solver gives the possibility of setting an initial temperature for a particular material. The initial temperature in the present case for PCM is 35.5 ° C ("patch" function in the initialization), with respect to the experimental results.

Value

Unit

**Table 10.** Boundary conditions use in case of experimental validation of the solar colector with integrated PCMs

	Velocity field obtained from the previous study	
Velocity magnitude (v inlet at 10De)	with values between 0.055-0.06 m/s for all 50	
	faces on the inlet	
Inlet temperature (T inlet 10De)	Variation imposed by the UDF created (user	
	defined function)	
PCM temperature (initial temperature imposed)	35.5	°C

**Boundary condition** 

To start from a stable solution I ran the simulation in the steady state regime and after stabilizing the solution I set the case for the numerical simulation in the transient regime imposing the following case conditions: 10s time step, 720 steps (7200 seconds) and 20 iterations on each time step. In addition to these settings, the case was also run for 1s, 5s, 10s, and 20s, respectively for 10 iterations, 15 interactions, 20 iterations, and 30 iterations. The conclusions were as follows: over 10s and less than 20 iterations, the phenomenon is not accurately rendered especially for the second stage of temperature variation (II).

In order to achieve the experimental validation of the numerical model of the solar collector with embodied PCMs I chose to compare the air temperature in the 2<sup>nd</sup> air cavity, in the middle of it at 100cm from the bottom part of the collector (T100). In figure 65 it is emphasised the T100 temperature variation both for the numerical study and experimental study.

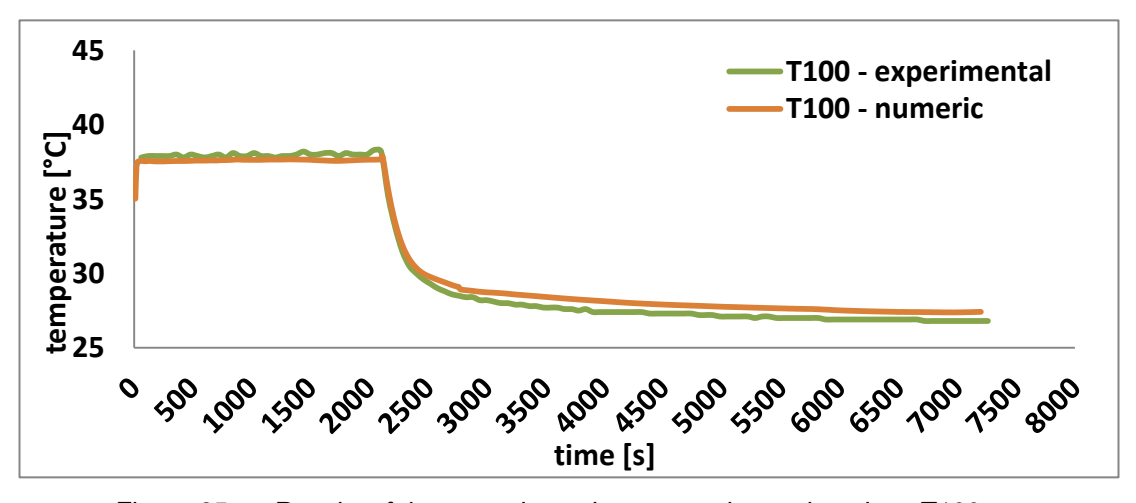


Figure 65 Results of the numeric study vs. experimental study at T100

Moreover, in order to validate the numeric model I also chose to compare the values obtained in the numerical study and in the experimental study for the air temperature variation at the collectors' outlet (Toutlet). In figure 66 we can observe the overlapped results. The temperature variation at 10De respects the variation imposed by the UDF created. Moreover, the allure of the exhaust air temperature variation curve (Toutlet) obtained in the case of numerical simulation is similar with the one obtained in an experimental manner with small differences that can be determined by the fact that the numerical model is a simplified one and doesn't

comprises all the solar collector components which can contribute to the thermal inertia of the systems (e.g.: OSB, thermal insulation etc.). By comparing the values obtained experimentally with the ones achieved in a numerical manner we can conclude that the numerical model created reproduces the real heat transfer phenomena within acceptable limits.

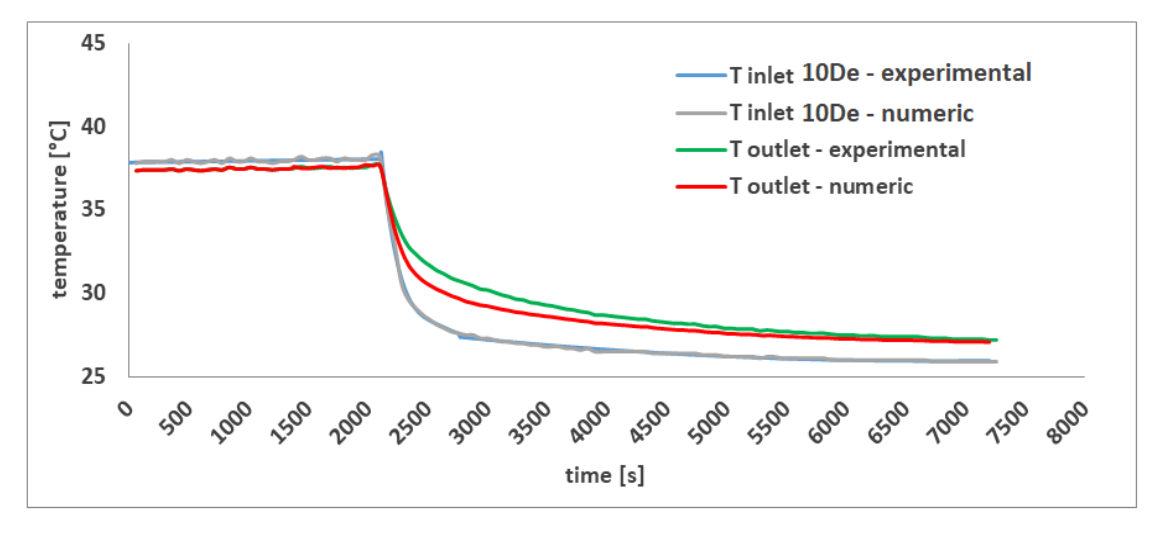


Figure 66 Results of the numeric study vs. experimental study: Toutlet and Tinlet

### 5.4. Final parameters of the numerical model and results

By considering the analyses elaborated in this chapter, we can conclude the final parameters of the numerical model that studies the solar collector with integrated phase changing materials.

The geometry is based on a simplified concept which represents a slice through the solar collector, the inlet in the computing domain consisting of 50 faces whose boundary limits (especially velocity fields) where obtained from the model that studies the airflow through the absorbent metal plate with lobed orifices.

According to the mesh independency study the geometry with 5 million tetrahedral cells has resulted to be the one that will not influence the results of the numerical simulations while being a stable solution. The mesh presents 2.5 million cells in the solar collectors' air cavity and 2.5 million cells in the PCMs enclosure.

The energy conservation model and k- $\Omega$  SST turbulence model (with corrections for a small Reynolds numbers as the case studied and curvature corrections etc.) have been chosen for the numerical case. According to the literature this kind of turbulence model is suitable for the time of airflow studied. Having the temperature values at different points from the experimental study, we did not use the heat transfer model for radiation in order to obtain a simplified model and to facilitate as much as possible the calculations. This model will be developed in the further studies and will underpin the continuation of post-doctoral studies.

For the air circulated in the computing domain I chose from the ANSYS Fluent database the corresponding properties, moreover regarding the PCMs I introduce the paraffin RT35 characteristics and I considered that the material is in solid state having the specific heat variable with temperature. Although the melting and solidification processes cannot be studied in this case, the thermal impact of PCMs is reproduced with accuracy. For the variable boundary conditions I used the velocity profiles obtained in the previous model and in order to study the collector in transient regime I have imposed user defined functions (UDFs) create in C++ programming language. Furthermore, for initialization I have imposed an initial temperature for the PCM.

The interpolation scheme used is "second order upwind" for the analysis of convective terms and the pressure-speed coupling scheme is determined by the "SIMPLE" algorithm. According to the studied literature, the convergence of the solution is achieved when the non-dimensional residuals of the flow equations are less than 10<sup>-3</sup>; as a result, in order to obtain the relevant results we have imposed a value less than 10<sup>-5</sup>. Typical images for the convergence of non-dimensional residues are shown in the figure below.

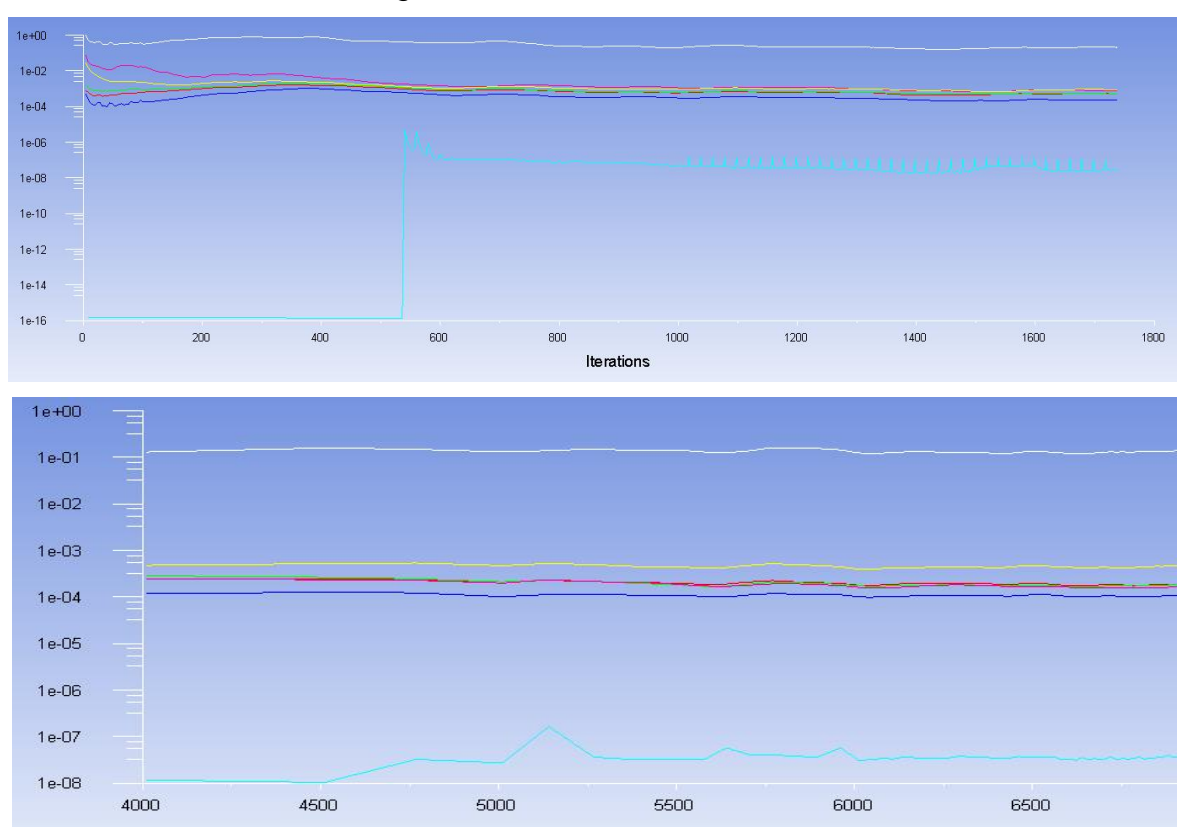


Figure 67 Typical images for the convergence of non-dimensional residues for the transient regime simulation: a – until 1700 iterations (until 550 iterations – steady state regime), b – after 4000 iterations

The model created will be further developed and studied in depth within the doctoral studies and after, the model presented being a preliminary simplified model. This model will underpin some complex parametric studies used to optimize the solar collector characteristics such as geometry or phase changing temperature. Below are presented temperature and velocity fields and profiles for

the solar collector with integrated PCMs in different stages of the numerical study conducted.

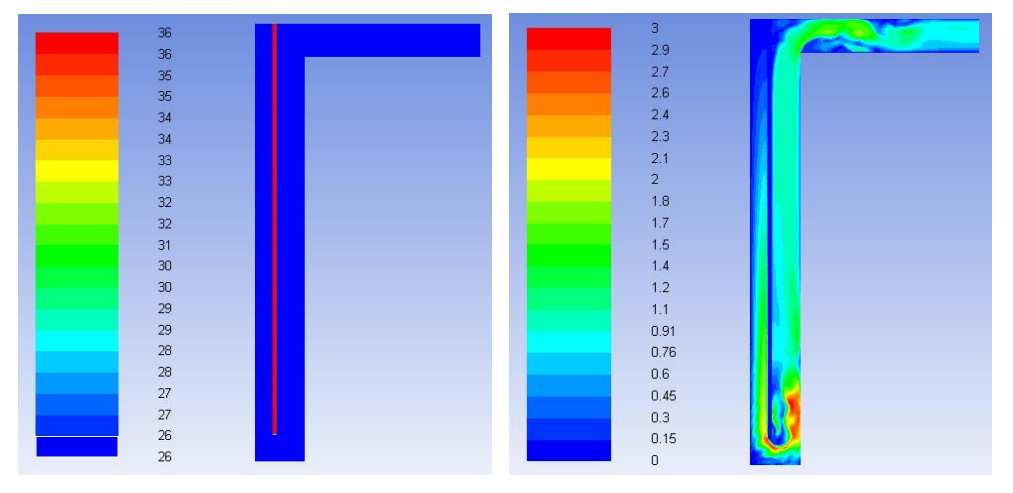


Figure 68 The results of the numerical study in steady state regime after 550 iterations (starting point for the transient regime study): a – temperature field, b – velocity field

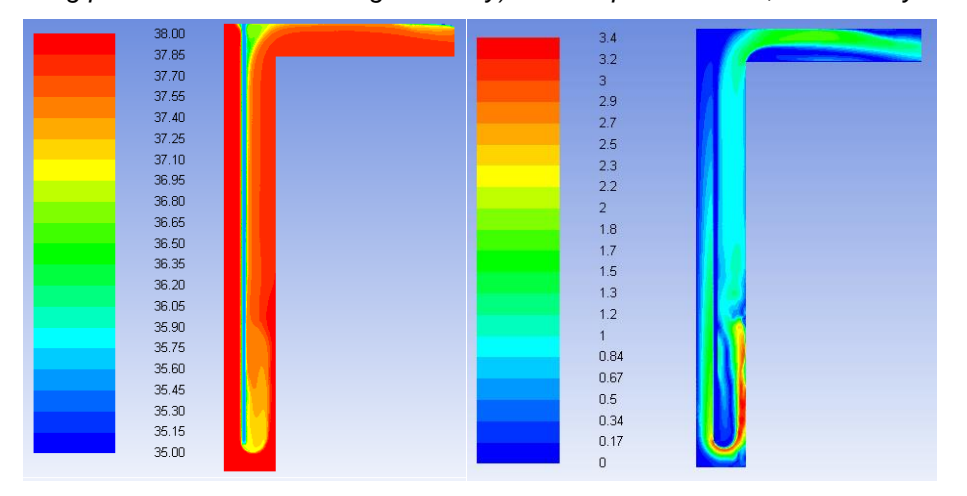


Figure 69 The results of the numerical study in transient regime after 600s: a – temperature field, b – velocity field

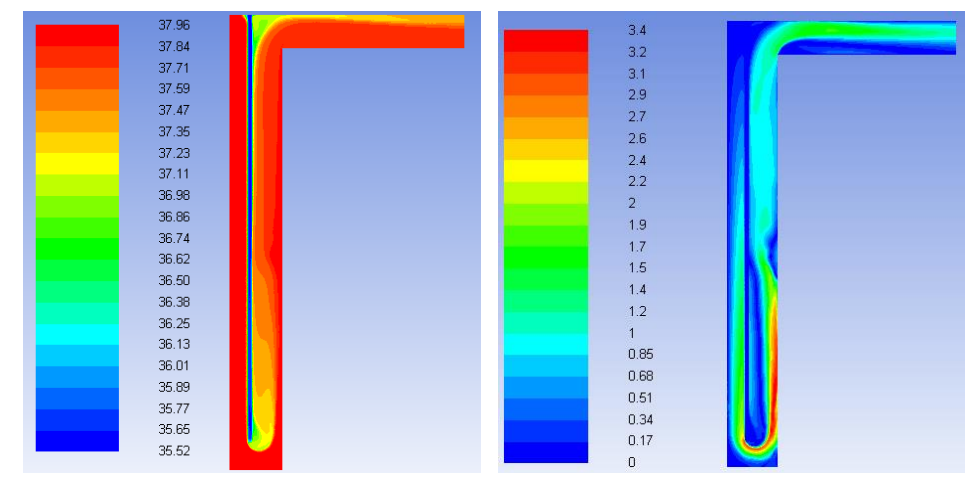


Figure 70 The results of the numerical study in transient regime after 1200s: a – temperature field, b – velocity field

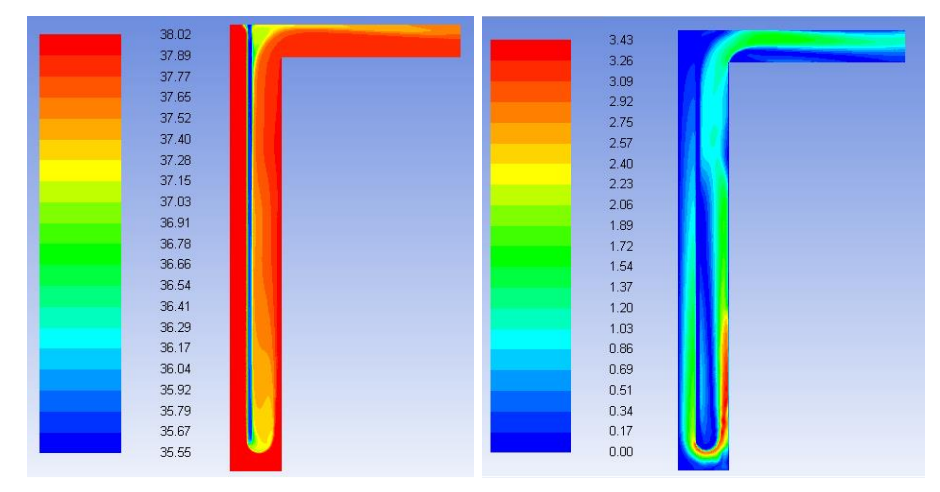


Figure 71 The results of the numerical study in transient regime after 1800s: a – temperature field, b – velocity field

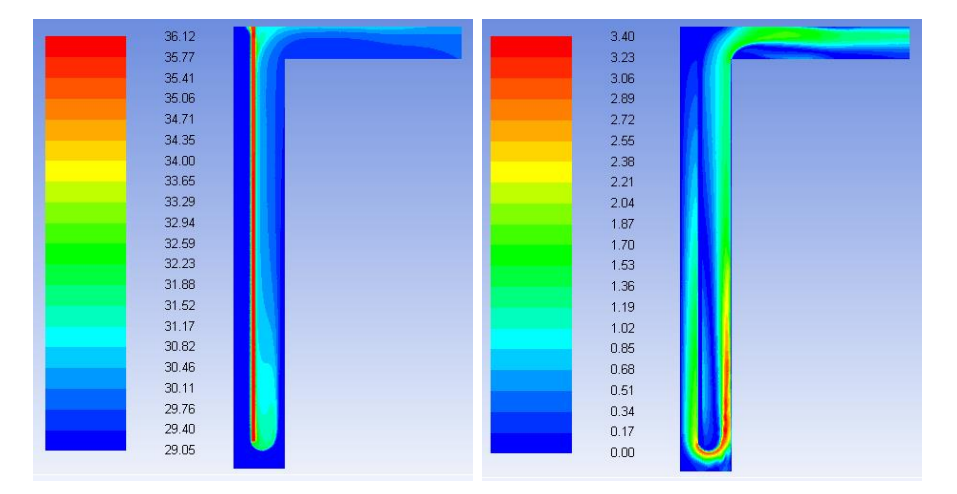


Figure 72 The results of the numerical study in transient regime after 2400s: a – temperature field, b – velocity field

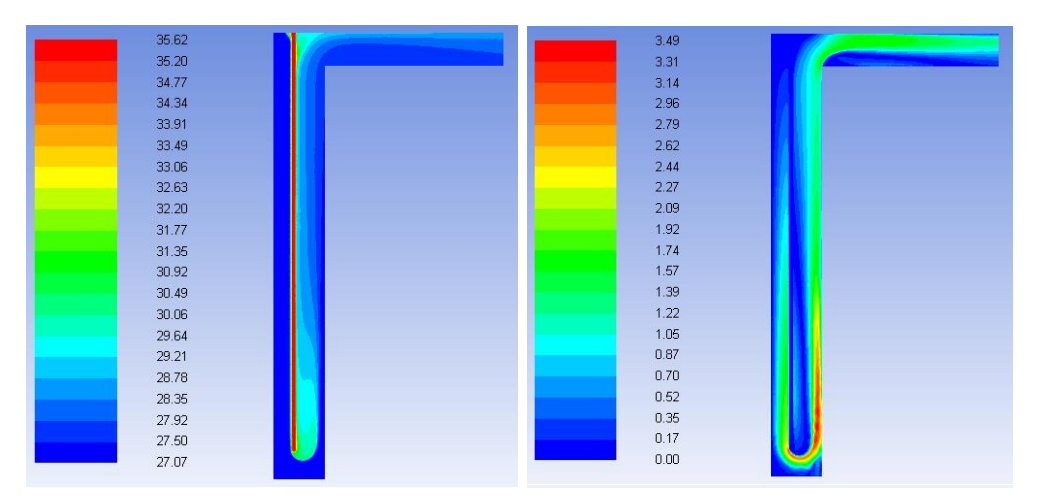


Figure 73 The results of the numerical study in transient regime after 3000s: a – temperature field, b – velocity field

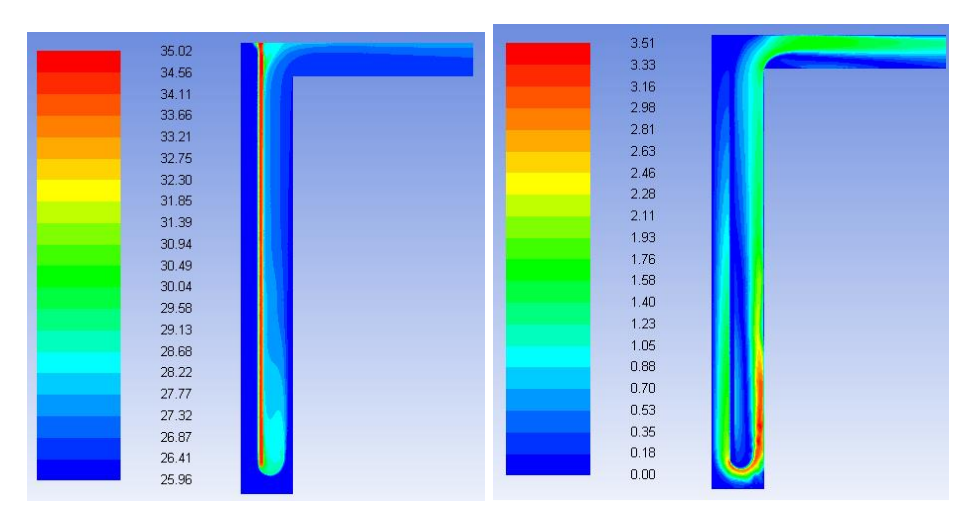


Figure 74 The results of the numerical study in transient regime after 7200s: a – temperature field, b – velocity field

### 6. Conclusions and perspectives

The current paper represents the third report within doctoral studies and presents the state of preliminary numerical studies conducted so far. The three research reports were structured as follows:

- a) Research Report no. 1, respectively the complex bibliographic study on the implementation of phase changing materials (PCMs) in buildings and solar collectors
- b) Research Report no. 2, respectively the experimental study regarding the implementation of phase changing materials within air solar collectors
- c) Research Report no. 3 (the current one), respectively the experimental study regarding the implementation of phase changing materials within air solar collectors.

The first report presents the complex bibliographic analysis carried out at the beginning of doctoral studies regarding the opportunity of implementing PCMs in buildings. According to the bibliographic study, the PCMs have not been implemented so far in transpired solar collectors, this system being an absolute novelty in literature. The solar collector with lobed geometry has the potential to increase thermal transfer and to increase the efficiency of the solar collector. Moreover, the TES materials have the potential to contribute to the improvement of temperature variations at collectors' outlet and to store large amounts of energy during the periods when the solar radiation is available and use it during when is needed (cloudy periods or during the night). The biggest advantage of the PCMs is that they have a very high energy storage capacity due to the latent heat stored during the phase change and that they occupy less space than the conventional materials like concrete for example.

The second report deals with the preliminary experimental studies carried out regarding the implementation of phase change materials integrated into transpired solar collectors that were further developed. Solar collectors with

embedded inertial materials have the potential to reduce energy consumption for space heating, reduce power consumption for fresh air preheating which is needed by the building occupants, dry indoor air, maintain a minimum safety temperature inside buildings and improve indoor thermal comfort. By using the PCMs integrated in the solar collectors, the number of hours of functioning increases thus improving its overall efficiency.

The present paper represents the third report within the doctoral program and studies the numerical modelling of TSCs with integrated PCMs. The report is structures in 5 main chapters addressing important aspects of the numerical analyses on the system proposed.

The first chapter of the present paper studies the current state of research regarding the numerical modelling of solar collectors and phase changing materials. One of the most used software in these cases is ANSYS Fluent and the main stages that must be achieved in a CFD study are:

- a) Creating the geometry of the model
- b) Creating the calculation grid mesh independency study
- c) Imposing boundary conditions and configuring the numerical case
- d) Validating the numerical model by comparing the numerical results with the experimental ones
- e) Calculation of the solution and post processing.

All the stages above are analysed in chapters 4 and 5. In the 2<sup>nd</sup> chapter it is emphasised the geometry of the real solar collector that was imported in Fluent. Moreover, a synthesis of the experimental results obtained until now is presented which will be used in order to experimentally validate the numerical models developed. In the time remained within the doctoral studies and afterwards the experimental studies will be completed and finalized in both the transient and permanent regime.

The 3<sup>rd</sup> chapter emphasises the objective of the present study, respectively:

- a) Numerical modelling of the airflow through the lobed orifices (absorbent metal plate)
- b) Designing the numerical model of the TSC with integrated PCMs

Moreover, the 3<sup>rd</sup> chapter presents the software and hardware infrastructure use for the numerical studied conducted, which is part of the Faculty of Building Services Engineering laboratories (Technical University of Civil Engineering Bucharest).

Chapters 4 and 5 are the most important chapters which are defining the present paper. Chapter 4 analyses the numerical model that studies the airflow through the lobed orifices. This study has the purpose to obtain the results at 10De distance from the metal plate that will be used as inlet data for the numerical model of the solar collector with PCMs and could be further used in order to study the impact of collectors' geometry. The simplified model analyses 4 equivalent orifices from the solar collector in order to optimize the computing time. A mesh independency study was conducted and we conclude that the geometry with 5.3

million cells determines an independent and stable solution and can be use further. The experimental validation was realised by comparing the velocity fields in longitudinal planes and also by comparing the air temperature on the outlet. The ANSYS Fluent case created is described by the energy conservation model and turbulence model k-ε RNG (with EWF) according to the literature and proper boundary conditions were imposed. By comparing the results obtained in an experimental manner with the numerical results at Re2500 we could conclude that the numerical model created reproduces the real phenomena in acceptable limits. Moreover, starting with 10De velocity profiles are similar, which confirms the premises assumed in the construction of geometry.

Having the temperature values at different points from the experimental study, we did not use the heat transfer model for radiation in order to obtain a simplified model and to facilitate as much as possible the calculations. This model will be developed in the further studies and will underpin the continuation of post-doctoral studies. This numerical model developed in the 4<sup>th</sup> chapter will be further used in order to:

- Study the impact of the orifices geometry on the solar
- Realise parametrical studies to optimize the solar collectors and its characteristics
- Obtaining boundary conditions for the solar collector with integrated PCMs.

The fifth chapter analyses the numerical model of the transpired solar collector with lobed orifices and integrated PCMs. The geometry created in ANSYS respects the real collector geometry, being practically a "slice" through it. The inlet in the computing domain is represented by 50 faces which will get as boundary conditions the outlet values of the model studied before, especially velocity profiles. Similar with the previous case a mesh independency study was conducted resulting that the mesh with 5 million cells (2.5 million in the air cavity and 2.5 million in the PCM enclosure) is the optimum solution in this case. The ANSYS Fluent case created is described by the energy conservation model and turbulence model k-Ω SST turbulence model (with corrections for a small Reynolds numbers as the case studied and curvature corrections etc.). This is one of the most feasible turbulence models and it is suitable, according to the literature, for small Reynolds numbers and for airflows within rectangular air cavities. In order to experimentally validate the numerical model in transient regime I used variable boundary conditions by creating user defined functions in C++ programming language. Also, to simplify the numerical model I considered that the PCMs are in solid state and they have a specific heat variable with temperature. By comparing the results obtained in an experimental manner with the numerical results at we could conclude that the numerical model created reproduces the real thermal transfer phenomena in acceptable limits.

Having the temperature values at different points from the experimental study, we also did not use the radiation heat transfer model in order to obtain a simplified model and to facilitate as much as possible the calculations. This model will be developed in the further studies and will underpin the continuation of post-

doctoral studies. This numerical model developed in the 5<sup>th</sup> chapter will be further used in order to:

- Parametrical studies and optimisation of the solar collector (geometry, phase change temperature, quantity of PCM, positioning of the PCM, air flow rates etc.)
- The study of melting/solidification of PCMs

Furthermore, within the doctoral studies and after, the numerical models will be enhanced in order to obtain more precise results. Moreover, the cases created will be studied in transient regime in different conditions: different time steps, different number of time steps, different amount of iterations per time step etc.

### 7. Conferences and publications

#### Published:

- a) Andrei-Stelian Bejan, Abdelouhab Labihi, Cristiana-Verona Croitoru, Florin Bode, Mihnea Sandu - Experimental Investigation of the Performance of a Transpired Solar Collector Acting as a Solar Wall, Solar World Congress 2017 Abu Dhabi, EUA
- b) Andrei Bejan, Abdelouhab LABIHI, Cristiana Croitoru, Daniel Bordianu and Hassan Chehouani - Transpired Solar Collectors Energy Efficiency Improvement Using Inertial Materials, 2017 International Conference on ENERGY and ENVIRONMENT (CIEM), Bucharest, Romania
- c) Andrei Stelian Bejan, Abdelouhab Labihi, Cristiana Verona Croitoru, Tiberiu Catalina, Hassan Chehouani and Brahim Benhamou Experimental investigation of the charge/discharge process for an organic PCM macroencapsulated in an aluminium rectangular cavity, Advances in Heat and Mass Transfer for the Built Environment (EENVIRO Workshop 2017), Bucharest, Romania
- d) Andrei-Stelian Bejan, Abdelouhab Labihi, Cristiana Croitoru, Tiberiu Catalina - Air solar collectors in building use, Advances in Heat and Mass Transfer for the Built Environment (EENVIRO Workshop 2017), Bucharest, Romania
- e) A. Bejan, C. Croitoru, F. Bode, I. Nastase, M. Sandu, A. Labihi Inertial elements integration on thermal solar collectors, 4th International Conference On Building Energy, Environment (COBEE 2018), Melbourne, Australia
- f) A. Bejan, M. Sandu, L. Tacutu, C. Croitoru, I. Nastase Airflow study inside an enclosure with a PCM wall and a solar collector, Roomvent & Ventilation 2018 Conference, 2-5 June, Finland

#### In process of publication:

 a) A.S. Bejan, T. Catalina, D.B. Mocanescu, A. Ene - Experimental study of an innovative glazed solar air collector tested in real conditions, 1<sup>st</sup> Doctoral School Conference 2018, Romania







Figure 75 Results dissemination – Solar World Congress SWC 2017, Abu Dhabi, EUA



Figure 76 Results dissemination – EENVIRO Conference 2017, București, România



Figure 77 Results dissemination – LP2M2E Laboratory, Cadi Ayyad University, Marrakech, Morocco

#### REFERENCES

- 1. Reichl, C., et al., Comparison of modelled heat transfer and fluid dynamics of a flat plate solar air heating collector towards experimental data. Solar Energy, 2015. **120**: p. 450-463.
- 2. Goyal, R.K., G.N. Tiwari, and H.P. Garg, *Effect of thermal storage on the performance of an air collector: A periodic analysis.* Energy Conversion and Management, 1998. **39**(3–4): p. 193-202.
- 3. Lai, C.-M. and S. Hokoi, Solar façades: A review. Building and Environment, 2015. 91: p. 152-165.
- 4. Croitoru, C.V., et al., *Thermodynamic investigation on an innovative unglazed transpired solar collector.* Solar Energy, 2016. **131**: p. 21-29.
- 5. Dymond, C. and C. Kutscher, *Development of a flow distribution and design model for transpired solar collectors*. Solar Energy, 1997. **60**(5): p. 291-300.
- 6. Molineaux, B., B. Lachal, and O. Guisan, *Thermal analysis of five unglazed solar collector systems for the heating of outdoor swimming pools.* Solar Energy, 1994. **53**(1): p. 27-32.
- 7. Gao, L., H. Bai, and S. Mao, *Potential application of glazed transpired collectors to space heating in cold climates.* Energy Conversion and Management, 2014. **77**: p. 690-699.
- 8. Alkilani, M.M., et al., *Review of solar air collectors with thermal storage units*. Renewable and Sustainable Energy Reviews, 2011. **15**(3): p. 1476-1490.
- 9. Nkwetta, D.N. and F. Haghighat, *Thermal energy storage with phase change material—A state-of-the art review.* Sustainable Cities and Society, 2014. **10**: p. 87-100.
- 10. Leon, M.A. and S. Kumar, *Mathematical modeling and thermal performance analysis of unglazed transpired solar collectors*. Solar Energy, 2007. **81**(1): p. 62-75.
- 11. Zhang, T., et al., *The application of air layers in building envelopes: A review.* Applied Energy, 2016. **165**: p. 707-734.
- 12. Zhang, T., et al., A glazed transpired solar wall system for improving indoor environment of rural buildings in northeast China. Building and Environment, 2016. **98**: p. 158-179.
- 13. Rosaria Ciriminna, F.M., Mario Pecoraino, Mario Pagliaro, *Solar Air Heating and Ventilation in Buildings: A Key Component in the Forthcoming Renewable Energy Mix.* Energy Technology, 2017. **5**: p. 1-9.
- 14. Paya-Marin, M.A., et al., *Large scale test of a novel back-pass non-perforated unglazed solar air collector.* Renewable Energy, 2015. **83**: p. 871-880.
- 15. Shukla, A., et al., *A state of art review on the performance of transpired solar collector.* Renewable and Sustainable Energy Reviews, 2012. **16**(6): p. 3975-3985.
- 16. Brown, C., et al., *Transpired Solar Collector Installations in Wales and England.* Energy Procedia, 2014. **48**: p. 18-27.
- 17. Januševičius, K., et al., *Validation of Unglazed Transpired Solar Collector Assisted Air Source Heat Pump Simulation Model.* Energy Procedia, 2016. **95**: p. 167-174.
- 18. Wang, X., et al., A simplified method for evaluating thermal performance of unglazed transpired solar collectors under steady state. Applied Thermal Engineering, 2017. **117**: p. 185-192.
- 19. Van Decker, G.W.E., K.G.T. Hollands, and A.P. Brunger, *Heat-exchange relations for unglazed transpired solar collectors with circular holes on a square or triangular pitch.* Solar Energy, 2001. **71**(1): p. 33-45.
- 20. Croitoru, C., et al., *Thermal Evaluation of an Innovative Type of Unglazed Solar Collector for Air Preheating.* Energy Procedia, 2016. **85**: p. 149-155.
- 21. Hami, K., B. Draoui, and O. Hami, *The thermal performances of a solar wall.* Energy, 2012. **39**(1): p. 11-16.
- 22. Kisilewicz, T., *Glazed building wall as a solar thermal collector.* Archives of Civil and Mechanical Engineering, 2009. **9**(1): p. 83-99.
- 23. Navarro, L., et al., Experimental study of an active slab with PCM coupled to a solar air collector for heating purposes. Energy and Buildings, 2016. **128**: p. 12-21.

- Khadiran, T., et al., Advanced energy storage materials for building applications and their thermal performance characterization: A review. Renewable and Sustainable Energy Reviews, 2016. 57: p. 916-928.
- 25. Soares, N., et al., Review of passive PCM latent heat thermal energy storage systems towards buildings' energy efficiency. Energy and Buildings, 2013. **59**: p. 82-103.
- 26. Kylili, A. and P.A. Fokaides, *Life Cycle Assessment (LCA) of Phase Change Materials (PCMs) for building applications: A review.* Journal of Building Engineering, 2016. **6**: p. 133-143.
- 27. Memon, S.A., *Phase change materials integrated in building walls: A state of the art review.* Renewable and Sustainable Energy Reviews, 2014. **31**: p. 870-906.
- 28. Kalnæs, S.E. and B.P. Jelle, *Phase change materials and products for building applications: A state-of-the-art review and future research opportunities.* Energy and Buildings, 2015. **94**: p. 150-176.
- 29. Giro-Paloma, J., et al., *Types, methods, techniques, and applications for microencapsulated phase change materials (MPCM): A review.* Renewable and Sustainable Energy Reviews, 2016. **53**: p. 1059-1075.
- 30. Tyagi, V.V. and D. Buddhi, *PCM thermal storage in buildings: A state of art.* Renewable and Sustainable Energy Reviews, 2007. **11**(6): p. 1146-1166.
- 31. Waqas, A. and Z. Ud Din, *Phase change material (PCM) storage for free cooling of buildings—A review.* Renewable and Sustainable Energy Reviews, 2013. **18**: p. 607-625.
- 32. Zhou, D., C.Y. Zhao, and Y. Tian, *Review on thermal energy storage with phase change materials* (*PCMs*) in building applications. Applied Energy, 2012. **92**: p. 593-605.
- 33. Cabeza, L.F., et al., *Materials used as PCM in thermal energy storage in buildings: A review.* Renewable and Sustainable Energy Reviews, 2011. **15**(3): p. 1675-1695.
- 34. Mehling, H.C., Luisa F., *Heat and cold storage with PCM An up to date introduction into basics and applications.* Springer, 2008.
- 35. Konuklu, Y., et al., Review on using microencapsulated phase change materials (PCM) in building applications. Energy and Buildings, 2015. **106**: p. 134-155.
- 36. Iten, M. and S. Liu, *A work procedure of utilising PCMs as thermal storage systems based on air-TES systems.* Energy Conversion and Management, 2014. **77**(Supplement C): p. 608-627.
- 37. Baïri, A., E. Zarco-Pernia, and J.M. García de María, *A review on natural convection in enclosures for engineering applications. The particular case of the parallelogrammic diode cavity.* Applied Thermal Engineering, 2014. **63**(1): p. 304-322.
- 38. Korti, A.I.N. and F.Z. Tlemsani, *Experimental investigation of latent heat storage in a coil in PCM storage unit.* Journal of Energy Storage, 2016. **5**(Supplement C): p. 177-186.
- 39. Bruno, F., USING PHASE CHANGE MATERIALS (PCMs) FOR SPACE HEATING AND COOLING IN BUILDINGS, in AIRAH performance enhanced buildings environmentally sustainable

#### design conference. 2005.

- 40. Arulanandam, S.J., K.G.T. Hollands, and E. Brundrett, *A CFD heat transfer analysis of the transpired solar collector under no-wind conditions*. Solar Energy, 1999. **67**(1–3): p. 93-100.
- 41. Gunnewiek, L.H., K.G.T. Hollands, and E. Brundrett, *Effect of wind on flow distribution in unglazed transpired-plate collectors*. Solar Energy, 2002. **72**(4): p. 317-325.
- 42. Gunnewiek, L.H., E. Brundrett, and K.G.T. Hollands, *Flow distribution in unglazed transpired plate solar air heaters of large area.* Solar Energy, 1996. **58**(4–6): p. 227-237.
- 43. Eryener, D. and H. Akhan, *The Performance of First Transpired Solar Collector Installation in Turkey.* Energy Procedia, 2016. **91**: p. 442-449.
- 44. Arkar, C., et al., *Performance analysis of a solar air heating system with latent heat storage in a lightweight building.* Applied Thermal Engineering, 2016. **95**: p. 281-287.
- 45. Osterman, E., V. Butala, and U. Stritih, *PCM thermal storage system for 'free' heating and cooling of buildings*. Energy and Buildings, 2015. **106**: p. 125-133.

- Li, S., Numerical Study of Convective Heat Transfer for Flat Unglazed Transpired Solar Collectors. Energy Procedia, 2012.
- 47. Gholampour, M. and M. Ameri, Energy and exergy analyses of Photovoltaic/Thermal flat transpired collectors: Experimental and theoretical study. Appl. Energy 164, 2016.
- 48. Badache, M., et al., Experimental and two-dimensional numerical simulatiion of an unglazed transpired solar air collector. Energy Procedia, 2012.
- 49. Li, Y., Thermal Performance Analysis of a PCM Combined Solar Chimney System for Natural Ventilation and Heating/Cooling (Thesis). 2013, Coventry University.
- 50. Hocine, H.B.C.e., et al., *A Three-Dimensional Modeling of Photovoltaic Thermal Collector.* INTERNATIONAL JOURNAL of RENEWABLE ENERGY RESEARCH, 2016. **Vol.6, No.2**.
- 51. Bejan, A.S., T. Catalina, and A.T. Munteanu, *Indoor Environmental Quality Experimental Studies in an Energy-efficient Building. Case study: EFdeN Project.* Energy Procedia, 2017. **112**: p. 269-276.
- 52. Entrop, A.G., H.J.H. Brouwers, and A.H.M.E. Reinders, Experimental research on the use of microencapsulated Phase Change Materials to store solar energy in concrete floors and to save energy in Dutch houses. Solar Energy, 2011. **85**(5): p. 1007-1020.
- 53. Kuznik, F. and J. Virgone, *Experimental assessment of a phase change material for wall building use.* Applied Energy, 2009. **86**(10): p. 2038-2046.
- 54. Kuznik, F., J. Virgone, and J.-J. Roux, *Energetic efficiency of room wall containing PCM wallboard: A full-scale experimental investigation.* Energy and Buildings, 2008. **40**(2): p. 148-156.
- 55. Navarro, L., et al., Experimental evaluation of a concrete core slab with phase change materials for cooling purposes. Energy and Buildings, 2016. **116**: p. 411-419.
- 56. Silva, T., et al., Experimental testing and numerical modelling of masonry wall solution with PCM incorporation: A passive construction solution. Energy and Buildings, 2012. **49**: p. 235-245.
- 57. Soares, N., et al., Experimental study of the heat transfer through a vertical stack of rectangular cavities filled with phase change materials. Applied Energy, 2015. **142**: p. 192-205.
- 58. Soares, N., et al., Experimental evaluation of the heat transfer through small PCM-based thermal energy storage units for building applications. Energy and Buildings, 2016. **116**: p. 18-34.
- 59. Dutil, Y., et al., *Modeling phase change materials behavior in building applications: Comments on material characterization and model validation.* Renewable Energy, 2014. **61**: p. 132-135.
- 60. Sharma, A., et al., *Review on thermal energy storage with phase change materials and applications.* Renewable and Sustainable Energy Reviews, 2009. **13**(2): p. 318-345.
- 61. Kuznik, F., J. Virgone, and K. Johannes, *Development and validation of a new TRNSYS type for the simulation of external building walls containing PCM.* Energy and Buildings, 2010. **42**(7): p. 1004-1009.
- 62. Borderon, J., J. Virgone, and R. Cantin, *Modeling and simulation of a phase change material system for improving summer comfort in domestic residence*. Applied Energy, 2015. **140**: p. 288-296.
- 63. Teodosiu Catalin, A.L., Raluca Teodosiu. Reducing Energy Consumption in Buildings Using Phase Change Material. in 4th Energy Performance of Buildings Abstract book (RCEPB IV). 2012.
- 64. Bogdan Diaconu, M.C. Phase Change Material (PCM) composite insulating panel with high thermal efficiency in International Conference on ENERGY and ENVIRONMENT TECHNOLOGIES and EQUIPMENT. 2010.
- 65. Johan Heier, C.B., Viktoria Martin. *Thermal energy storage in Swedish single family houses a case study.* in *The 12th International Conference on Energy Storage*. 2012. Innostock.
- 66. Sage-Lauck, J.S. and D.J. Sailor, *Evaluation of phase change materials for improving thermal comfort in a super-insulated residential building*. Energy and Buildings, 2014. **79**: p. 32-40.
- 67. Solgi, E., R. Fayaz, and B.M. Kari, Cooling load reduction in office buildings of hot-arid climate, combining phase change materials and night purge ventilation. Renewable Energy, 2016. **85**: p. 725-731.
- 68. Saffari, M., et al., Economic impact of integrating PCM as passive system in buildings using Fanger comfort model. Energy and Buildings, 2016. **112**: p. 159-172.

- 69. Tabares-Velasco, P.C., C. Christensen, and M. Bianchi, *Verification and validation of EnergyPlus phase change material model for opaque wall assemblies.* Building and Environment, 2012. **54**: p. 186-196.
- 70. Guarino, F., et al., *PCM Thermal Energy Storage in Buildings: Experimental Study and Applications.* Energy Procedia, 2015. **70**: p. 219-228.
- 71. Berardi, U. and M. Manca, *The Energy Saving and Indoor Comfort Improvements with Latent Thermal Energy Storage in Building Retrofits in Canada*. Energy Procedia, 2017. **111**: p. 462-471.
- 72. Sigalas, G., Computational Optimization of Passive use of Phase Change Materials in Lightweight Low-Energy Houses. 2011, Technische Universiteit Endhoven University of Technology.
- 73. Vikas, A. Yadav, and S.K. Soni, Simulation of Melting Process of a Phase Change Material (PCM) using ANSYS (Fluent). International Research Journal of Engineering and Technology (IRJET), 2017.
- 74. Bejan, A.S. and T. Catalina, *The Implementation of Phase Changing Materials in Energy-efficient Buildings. Case Study: EFdeN Project.* Energy Procedia, 2016. **85**: p. 52-59.
- 75. Andrei Stelian Bejan, T.C., Joseph Virgone. Comparison of different PCMs impact on indoor comfort in a energy positive house. in CLIMA 2016, Aalborg University. 2016.
- 76. Kuznik, F., J. Virgone, and J. Noel, *Optimization of a phase change material wallboard for building use.* Applied Thermal Engineering, 2008. **28**(11–12): p. 1291-1298.
- 77. Shrestha, M., *PCM Application Effect on Energy Use and IA Temperature*. 2012, Norwegian University of Science and Technology, Faculty of Architecture and Fine Arts.
- 78. Janis Kazjonovs, D.B., Aleksandrs Korjakins, Ansis Ozolins, Andris Jakovics. *ANALYSIS OF SIMULATION MODELS OF PCM IN BUILDINGS UNDER LATVIA'S CLIMATE CONDITIONS.* in *4th International Conference CIVIL ENGINEERING.* 2013.
- 79. Sharifi, N.P., A.A.N. Shaikh, and A.R. Sakulich, *Application of phase change materials in gypsum boards to meet building energy conservation goals.* Energy and Buildings, 2017. **138**: p. 455-467.
- 80. Kuznik, F., et al., *A review on phase change materials integrated in building walls.* Renewable and Sustainable Energy Reviews, 2011. **15**(1): p. 379-391.
- 81. Navarro, L., et al., *Thermal energy storage in building integrated thermal systems: A review. Part 1. active storage systems.* Renewable Energy, 2016. **88**: p. 526-547.
- 82. Navarro, L., et al., *Thermal energy storage in building integrated thermal systems: A review. Part 2. Integration as passive system.* Renewable Energy, 2016. **85**: p. 1334-1356.
- 83. Manual. *ANSYS Fluent Chapter 12.4.2 RNG k-epsilon Model.* accesat martie 2018; Available from: <a href="https://www.sharcnet.ca/Software/Fluent6/html/ug/node479.htm">www.sharcnet.ca/Software/Fluent6/html/ug/node479.htm</a>.
- 84. Croitoru, C. and I. Colda, Studii teoretice si experimentale referitoare la influenta turbulentei aerului din incaperile climatizate asupra confortului termic. 2011.
- 85. Bordianu, D., C. Croitoru, and I. Nastase, *Studiul termoaeraulic al elementelor de anvelopă cu colector solar integrat.* 2016.
- 86. Manual, Ansys Fluent Chapter 4.1.5. The k-omega and SST Models. accessat aprilie 2018.
- 87. Ji, Y., CFD modelling of natural convection in air cavities. CFD Letters, 2014. Vol. 6(1).
- 88. Rubitherm. [cited June 2017; Available from: https://www.rubitherm.eu/media/products/datasheets/Techdata -RT35 EN 31052016.PDF.